NASA TECHNICAL TRANSLATION

NASA TT F-497

NASA TT F-497

DIRECTIONAL DISTRIBUTION IN THE REFLECTION OF HEAT RADIATION AND ITS EFFECT ON HEAT TRANSFER

by B. Münch

Doctoral Dissertation, Swiss Technical College of Zürich, Zürich, 1955

NATIONAL AERONAUTICS AND SPACE ADMINISTRATION • WASHINGTON, D. C. • APRIL 1968

DIRECTIONAL DISTRIBUTION IN THE REFLECTION OF HEAT RADIATION AND ITS EFFECT ON HEAT TRANSFER

By Benjamin Münch

Translation of "Die Richtungsverteilung bei der Reflexion von Wärmestrahlung und ihr Einflus auf die Wärmeübertrangung." Institut für Thermodynamik und Verbrennungsmotorenbau an der Eidgenössischen Technischen Hochschule, Zürich, 1955.

NATIONAL AERONAUTICS AND SPACE ADMINISTRATION

For sale by the Clearinghouse for Federal Scientific and Technical Information
Springfield, Virginia 22151 – CFSTI price $3.00

FOREWORD

This work was undertaken at the instigation of Prof. Dr. G. Eichelberg. Starting with the problem of the heat exchange through radiation, the work continued with experimental and theoretical considerations for practical application.

The experimental investigations were conducted at the Machine Laboratory of the Swiss Technical College at Zürich.

I wish to express my sincere thanks to my highly esteemed teacher, Prof. Eichelberg, for his interest in seeing this work carried out to its successful conclusion. I thank the Study Commission for Aeronautics at the Swiss Technical College for their financial assistance in facilitating the printing. To the personnel of the Machine Laboratory, especially Mr. P. Hollenstein, I express my appreciation and thanks for the careful design of the experimental apparatus.

Zürich, November 1954

Benjamin Münch

FOREWORD TO THE ENGLISH TRANSLATION

The recommendation that an Engish edition of this work be published was made by scientists at the NASA Lewis Research Center in Cleveland, Ohio. Since the appearance of the original German edition in 1955, requirements for space travel and earth satellite technology have produced a growing interest everywhere in the precise calculation of heat exchange through radiation. The calculation methods developed in this present work are numerically exact and can be programmed in a digital computer.

Zürich, November 1966

Benjamin Münch

CONTENTS

Most Important Symbols

E	total radiation energy per unit surface
E_ν	radiation energy per unit surface and unit solid angle in direction of angle ν
E_n	radiation energy per unit surface and unit solid angle in direction of surface normal
F	surface
f	reflection factor
f'	direction-dependent reflection factor
H	brightness
Q, q	radiation energies
ϵ	emission coefficient of total radiation
ϵ_ν	emission coefficient for angle ν
ρ	reflection coefficient taken over all directions of space and all incidence angles
ρ_ν	reflection coefficient for incident angle ν
$\rho_{\nu\mu\psi}$	$= \rho'$ reflection coefficient for the incidence angle ν and direction of reflection (μ, ψ)
ν	incidence angle of radiation
μ, ψ	angles of reflection
φ	solid angle ratio
Ω	solid angle

ABSTRACT. The thermal radiation properties of a surface can be characterized by its emission and reflection coefficients. An experimental apparatus is described for measuring the reflection coefficient as a function of the incident and reflected directions. All directional distributions from the purely specular to the strongly scattering were found by superposition of purely specular and diffuse results. A good approximation was found for the tests on concentric spheres.

CUT ALONG THIS LINE

FOLD LINE

NATIONAL AERONAUTICS AND SPACE ADMINISTRATION
WASHINGTON, D.C. 20546

OFFICIAL BUSINESS

POSTAGE AND FEES PAID
NATIONAL AERONAUTICS & SPACE ADMINISTRATION

NATIONAL AERONAUTICS AND SPACE ADMINISTRATION
CODE USS-T
WASHINGTON, D.C. 20546

NASA TTF No.
497

FOLD LINE

CUT ALONG THIS LINE

NATIONAL AERONAUTICS AND SPACE ADMINISTRATION

TECHNICAL TRANSLATION EVALUATION

Budget Bureau No. 104-R037
Approval Expires: Sept. 30, 1969

TO: THE USERS OF THIS TRANSLATION →

NASA TTF NO. 497

MAINTAINING THE QUALITY OF NASA TRANSLATIONS REQUIRES A CONTINUOUS EVALUATION PROGRAM. PLEASE COMPLETE AND MAIL THIS FORM TO AID IN THE EVALUATION OF THE USEFULNESS AND QUALITY OF THE TRANSLATING SERVICE.

THIS PUBLICATION *(Check one or more)*

- [ ] FURNISHED VALUABLE NEW DATA OR A NEW APPROACH TO RESEARCH.
- [ ] VERIFIED INFORMATION AVAILABLE FROM OTHER SOURCES.
- [ ] FURNISHED INTERESTING BACKGROUND INFORMATION.
- [ ] OTHER *(Explain)*: _____

FOLD LINE FOLD LINE

TRANSLATION TEXT *(Check one)*

- [ ] IS TECHNICALLY ACCURATE.
- [ ] IS SUFFICIENTLY ACCURATE FOR OUR PURPOSE.
- [ ] IS SATISFACTORY, BUT CONTAINS MINOR ERRORS.
- [ ] IS UNSATISFACTORY BECAUSE OF *(Check one or more)*:
  - [ ] POOR TERMINOLOGY.
  - [ ] NUMERICAL INACCURACIES.
  - [ ] INCOMPLETE TRANSLATION.
  - [ ] ILLEGIBLE SYMBOLS, TABULATIONS, OR CURVES.
  - [ ] OTHER *(Explain)*:

FOLD LINE FOLD LINE

REMARKS

FROM

DATE

NOTE: REMOVE THIS SHEET FROM THE PUBLICATION, FOLD AS INDICATED, STAPLE OR TAPE, AND MAIL. NO POSTAGE NECESSARY.

NASA Form 1332 AUG 66

GPO 915-777

CUT ALONG THIS LINE

CUT ALONG THIS LINE

DIRECTIONAL DISTRIBUTION IN THE REFLECTION OF HEAT RADIATION AND ITS EFFECT ON HEAT TRANSFER*

By Benjamin Münch

INTRODUCTION

If two or more surfaces at different temperatures exchange heat by radiation, the amounts of energy transferred depend both on the geometric arrangement and on the radiation properties of the participating surfaces. If the surfaces are only slightly reflecting, that is, approximately a blackbody in their properties, only the direct emission needs to be considered in computing the heat transfer. The contribution of the reflected radiation may be neglected. This well known simplification, known as the Nusselt approximation, makes it possible to treat even very complicated geometric arrangements with reasonable computational labor. However, the often required computation of the reflections is treated in the literature for only a few rather simple cases such as parallel plates, and concentric, spherical, and cylindrical surfaces. Here, almost without exception, the reflections are treated like emissions in that the same directional distribution (the Lambert cosine law), is assumed for both emission and reflection.

The problem of the radiation exchange between eccentric spherical surfaces had been studied some years ago at the Institute for Thermodynamics and Combustion Engines of the Swiss Technical Institute. Approximation computations, which similarly assume the reflections to obey the Lambert cosine law while they take into account their local distribution on the surface, have been carried out by Eichelberg and H. H. Ott (ref. 8). The results are in good qualitative agreement with those obtained in section 4. In accordance with these results, the heat transfer must decrease if the spherical surfaces are brought from the concentric to an eccentric position. On the contrary, tests conducted in 1949 by K. Elser (ref. 7) showed an increase of the heat transfer with increasing eccentricity. This was also found to be true when using matte, diffusely reflecting surfaces for which it was believed that the assumptions of the calculation were satisfied. The qualitatively different result of the experiment makes it appear likely that not only the local distribution of the reflections but also their distribution of direction plays an important part.

Measurements of the reflections and their directional distributions of

*"Die Richtungsverteilung bei der Reflexion von Wärmestrahlung und ihr Einfluss auf die Wärmeübertragung." Mitteilung Nr. 16, Institut für Thermodynamik und Verbrennungsmotorenbau an der Eidgenossischen Technischen Hochschule, Zürich, 1955.

energy were conducted by E. Eckert (ref. 3), with emission temperatures between 273.4° and 280° C and with the incident radiation predominantly normal to the surface. The measurements, described in the first section of this report, of the directional distribution of the reflections go into more detail on the dependence on the incident angle of the radiation. The emission temperatures employed are higher throughout than those of Eckert and generally vary between 500° and 1000° C. This has the advantage, in regard to the measuring technique, that greater radiation energies are available and, consequently, the aperture angle of the bundle of rays used can be made smaller.

The theoretical computations, given in sections 2 to 4, are for the purpose of applying the obtained results to the determination of the heat exchange. Finally, in section 5, the results are experimentally tested for the example of eccentric spherical surfaces.

The present work refers only to the total radiation emitted by a surface that is composed of the various wavelengths of the spectrum. The radiating surfaces are always (except as noted in sections 11 and 15) assumed as gray radiators whose emission is proportional to the fourth power of the absolute temperature, according to the Stefan-Boltzmann law. In accordance with the usual practice for technical computations of radiation exchange, the deviations from the gray radiator assumptions are taken into account by assuming the radiation properties (emission and reflection coefficients) to be dependent on the temperature.

1. DIRECTIONAL DISTRIBUTION OF REFLECTIONS, DETERMINATION OF ABSORPTION COEFFICIENTS THROUGH MEASUREMENT OF REFLECTION COEFFICIENTS

11. Emission and Reflection Magnitudes

According to the Stefan-Boltzmann law, a heated surface gives off the total radiation energy

$$E = \epsilon E_s = \epsilon C_s \left(\frac{T}{100}\right)^4 \tag{1}$$

per unit surface per unit time. Here C_s denotes the radiation constant of a blackbody, T is the absolute temperature in °K, and the emission ratio or emission coefficient ϵ is the ratio of the total radiation of the surface under consideration to the radiation of the blackbody, referred to all wavelengths and directions of space. For the radiation per unit surface and unit solid angle emitted at angle ν to the surface normal there are defined an ϵ_ν and, in particular for the direction of the normal to the surface, an ϵ_n:

$$\left.\begin{aligned} E_\nu &= E_{\nu_s} \epsilon_\nu \\ E_n &= E_{n_s} \epsilon_n \end{aligned}\right\} \tag{2}$$

The subscript s refers to the blackbody, the subscript ν to the angle ν between the direction of the emission and the surface normal. The emission of a blackbody is distributed, according to the Lambert cosine law, as

$$E_{\nu_s} = E_{n_s} \cos \nu \tag{3}$$

and always forms an upper limit for the emission of a surface radiating due to its temperature alone. If ψ denotes the angle of rotation about the surface normal, the solid angle element is given by

$$d\Omega = \sin \nu \, d\nu \, d\psi$$

and, by integration over all directions of the half-space, the total radiation is

$$E = \int E_\nu \, d\Omega$$

With account taken of equation (3) there is obtained for a blackbody

$$E_s = \pi E_{n_s}$$

and finally, for the emission ratio of the total radiation,

$$\epsilon = \int_0^{\pi/2} \epsilon_\nu \sin(2\nu) d\nu \tag{4}$$

If heat radiation falls on a nonblackbody in the direction ϵ, as shown in figure 1, the nonabsorbed energy is in general reflected in all directions of the half-space. In figure 1, ϵ denotes the ray with angle of incidence ν to the surface normal n and r a reflected ray whose direction is fixed by the angles of reflection μ and ψ. If E_ν is the incident energy per unit surface, R_ν the total reflected energy per unit surface and $R_{\nu\mu\psi}$ the reflected energy per unit surface and unit solid angle in the direction r we define the reflection coefficient, referred to the angle of incidence ν and the angles of reflection μ and ψ, as

$$\rho_{\nu\mu\psi} = \rho' = \frac{2\pi R_{\nu\mu\psi}}{E_\nu} \tag{5}$$

The double integration over all reflection directions of the half-space gives the reflection coefficient corresponding to the direction of incidence ν

$$\rho_\nu = \frac{R_\nu}{E_\nu} = \frac{1}{2\pi} \int \rho' \, d\Omega = \frac{1}{2\pi} \int_0^{\pi/2} \int_0^{2\pi} \rho' \, d\psi \sin \mu \, d\mu \tag{6}$$

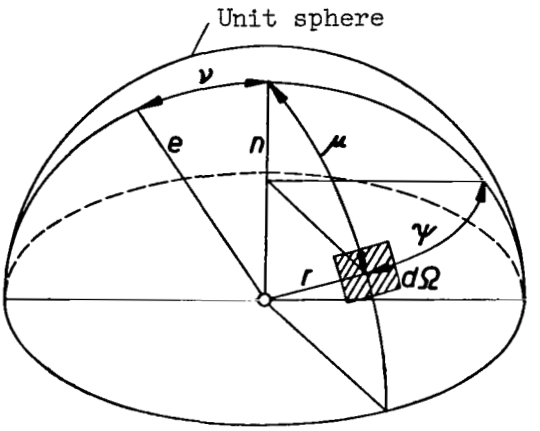

Figure 1. - Direction of incidence and reflection.

If ρ' is constant over all directions, ρ_ν and ρ' are of the same magnitude. The double integral, equation (6) is, for the purpose of determining ρ_ν from measured reflection coefficients ρ', separated into two simple integrals:

$$\left.\begin{aligned} \bar{\rho} &= \frac{1}{2\pi}\int_0^{2\pi} \rho'\, d\psi \\ \rho_\nu &= \int_0^{\pi/2} \bar{\rho}\, \sin\mu\, d\mu \end{aligned}\right\} \qquad (7)$$

The Kirchhoff law, which follows from the second principle of thermodynamics, connects the emission and reflection magnitudes with each other. Imagine having two surface elements in a black cavity according to figure 2: the one element dF_1 with the emission coefficient ϵ_ν and reflection coefficient ρ_ν in the direction ν; the second element dF_2 with $\epsilon_{\nu'}$ and $\rho_{\nu'}$ in the direction ν'. The cavity and the two surface elements have the same temperature. From dF_1 there is emitted the radiation

$$dF_1 E_\nu = dF_1 E_{n_s} \cos\nu\, \epsilon_\nu$$

Of this radiation the fraction

$$dF_1 E_\nu\, d\Omega = \frac{dF_1\, dF_2}{r^2} E_{n_s} \cos\nu \cos\nu'\, \epsilon_\nu$$

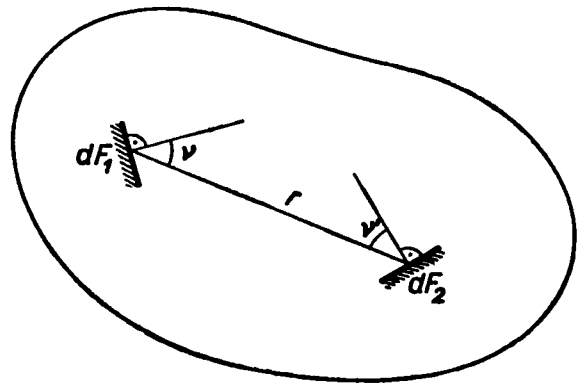

Figure 2. - For proving Kirchhoff's law.

strikes the surface element dF_2, that absorbs this amount multiplied by $1 - \rho_{\nu'}$. Hence, dF_2 receives from dF_1 the energy stream

$$dQ_{12} = E_{n_s} \frac{dF_1\, dF_2}{r^2} \cos \nu \cos \nu' \epsilon_\nu (1 - \rho_{\nu'})$$

The emission from dF_2 leads to the radiation heat dQ_{21} transferred to dF_1. The expression for it is obtained from the formula for dQ_{12} by interchanging the subscripts ν and ν' and differs from it only through the last two factors. The second principle forbids the heat exchange between two bodies of equal temperature and therefore requires $dQ_{12} = dQ_{21}$. From this follows the condition

$$\epsilon_\nu (1 - \rho_{\nu'}) = \epsilon_{\nu'} (1 - \rho_\nu)$$

and when the surface element dF_2 is a blackbody

$$\epsilon_\nu = 1 - \rho_\nu \tag{8}$$

The result, according to which the emission coefficient must be equal to the absorption coefficient $1 - \rho_\nu$ for every direction of emission, we shall denote as the differential Kirchhoff law, in contrast to the less general relation

$$\epsilon = 1 - \rho$$

obtained from equation (8) through integration and which is normally denoted as Kirchhoff's law and requires the equality of the emission and absorption coefficients of the total radiation. The law of equation (8), according to the assumptions of the proof, holds for every surface, including a nongray radiator. It holds without restriction for the gray radiator (whose emission and absorption coefficients are independent of the temperature) upon which gray radiation of

corresponding temperature falls. Since nothing must be assumed as to the emission temperature it also holds for each individual wavelength of the spectrum.

According to the differential Kirchhoff's law no surface can emit in any direction more than the blackbody, that is, ϵ_ν can never be greater than 1. It is significant to compare the directional distribution of the emissions with the Lambert cosine law that holds for the directional distribution of the upper limit, namely the blackbody. For the reflection coefficient ρ' there is no such limit. It may become arbitrarily large for individual directions and its definition does not depend on the Lambert cosine law.

12. Apparatus for Determining Reflection Coefficients

For measuring the reflection coefficients ρ' on a surface that is in the form of a test plate, the latter is irradiated by a radiation source with definite intensity and at a given angle of incidence. A radiation measuring apparatus receives the reflections in a small solid angle interval in the desired direction of reflection.

Figure 3 shows the design of the experimental setup. The stand 1 carries on its fixed arm 2, formed like an "optical bench," the cavity radiator 4 as a radiation source. The interchangeable diaphragm 5 with the circular cross section F_2 has an aperture of diameter of 10, 20, or 40 millimeters and together with the adjustable distance r_1 (for the tests r_1 was equal to 40 or 60 cm) determines the energy stream that falls per unit area on the test plate 9. The arm 3, which can swing out in the direction of the arrow, carries the vacuum thermocouple 17 as a radiation measuring instrument. For quantitatively regulating the radiation output to be measured the rectangular diaphragm 14 and the diaphragm 16 with the circular cross section F_3 are used (diameter of aperture 20 or 40 mm). Both diaphragms are interchangeable and are at the fixed distance $r_2 = 87.5$ centimeters from each other. For interrupting the radiated energy stream, screen slide 7 is used. This slide shuts off the cavity radiator directly, and the valve 13, which (as protection against an undesired overstressing of the vacuum thermocouple) is normally closed, is raised during the measurement by means of a photo release lever. The desired angles of incidence and reflection can be adjusted by deflecting the arm 3 (angle scale on the stand) and by rotating the test plate about the vertical axis (indicator 11 and circular scale on the cover of the stand). Furthermore, the plate 9 can be deflected in the arc 10 (rotation about a horizontal axis).

The radiation protective tunnels 6 and 15 and jacket sheet metal 12 screen off the radiation to the outside. The numerous intermediate screens and the auxiliary diaphragm 8, which restricts the incident beam to a minimal required diameter, prevent the falsifying of the measurement by disturbing reflections at the wall. The jacket of the cavity radiator, diaphragms 5 and 8, the test plate and a part of the radiation screens 6 are water-cooled.

The electrically heated radiation source (fig. 4) is designed for a maximum emission temperature of 1000° C. The radiating part consists of the hollow body

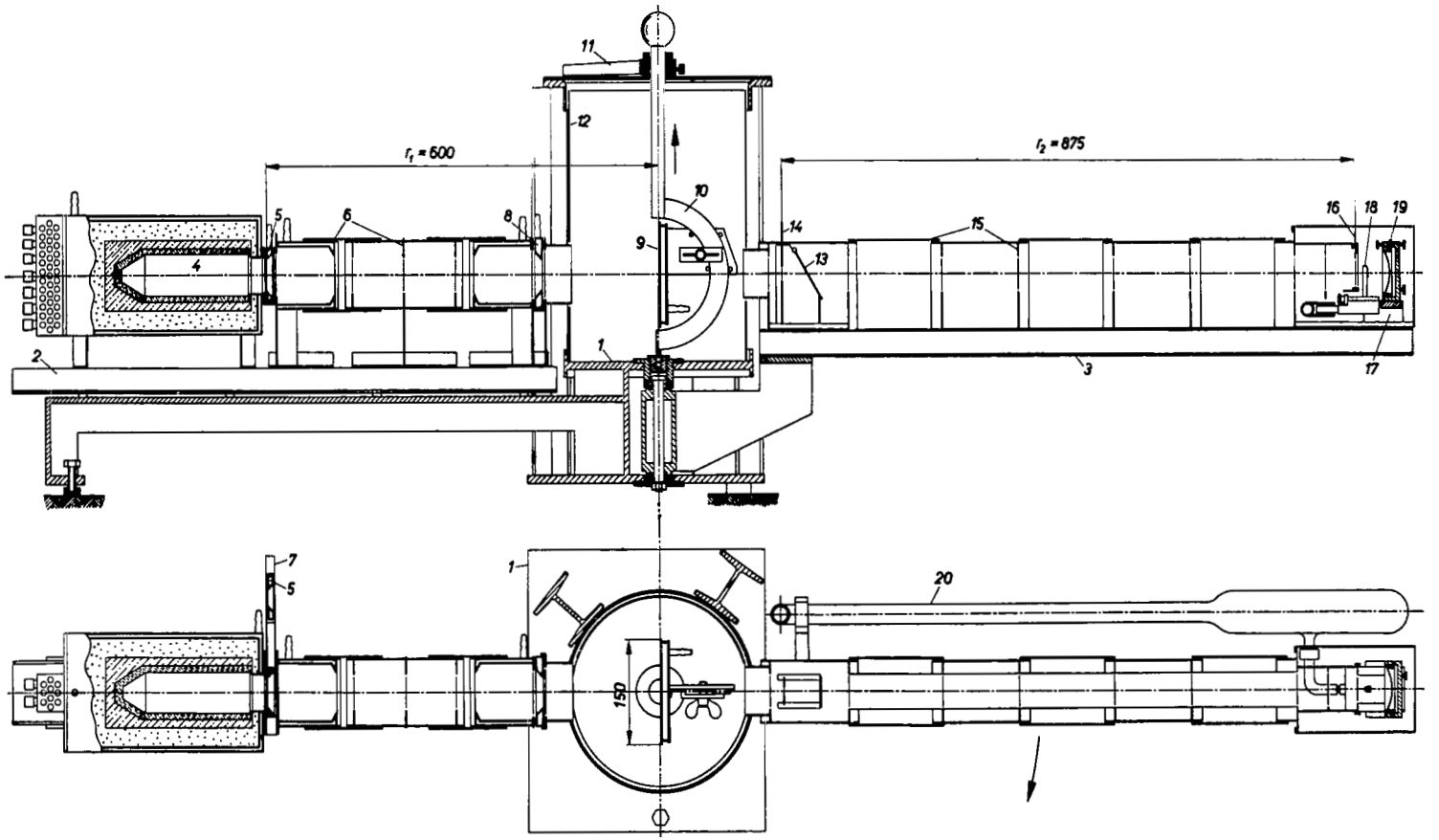

Figure 3. - Apparatus for determining reflection coefficients.

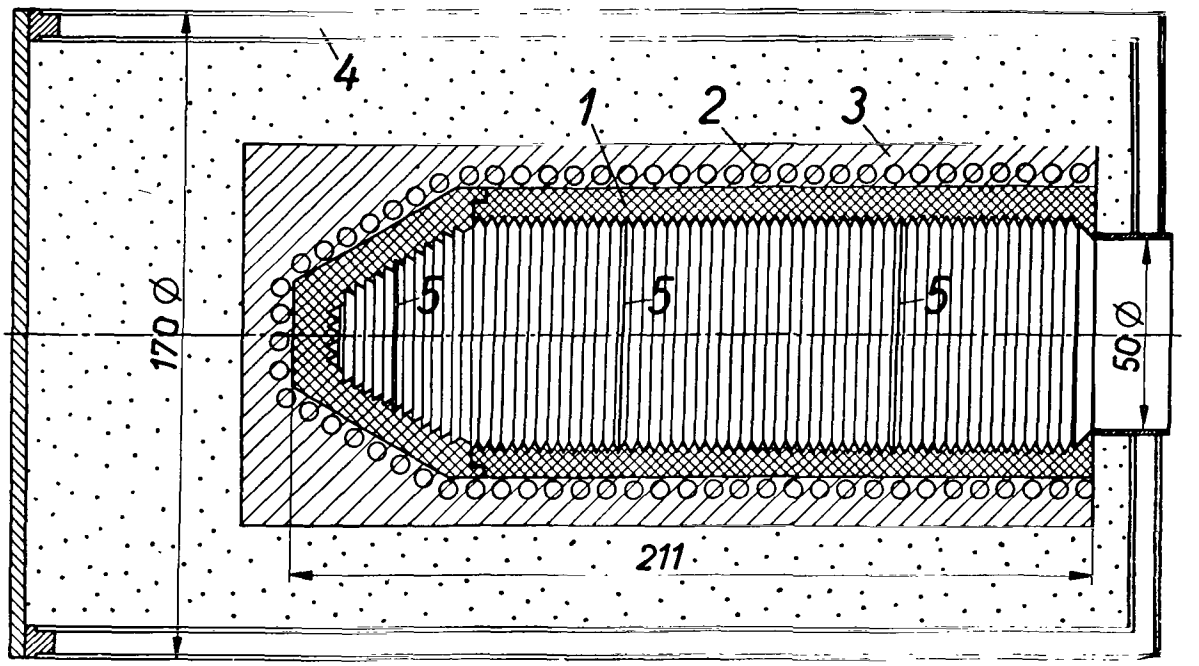

Figure 4. - Section through radiation source.

1, whose inner surface is grooved for the purpose of more nearly approximating a blackbody and was prepared from the steatite material "calorstea" of the Swiss Isola Works of Breitenbach. The heating coil 2 of canthal wire is embedded in the cement jacket 3 and is made up of 4 partial coils whose loading can be regulated with the aid of series-connected resistances so that the cavity radiator assumes the desired steady temperature constant over the entire length within about $\pm 10^{\circ}$ C. The temperature is measured with the three platinum-platinum rhodium thermocouples 5 which, with stretched sides, were cemented into a groove of the hollow body 1. The cold soldered joints were situated near the switch panel on the rear side of the radiator and were approximately at room temperature. The temperature measured with the rearmost thermocouple serves as the emission temperature of the blackbody. The measurement need be accurate only to 5° C since the emission temperature is required only as a parameter. The heated part of the radiator is surrounded by an asbestos insulation and by the water-cooled jacket 4. The heating and thermocouple wires were led out on the rear side on a switch panel.

The vacuum thermocouple 17 (fig. 3), from the firm of Kipp and Sons in Delft (Holland), contains a radiation receiver two 0.1 millimeter-wide thermocouples and 0.001 millimeter-thick band-shaped manganin-constantan thermocouples (thermocouple voltage about 4.1 mV/100° C) in the arrangement indicated in figure 5, where the dimensions are given under the dimension lines. The two thermocouples are connected in opposition if the thermoelectric voltage is tapped off the terminals K_1 and K_2; one receives the radiation while the other forms the cold joint for eliminating the instrument temperature. The adjustable elliptical

mirror 19, with the focal lengths 35 and 285 millimeters, concentrates the radiation near the soldered joint of one of the two thermocouples. The mirror (with r_2 = 875 mm) forms an image of the manganin-constantan strips enlarged 28.8-14 times (fig. 3). For example, if the diaphragm 14 has an aperture of height B = 20 millimeters, the portion of the thermocouple indicated by the hatched part in figure 5 is acted upon. The effective area F_2 (aperture cross sec. of diaphragm 14) is then 2.9 × 20 millimeters squared. The interchangeable diaphragms 14 are all 10 millimeters wide and have various heights B (from 0.5 to 20 mm). The thermoelectric voltage is not accurately proportional to F_2 because the sensitivity of the measuring system depends to some extent on the impingement width B. The diaphragms must therefore be compared with each other in a checking experiment in order to determine the ratios of the measurement readings for any two different apertures F_2 (determination of the diaphragm ratios F_2'/F_2, see sec. 13).

The measuring system is enclosed in the small tube 18 (fig. 3) and, for the purpose of raising its sensitivity by excluding the heat conduction of the surrounding air, is placed in a high vacuum. A rock salt window that sufficiently passes all wavelengths between 2000 A and 16 μ provides the vacuum sealing. A mercury diffusion pump, which is connected to a rotary pump for producing the prevacuum, furnishes the high vacuum. Connected in series with it is a liquid air-cooled cold trap which serves to freeze out the condensable vapors, especially the mercury vapors. The high vacuum is conducted to the small tube 18, over a neoprene hose and the glass tube 20.

The sensitivity of the vacuum thermocouple during the measurements was about 7 μV/μW when evacuated and about 0.5 μV/μW without vacuum.

A mirror galvanometer with high voltage sensitivity measured the thermoelectric voltage. For a light pointer length of 2.5 millimeters a scale reading of 53 mm/μV was obtained. Therefore, radiation powers of 0.1 μW could still be accurately measured, while those of 0.01 μW could be estimated. The measuring instrument constructed as a dual coil galvanometer is, with its coil of 50 Ω internal resistance, connected over a shunt box S, shown in figure 6. The shunt box permits the reduction of the sensitivity by the factors indicated whereby the resistance of the galvanometer with shunt is always 50 Ω. Furthermore, in the galvanometer circuit there is the resistance R_1 of 0.1 of the calibration box E. R_1 together with R_2 are part of a voltage divider to which a voltage of 2 volts from a storage battery is applied by closing the switch P. The voltage drop over the resistance R_1 is 0.0001 V and is introduced in the galvanometer circuit as calibration voltage. Thereby the sensitivity of the galvanometer can be checked each time.

13. Measuring Procedure

The measurements of the reflection coefficients were conducted as relative measurements through comparison of the reflected amounts of radiation with a measurement of the emission output (calibration). In this way the temperature

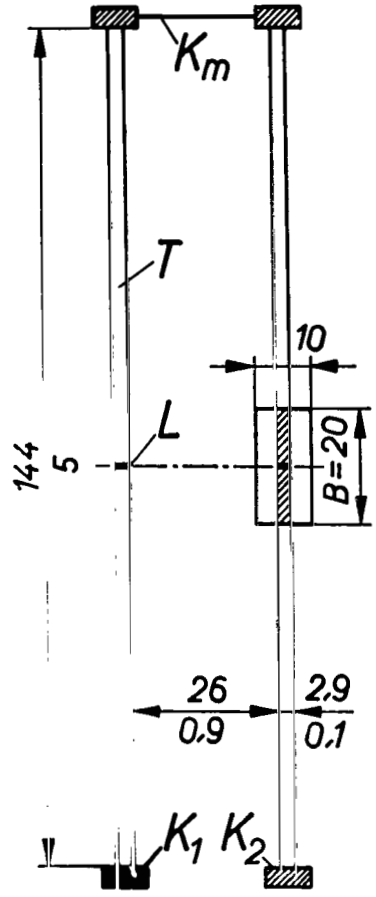

Figure 5. - Measuring system of vacuum thermocouple.

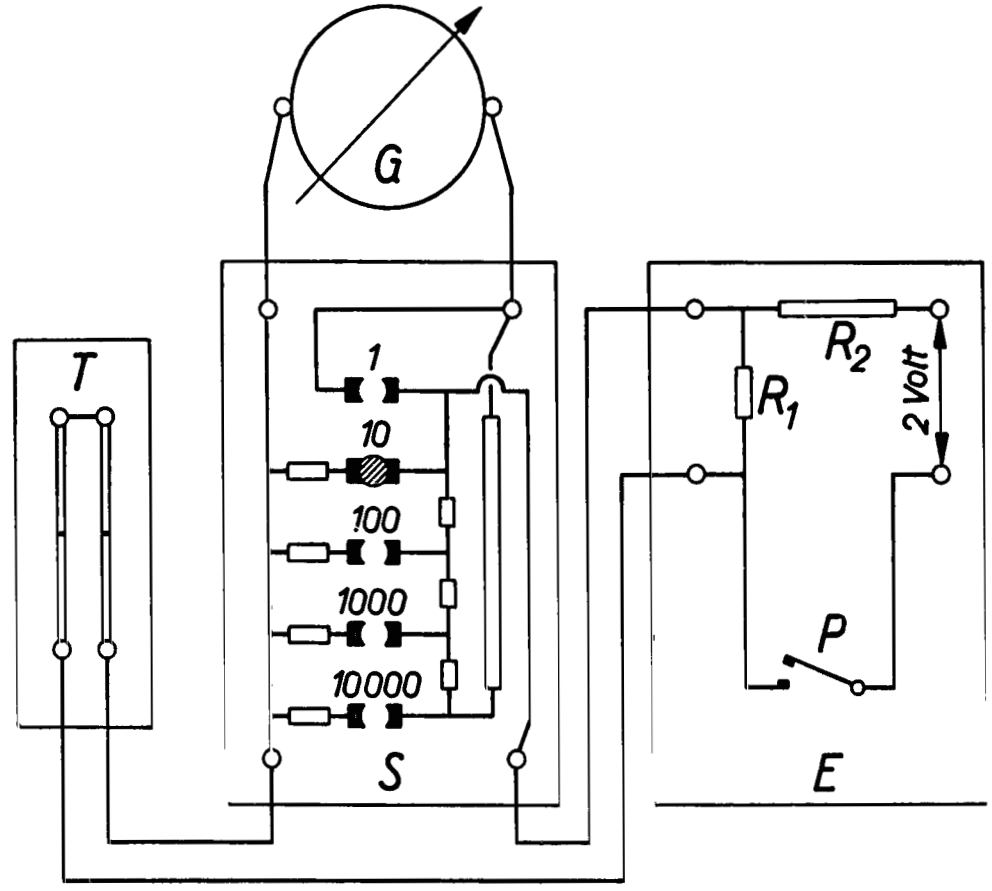

Figure 6. - Circuit diagram of galvanometer circuit.

of the radiation source, the sensitivities of the thermocouples and the galvanometer and several geometric magnitudes were eliminated from the formulas for the evaluation.

Figure 7 shows a geometric scheme of the apparatus. F_1 and F_3 denote the aperture cross sections of the diaphragms beyond the hole radiator and ahead of the vacuum thermocouple and F_2 is the effective aperture of the rectangular diaphragm. The optical axes of the radiator and of the vacuum thermocouple and the surface normal n of the test plate need not (as drawn in the figure), fall in the same plane.

For calibrating the radiation source and the measuring apparatus the swiveling arm 3 is brought into the extended position shown in figure 3 and the test plate drawn up high in the stand in the direction of the arrow. The radiator with the large diaphragm F_1 (40 mm diam.) is shifted so near the diaphragm F_2 that from each point of the diaphragm aperture F_3 behind the aperture F_2 only the emitting surface of the blackbody can be seen. The emission energy of the radiator is

$$E_e = C_s\left[\left(\frac{T_e}{100}\right)^4 - \left(\frac{T_u}{100}\right)^4\right]$$

if its emission coefficient is assumed to be 1. With

$$\varphi_{23} = \frac{F_3}{\pi r_2^2}$$

as solid angle ratio for the radiation exchange from F_2 to F_3. F_2' as effective aperture of the rectangular diaphragm during the calibration the energy stream falling on the thermocouple, is obtained as

$$Q_e = E_e \frac{F_2' F_3}{\pi r_2^2} \qquad (9)$$

During the measurement the blackbody emits the radiation output $E_e F_1$. The amount of radiation

$$E_\nu = E_e \frac{F_1 \cos \nu}{\pi r_1^2} \qquad (\text{watt/cm}^2)$$

falls on the test plate that reflects the portion $R_\nu = E_\nu \rho_\nu$. The radiation emitted per unit area and unit solid angle in the reflection direction considered becomes

$$R_{\nu\mu\psi} = \frac{\rho' E_\nu}{2\pi}$$

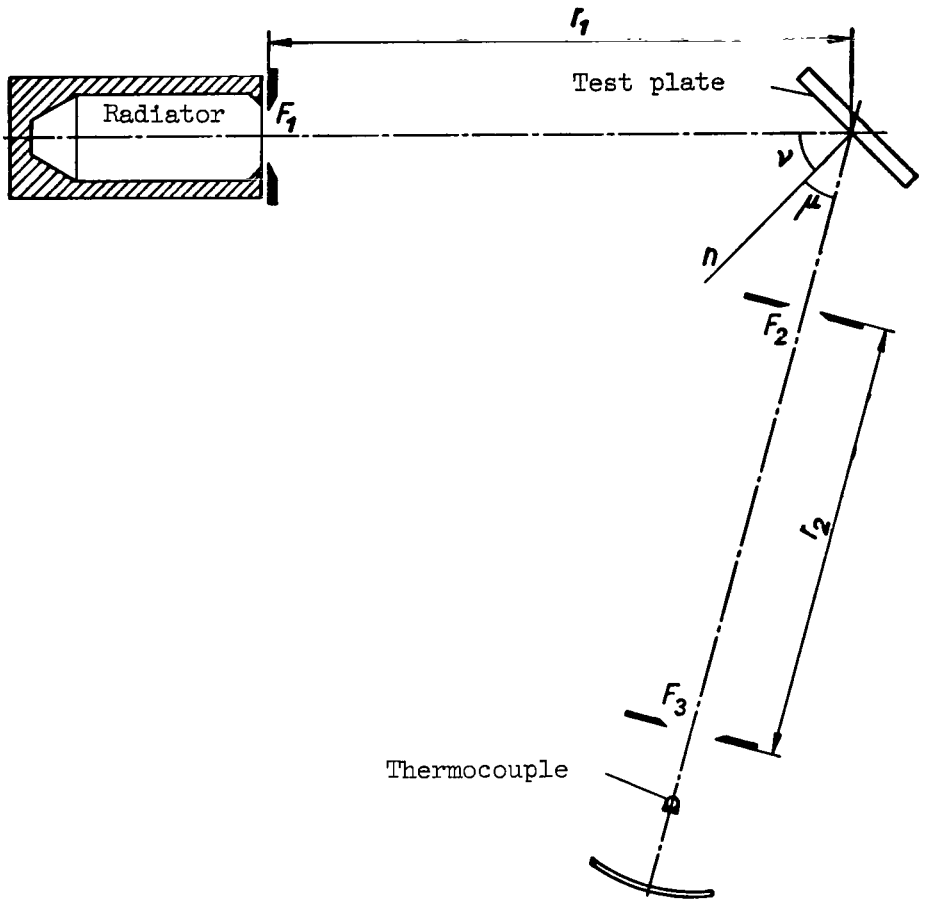

Figure 7. - Geometric scheme of apparatus.

Since $F_2/\cos\mu$ is the area of the test plate as viewed from the measuring instrument and the diaphragm F_3 at the distance r_2 from the rectangular diaphragm subtends the solid angle

$$\Delta\Omega = \frac{F_3}{r_2^2}$$

the thermocouple, during the measurement, receives the radiation

$$R_{\nu\mu\psi}\frac{F_2}{\cos\mu}\Delta\Omega = R_{\nu\mu\psi}\frac{F_2}{\cos\mu}\frac{F_3}{r_2^2}$$

or

$$Q_m = E_e\rho'\frac{F_1F_2F_3}{2\pi^2r_1^2r_2^2}\frac{\cos\nu}{\cos\mu} \qquad (10)$$

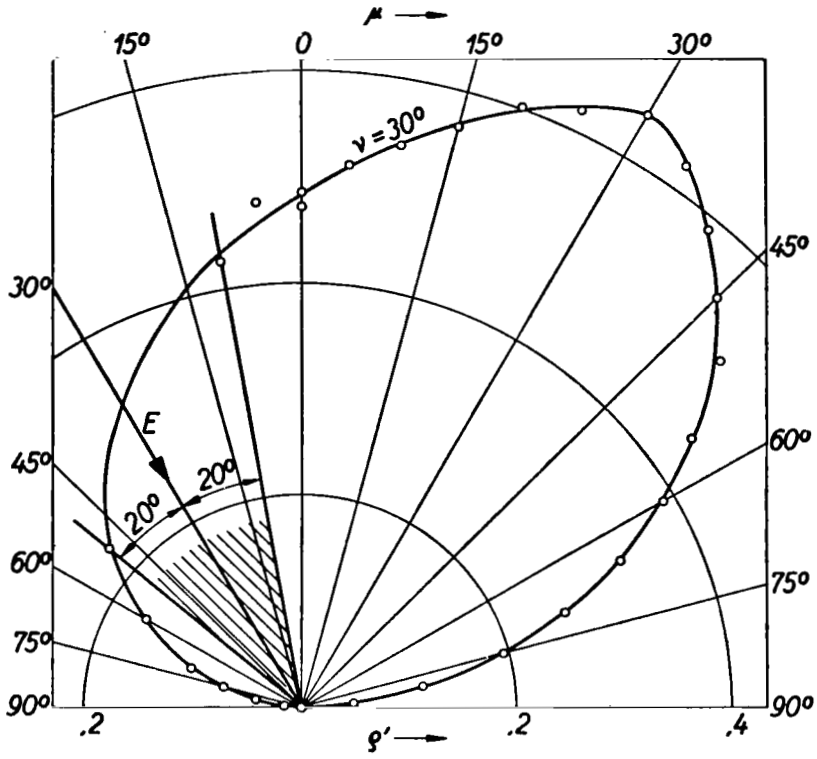

Figure 8. - Directional distribution of ρ' for white typewriting paper, emission temperature, 905° C; ν = 30°; ψ = 0.

The formula required for the evaluation

$$\rho' = \frac{Q_m}{Q_e} \frac{2\pi r_1}{F_1} \frac{F_2'}{F_2} \frac{\cos \mu}{\cos \nu} \tag{11}$$

follows from comparing figures 9 and 10 and holds only for diffuse reflectors. The applicability can be tested through obtaining the same value ρ' with altered geometric parameters F_1 and r_1. The presence of diffuse reflection is also recognizable by the naked eye if the heat radiation employed contains an appreciable part of visible wavelengths, that is, if the emission temperature lies above 600° C, for example. On the test plate there is then seen a reddish shimmer, not sharply defined, that appears to be lodged in the surface.

The specular reflectors reflect only in a direction that is given by the equality of the angle of incidence ν and angle of reflection μ and by $\psi = 0$. The visual observation shows a sharp mirror image of the radiation source with the diaphragm aperture F_1 on the test plate. The specification of ρ' has no purpose here since for the particular direction of the mirror reflection, ρ' is infinitely great; for all other directions of the half-space it becomes zero in

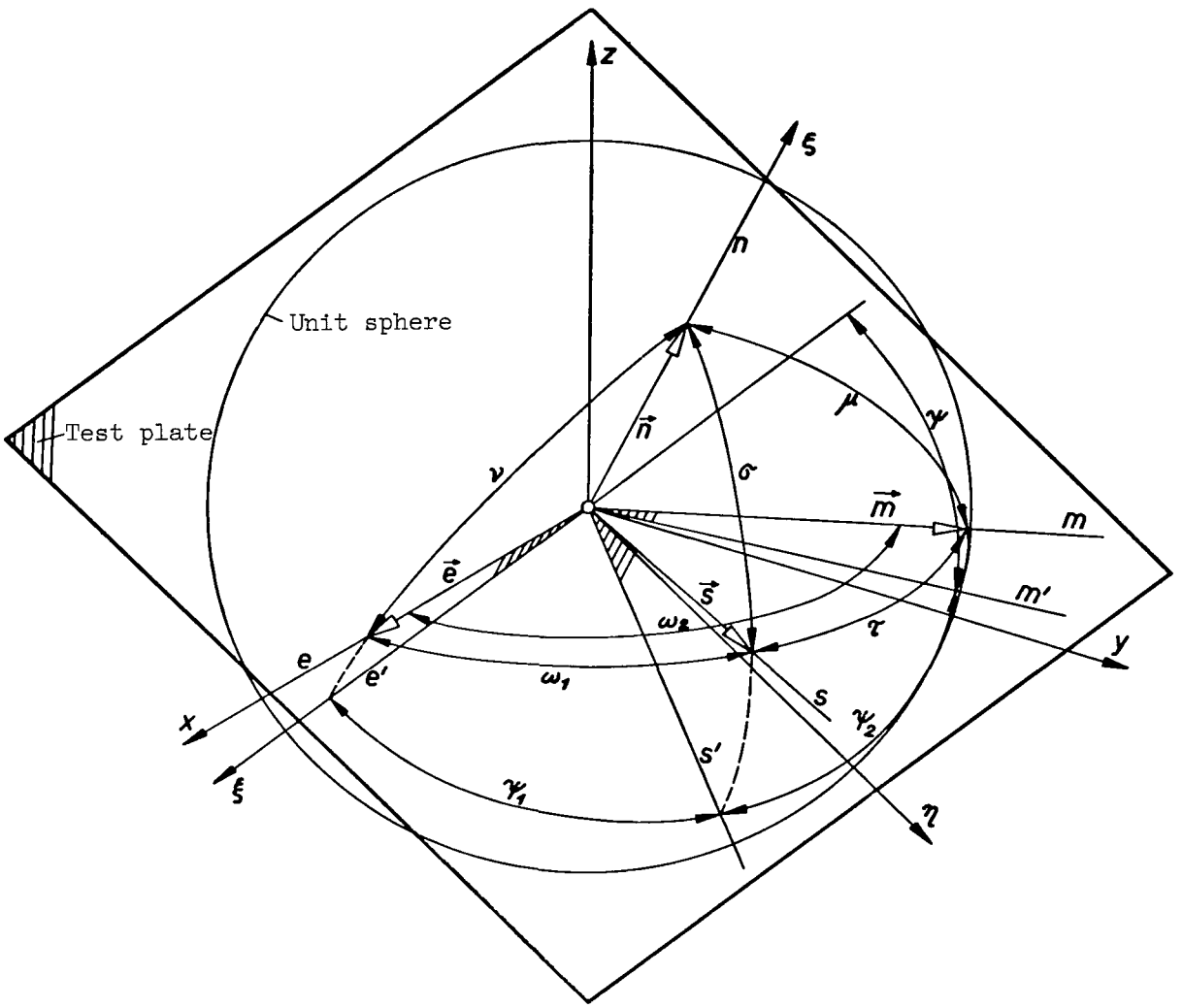

Figure 9. - Relation between angles introduced.

such manner that the double integral equation (6) gives the correct value for the reflection coefficient ρ_ν. For reflectors, ρ_ν can be determined by a single measurement for each angle of incidence. The diaphragm aperture F_1 must be chosen so large and for r_1 so small that from each point of the aperture F_3 behind the rectangular diaphragm only a piece of the mirror image of the whole radiator can be seen. The mirror image of the blackbody illuminates more weakly than the blackbody itself by the factor ρ_ν and the radiation falling on the thermocouple during the measurement is

$$Q_m = \rho_{\nu_{spec}} E_e \frac{F_2 F_3}{\pi r_2^2} \tag{12}$$

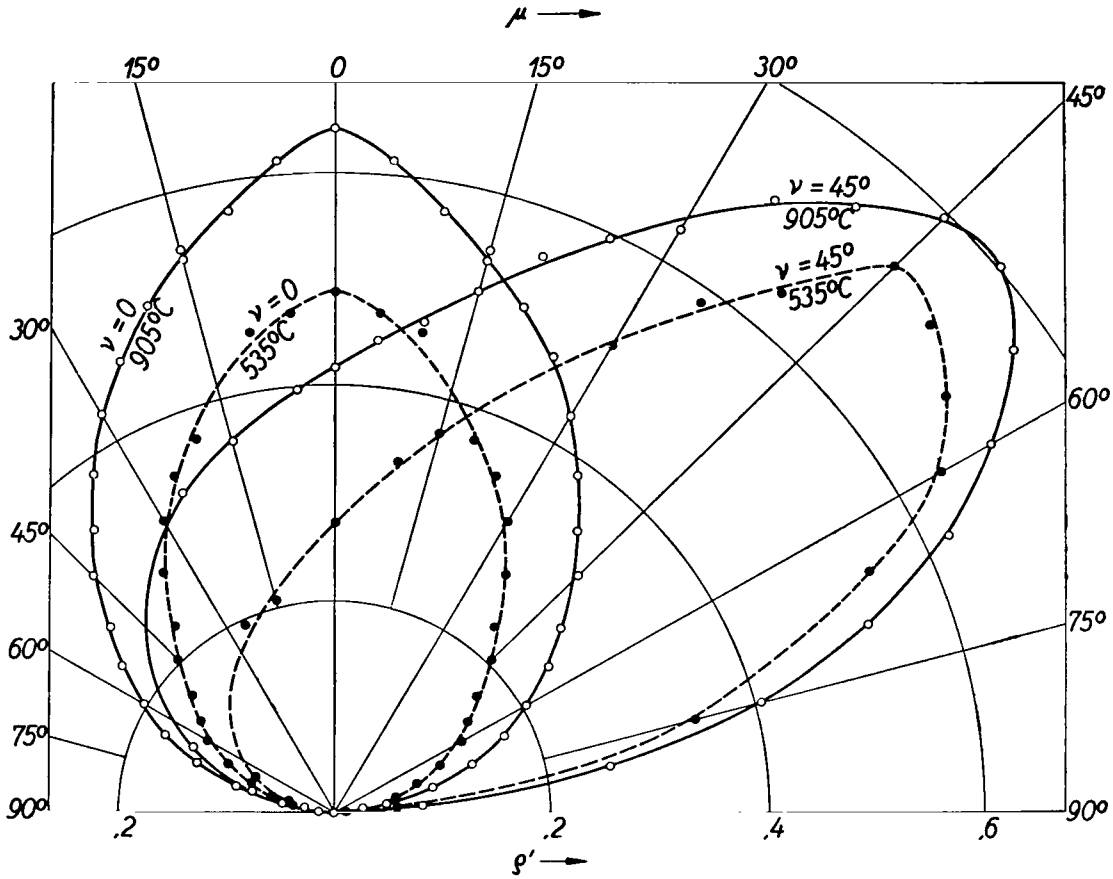

Figure 10. - Directional distribution of reflection coefficient in incident plane for white paper; emission temperatures, 535° and 905° C.

Comparison with equation (9) gives the formula for the reflection coefficient ρ_ν for specular reflection:

$$\rho_{\nu_{sp.}} = \frac{Q_m}{Q_e} \frac{F_2'}{F_2} \tag{13}$$

The experimental criterion for the presence of specular reflection is the independence of the measured reading Q_m on F_1 and r_1 provided F_1 is chosen sufficiently large and r_1 is chosen sufficiently small.

For the measurements on specular reflectors no evacuation of the thermocouple is required since its sensitivity is sufficient for this purpose. The value of $\rho_{\nu_{sp}}$ generally lies in the neighborhood of 0.9 so that $F_2' = F_2$ was chosen in the tests. Readings for Q_m and Q_e of the same order of magnitude are then obtained.

On the contrary, for diffuse reflectors, the radiation measuring instrument must be evacuated in order to utilize its full sensitivity. As a rule the measured energy streams for Q_m fluctuated between 0.1 and 1 μW; for Q_e, approximately 10 μW.

In the evaluation formulas (11) and (13) the galvanometer deflections can be directly substituted in place of the radiation energies Q_m and Q_e, since the calibration constants of the instruments are divided out. In the development of the test program about 10 test points were taken each time between two calibrations in regular time sequence. Voltage fluctuations of the supply line and other effects caused the emission output of the blackbody to fluctuate somewhat so that the two calibrations generally differed. According to the measuring experiences the radiation output reacts so inertly on the disturbance factors that their time variation may be assumed as linear provided the time interval between the calibrations does not exceed about 20 minutes. The calibration values Q_e corresponding to the measuring points may thus be obtained by linear interpolation.

The measurements on the investigated diffuse reflectors usually refer to the incident directions which, formed in the plane through the incidence direction and the surface normal, lie in the incidence plane. The incidence plane is distinguished by the value $\psi = 0$ or 180° (fig. 1). The directional distribution of the reflection coefficient ρ' in the incident plane gives well defined diagrams for the characterization of the investigated surfaces (e.g., the polar diagram in fig. 8). Here the directional distribution of ρ' can be seen for white typewriter paper that was irradiated at an incident angle of $\nu = 30^\circ$ with radiation of the emission temperature of 905° C. The incident ray E in the diagram comes from the left and is marked by the arrow. The apparatus can no longer be used beyond 20° to the left and right of E because the swivel with the thermocouple strikes against the fixed arm. In the hatched angular dead region, therefore, there are no measuring points (no small circles).

For evaluating the integrals (7) and determining ρ_ν, measurements are also required outside the incident plane. Figure 9 shows the relation between the angles of incidence and reflection ν, μ, and ψ and the angles ω_1, ω_2, and σ to be adjusted on the apparatus. The straight line e is the optical axis of the radiation source, m is the measuring apparatus, n is the surface normal of the test plate, s is the direction setting of the arc 10 in figure 3 and e', m', and s' are the normal projections of e, m, and s on the test plate. On the apparatus the angle ω_1 is adjustable between e and s (angle of rotation of the arc 10), the angle ω_2 between e and m (swiveling angle of the rotatable arm), and finally the angle of inclination σ of the test plate as the angle between n and s. The x,y-plane of the introduced coordinate system (x,y,z) coincides with the plane determined by e and m, the $\xi\eta$-plane of the system (ξ, η, ζ) coincides with the surface of the test plate. The unit vectors $\vec{e}$, $\vec{m}$, $\vec{n}$, and $\vec{s}$ of the directions e, m, n, and s have the following components in the system (x,y,z):

Vector	x-Component	y-Component	z-Component
$\vec{e}$	1	0	0
$\vec{s}$	$\cos \omega_1$	$\sin \omega_1$	0
$\vec{m}$	$\cos \omega_2$	$\sin \omega_2$	0
$\vec{n}$	$\cos \omega_1 \cos \sigma$	$\sin \omega_1 \cos \sigma$	$\sin \sigma$

The angle between two directions is equal to the scalar product of the unit vectors of the two directions

$$\cos \nu = \vec{e}\vec{n}$$

$$\cos \nu = \cos \omega_1 \cos \sigma; \qquad \cos \omega_1 = \frac{\cos \nu}{\cos \sigma} \tag{14}$$

and

$$\cos \mu = \vec{m}\vec{n}$$

where

$$\left.\begin{aligned} &\cos \mu = \cos \sigma \cos \tau; \qquad \cos \tau = \frac{\cos \mu}{\cos \sigma} \\ &\tau = \omega_2 - \omega_1 \end{aligned}\right\} \tag{15}$$

For the computation of ψ_1, ψ_2, and finally of ψ, we start more simply from the components of the unit vectors in the coordinate system (ξ, η, ζ):

Vector	ξ-Component	η-Component	ζ-Component
$\vec{e}$	$\sin \nu$	0	$\cos \nu$
$\vec{s}$	$\cos \psi_1 \sin \sigma$	$\sin \psi_1 \sin \sigma$	$\cos \sigma$

The scalar product of the two vectors gives

$$\vec{e}\vec{s} = \cos \omega_1 = \cos \psi_1 \sin \nu \sin \sigma + \cos \nu \cos \sigma$$

whence

$$\cos \psi_1 = \frac{\cos \omega_1 - \cos \nu \cos \sigma}{\sin \nu \sin \sigma}$$

Taking relation (14) into account we have

$$\left.\begin{aligned} \cos \psi_1 &= \cot \nu \tan \sigma \\ \text{and analogously} \\ \cos \psi_2 &= \cot \mu \tan \sigma \\ \text{with} \\ \psi &= 180^\circ - \psi_1 - \psi_2 \end{aligned}\right\} \qquad (16)$$

In practice, ν, μ, and σ are generally given and ω_1, ω_2, and ψ are required. For the special case of the measurements in the incident plane, relations (14), (15), and (16) simplify to

$$\left.\begin{aligned} \sigma &= 0 \\ \omega_1 &= \nu \\ \omega_2 &= \nu + \mu \\ \psi &= 0; \qquad 180^\circ \end{aligned}\right\} \qquad (17)$$

In the determination of the reflection coefficients ρ' for the incident angle $\nu = 0$ the interval of reflection angles that is of most interest μ is situated in the dead region where angles cannot be measured ($0 \leq \mu \leq 20^\circ$). As an expedient, for the incidence angles $\nu = 10^\circ$, 15°, and 20°, measurements in the incidence plane are carried out for $\mu = \nu + \mu_0$. It is found that the measured reflection coefficients are primarily a function of the parameter μ_0 and depend only slightly on the incident angle ν. Therefore, the extrapolation to $\nu = 0$ with $\mu = \mu_0$ is permissible.

The measuring program comprised the measurement of the reflection distribution for the six following surfaces, which were selected as typical representatives from the large manifold of diffuse reflectors:

(1) Brass sheet, oxidized black with a dull and rough surface.

(2) White matte paper (typewriting paper) as an example of a fibrous surface.

(3) White pine, planed and polished. Surface parallel to direction of fibers.

(4) Steatite material "calorstea" of the Swiss Isola-Werke, Breitenbach, as an example of a fire-resistant stone.

(5) Aluminum alloy "anticorodal," colorless and anodically oxidized.

(6) Anticorodal sheet, roughened with fine grain by sand blast, surface fine grained and matte.

The measurements served principally for the determination of the directional distribution of ρ' in the incident plane, at various emission temperatures. Reflection coefficients were measured for only two of the surfaces (black oxidized brass and paper, outside the plane of incidence in order to determine ρ_ν by integration.

In addition the following four polished metal surfaces were investigated: a copper, a brass, an anticorodal and an iron sheet, and also a bright-rolled slightly tarnished anticorodal sheet at various emission temperatures between 350° and 1000° C. The polished metal plates were specular reflectors. The bright-rolled anticorodal sheet also had specular reflection except for a slight proportion that reflected diffusely.

14. Measuring Errors

The scatter of the measuring points in the measurements without vacuum (specular reflectors) was somewhat less than 1 percent and for the measurements with vacuum (diffuse reflection) about 1.5 percent.

Inaccurate adjustment of the geometric magnitudes and incomplete knowledge of the diaphragm ratios F_2'/F_2 can, as the consideration of formula (11) shows, lead to systematic errors, which however can be kept within the scatter. In the tests with the specular reflectors, such errors are exluded because F_2' was chosen equal to F_2.

The incident and reflected beams had finite aperture angles that lay between 1.5° and 5°, as could easily be computed from the dimensions. Measuring errors due to finite aperture angles could be of importance where the reflection coefficient ρ' varies strongly with the direction of the reflection. In the conducted measurements they are negligible.

Disturbance reflections at the inner walls of the apparatus are also negligible since they are sufficiently suppressed by the built-in diaphragms. Only in very extreme cases, when the reflection coefficient ρ' varies within wide limits (e.g., in the measurement of the diffuse portion in the case of nearly specular reflectors), can such disturbances sometimes lead to a falsification of the results.

The heating of the test plates during the taking of a test point leads, in the case of a few surfaces, to systematic errors that cannot be eliminated. Until the galvanometer has reached its final deflection and can be read off, radiation falls for 45 seconds on the test plate. The surface of the plate is slightly warmed and emits radiation that falsifies the measurement. The smaller the heat penetration coefficient $\sqrt{\lambda\gamma c}$ the greater the error of the test plate because the predominant part of the absorbed radiation energy is conducted away by the heat conduction in the plate. The heat radiated due to the temperature increase ΔT gives the absolute measuring error

$$Q_t = C_s \underbrace{\left[\left(\frac{T_u + \Delta T}{100}\right)^4 - \left(\frac{T_u}{100}\right)^4\right]}_{\approx 0.976\ \Delta t\ (\text{in } ^\circ C)} \epsilon_\mu \frac{F_2 F_3}{\pi r_2^2}$$

The ratio to the reflected energy stream which, according to relation (10), falls on the thermocouple is

$$\frac{Q_t}{Q_m} = 2C_s \frac{0.976\ \Delta T}{W} \frac{\epsilon_\nu \epsilon_\mu}{\rho'} \cos \mu$$

where

$$W = E_e \frac{F_1 \cos \nu}{\pi r_1^2} \epsilon_\nu$$

is the absorbed radiation energy per unit surface of the test plate. From the relative error the correction to be applied to the measured reflection coefficients ρ' is

$$\Delta\rho' = \rho' \frac{Q_t}{Q_m} = 1.95\ C_s \frac{\Delta T}{W} \epsilon_\nu \epsilon_\mu \cos \mu$$

The temperature increase ΔT, which the surface of the plate undergoes after 45 seconds with constant heating W, must also be known. This increase is obtained by solving the one-dimensional nonsteady heat conduction problem with the initial and boundary conditions

$$\Delta T = 0 \qquad \text{for} \qquad t \leq 0$$

and

$$\left[\frac{\partial(\Delta t)}{\partial x}\right]_{x=0} = \frac{W}{\lambda}$$

where x is the penetration depth in the plate and t is the time. In the case of the investigated surfaces the correction is to be considered only for white pine (heat penetration coefficient 400 Joule $\sec^{-1/2} m^{-2} deg^{-1}$) and calorstea (heat penetration coefficient 1700 Joule $\sec^{-1/2} m^{-2} deg^{-1}$) and amounts to

For white pine

$$\Delta\rho' = 0.22\ \epsilon_\nu \epsilon_\mu \cos \mu$$

For calorstea

$$\Delta\rho' = 0.057\ \epsilon_\nu \epsilon_\mu \cos \mu \qquad (18)$$

The numerical factor in the formulas is independent of the radiation load of the surfaces. With the radiations used, the temperature increments ΔT in the case of white pine and calorstea were 3.2° and 0.75° C, respectively, and the corrections to be applied were of the order of 20 and 2 percent of the measured value, respectively.

Finally, we also consider what errors are committed if a false emission temperature or surrounding temperature is substituted in the computation of the radiation outputs

$$Q = k\left(T_e^4 - T_u^4\right)$$

The differential dQ gives the change of Q for a change dT_e, or dT_u of T_e and T_u, respectively, so that

$$dQ = 4k\left(T_e^3\, dT_e - T_u^3\, dT_u\right)$$

Compared with $Q \approx kT_e^4$, the relative error of the radiation outputs for falsely substituted emission temperature is found to be

$$\frac{\Delta Q}{Q} = 4\,\frac{\Delta T_e}{T_e}$$

and for falsely substituted surrounding temperature

$$\frac{\Delta Q}{Q} = 4\,\frac{\Delta T_u}{T_u}\left(\frac{T_u}{T_e}\right)^4$$

It is found that the emission temperature must be measured very accurately if it is to be used as the basis for determining the emitted radiation. The measurements were therefore conducted as relative measurements with reference to Q_e and Q_m. The temperature of the surroundings on the contrary, for the emission temperatures used, need be known with an accuracy of only about 20° C. In the measurement of large radiation powers (10 to 100 μW) the excess temperature at the soldered joint of the thermocouple could have played a part as an error of T_u. However, Q_e always remained within such limits that the excess temperature of the joint did not exceed 5° C. This error is, therefore, negligible and very accurate proportionality occurred between the thermoelectric voltage and the measured radiation power.

15. Results of Measurements

For the six investigated diffuse reflectors, the reflection coefficients ρ' for various angles of incidence ν were obtained first. The results for paper, black-oxidized brass, white pine, and calorstea are plotted in the polar diagrams of figures 10 to 14. The results for the anodically oxidized and sandblasted anticorodal sheet are plotted in semilogarithmic presentation in figures 15 and 16. The beam with incident angle ν is, in the polar diagrams, always

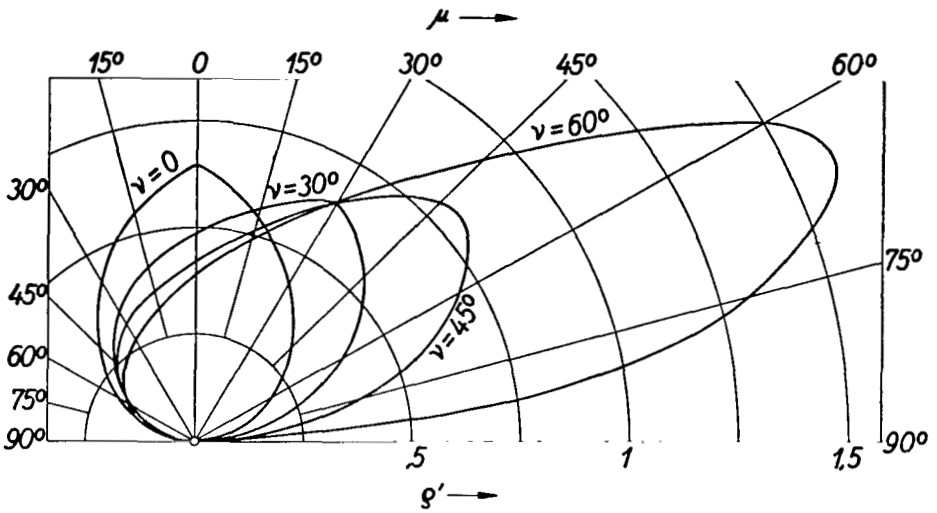

Figure 11. - Directional distribution of reflection coefficient in incident plane for white paper; emission temperature, 905° C.

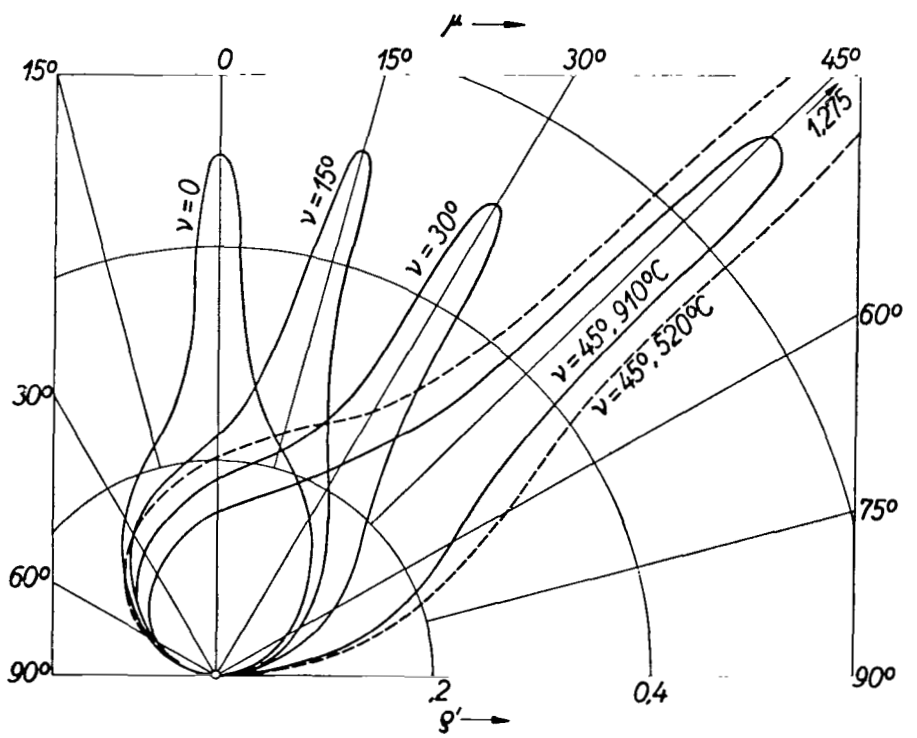

Figure 12. - Directional distribution of reflection coefficient in incident plane for black-oxidized brass; emission temperatures, 520° and 910° C.

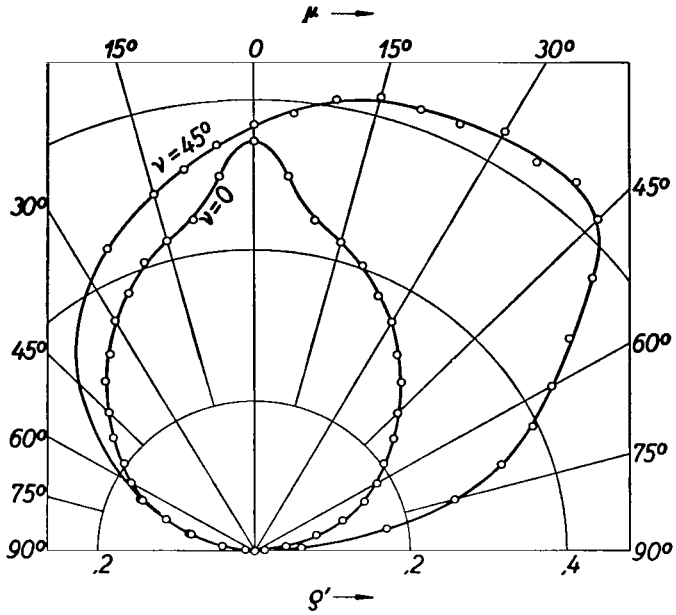

Figure 13. - Directional distribution of reflection coefficient in incident plane for white pine, irradiated at right angles to fiber direction; emission temperature, 910° C.

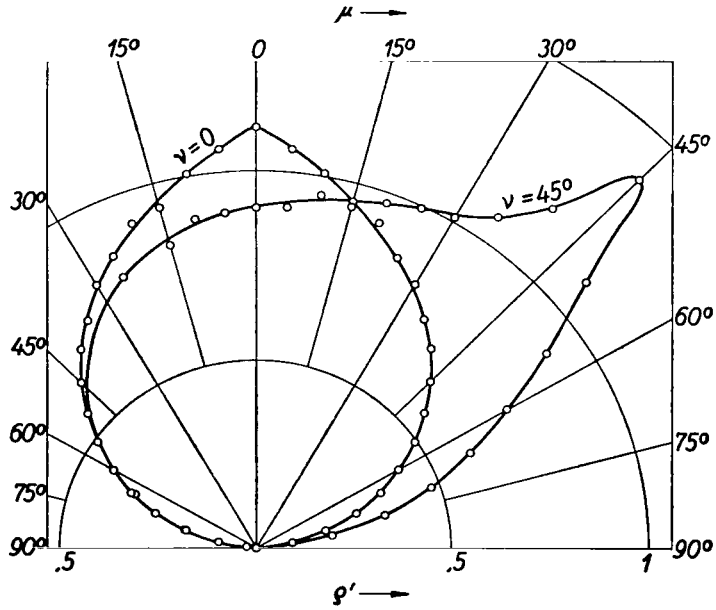

Figure 14. - Directional distribution of reflection coefficient in plane of incidence for calorstea (steatite substance); emission temperature, 905° C.

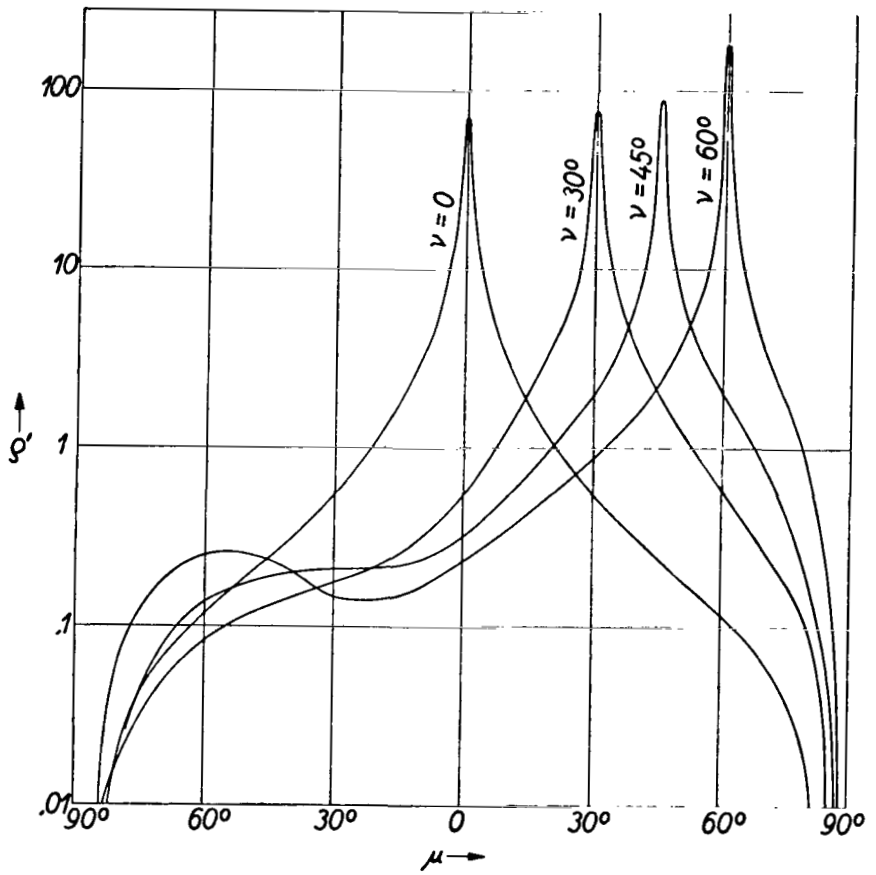

Figure 15. - Directional distribution of reflection coefficient in incident plane for anodically oxidized anticorodal sheet; emission temperature, 920° C.

assumed to be incident from the left. It is also found that in the case of matte, strongly scattering surfaces in the direction of the specular reflection are much preferred. The most diffuse reflection is obtained by fibrous or porous materials, like paper, wood, and fire-resistant stone. The black-oxidized brass with its more compact surface shows reflection coefficients that rise strongly in the direction $\mu = \nu$. Still more strongly dependent on μ are the ρ' values of the two investigated treated anticorodal sheets, which closely approach the specular reflector.

The reflection distributions in the cases investigated approach those of specular reflectors the flatter the incidence of the radiation (i.e., the greater the value of ν). The effect is seen in table I through the reflection coefficients ρ' for the direction of the specular reflection ($\mu = \nu$), which rapidly increase with the incident angle. The phenomenon can be well observed by the naked eye at emission temperatures above 600° C. For glancing incidence (ν al-

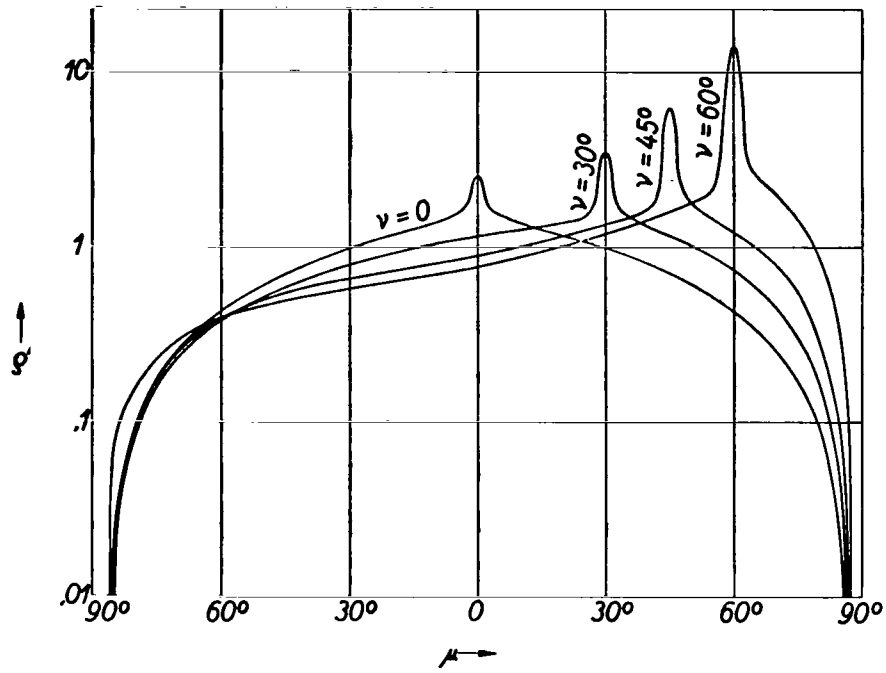

Figure 16. - Directional distribution of reflection coefficient in incident plane for sandblasted anticorodal sheet; emission temperature, 920° C.

most 90°), an unsharp mirror image of the radiation source on the test plate is seen in the direction of the specular reflection instead of the blurred reddish shimmer.

The effect of the emission temperature on the reflection properties was investigated on the surfaces of both white paper and black-oxidized brass. In both cases the distribution of the reflection coefficients at low emission temperature approaches somewhat more that of the specular reflector. This can be clearly explained on the basis of the wave character of the heat radiation. The radiation of low emission temperature is, according to the Wien displacement law, richer in the longer waves, for which the fine structure of the surface does not show up (i.e., the surface appears more even, smoother and more mirror like). The absolute magnitude of the reflection coefficient ρ' varies corresponding to the color of the reflector, if the emission temperature is raised to such an extent that the emitted radiation contains an increasingly larger proportion of visible wavelengths. Thus, ρ' increases for an increase of the emission temperature from about 500° to about 900° C for white paper but, decreases for the case of the black-oxidized brass sheets.

A clear comparison basis for evaluating a reflector is given by the normed 45° distributions in figure 17. They are obtained by redrawing the polar diagrams of the distributions of ρ' for the incident angle $\nu = 45°$ and for the incident plane in such manner that the distance in the diagram corresponding to

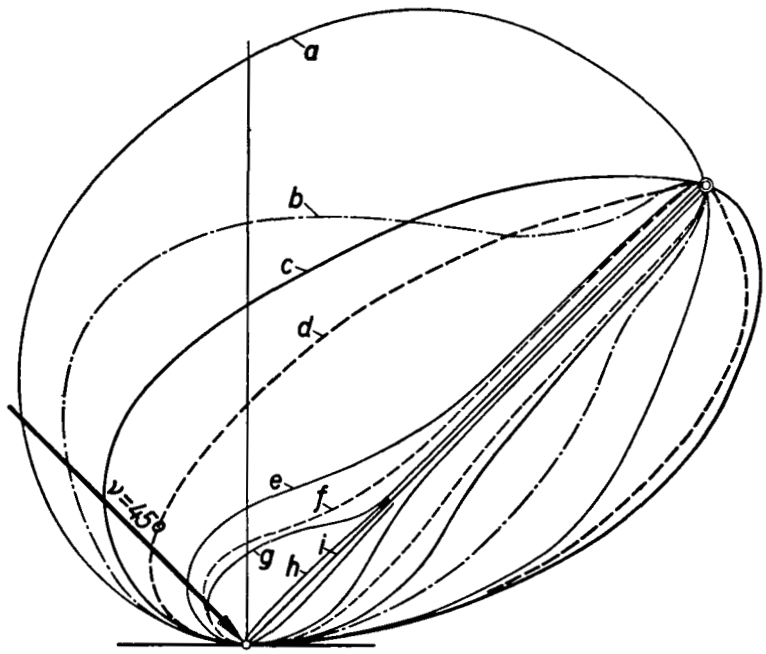

(a) White pine; emission temperature, 910° C.
(b) Calorstea; emission temperature, 905° C.
(c) White paper; emission temperature, 905° C.
(d) White paper; emission temperature, 535° C.
(e) Black-oxidized brass; emission temperature, 910° C.
(f) Black-oxidized brass; emission temperature, 520° C.
(g) Sandblasted anticorodal sheet; emission temperature, 920° C.
(h) Anodically oxidized anticorodal sheet; emission temperature, 920° C.
(i) Specular reflector (for comparison).

Figure 17. - Normal directional distributions of reflection coefficient in incident plane for $\nu = 45°$.

the reflection coefficient in the direction of the specular reflection ($\mu = \nu$, $\psi = 0$) is the same for all reflectors to be compared. The figure shows that the investigated six surfaces cover the entire span between the strongly scattered and the almost specular reflectors.

The measurements of ρ' can be used for the evaluation of the integrals (7) from which ρ_ν, and therefore, also the absorption coefficient $(1 - \rho_\nu)$ of the direction ν, is obtained, and finally by repeated integration according to (4) for the determination of the total absorption coefficient $(1 - \rho)$. The evaluation, to be conducted graphically, of the triple integral assumes a large number of measured ρ' values and a considerable amount of computation, but has the advantage that in this manner absorption coefficients can be determined that cannot be obtained from emission measurements because the investigated surface is not suited for the high emission temperatures encountered (determination of

(1 - ρ) of paper for an emission temperature of 900° C), or has other physical properties at these temperatures.

For white paper and black-oxidized brass the required measurements of ρ' for the evaluation of (7) were made outside the incidence plane for the two incident angles $\nu = 30^\circ$ and 60° and for the reflection angles $\mu = 15^\circ$, 30°, 45°, 60°, and 75° for each of the two ν-values. Figure 18 gives the result for white paper and for $\nu = 30^\circ$. The reflection coefficient ρ' is plotted as a function of ψ with μ as parameter. The first integral of (7) is obtained by planimetering the area $\bar{\rho}$. The second integration leads to the reflection coefficient ρ_ν and, thus, to $(1 - \rho_\nu)$. To the angle of incidence $\nu = 0$ (normal incidence) there corresponds a rotation-symmetrical direction distribution of ρ', with the surface normal of the test plate as axis of symmetry, and the reflection coefficient ρ_ν is obtained for the direction of normal incidence

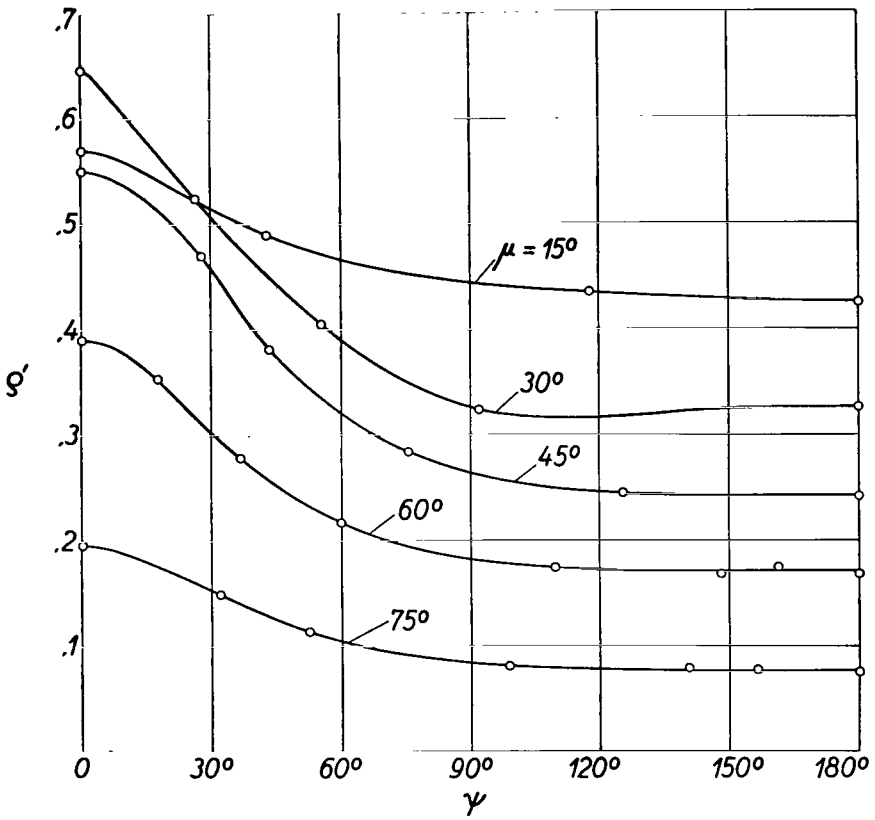

Figure 18. - Reflection coefficient ρ' for white paper; angle of incidence ν = 300°; emission temperature, 905° C.

through a single integration by substituting ρ' directly in place of ρ in the second integral of (7).

$$\rho_{\nu=0} = 1 - (1 - \rho_n) = \int_0^{\pi/2} \rho' \sin \mu \, d\mu \qquad (19)$$

The determination of the absorption coefficient $(1 - \rho_n)$ according to equation (19) was carried out for all investigated diffuse reflectors. Finally, for white paper and black-oxidized brass, there are three $(1 - \rho_\nu)$ values for the three incidence angles $\nu = 0^\circ$, 30°, and 60°. The first two angles coincide within the accuracy of the evaluations. The knowledge of the fundamental trend of the directional distribution of the absorption coefficients in the case of nonmetals, for example, according to the measurements of the emission coefficients of E. Schmidt (ref. 2), enables their reconstruction with the aid of the three measurement values. The integral

$$(1 - \rho) = 1 - \int_0^{\pi/2} \rho_\nu \sin(2\nu) d\nu$$

then leads to the absorption ratio $(1 - \rho)$ of the entire radiation.

The four tested bright-metal surfaces are specular reflectors. A diffuse portion of the reflected radiation could not be confirmed and therefore may be neglected. According to the results of section 13, a test point here gives the absorption ratio $1 - \rho_\nu$ for the angle ν to the surface normal. The measurements, as shown in figure 19, for the polished iron sheet, led to the already familiar directional distributions of the absorption coefficient for electrically conducting materials, as required by the electromagnetic theory of light (refs. 1 and 2) and as confirmed by the measurements of the emission coefficients by E. Schmidt (ref. 2). In accordance with these results the absorption ratio for smooth metal surfaces strongly increases at large angles to the surface normal and again drops only in the neighborhood of the glancing incidence. The large scatter of the test points is explained by the circumstance that the absorption coefficients are obtained through the formation of the differences $1 - \rho_\nu$, which are small compared with the test values. The increase of the absorption ratios with rising emission temperature, likewise predicted by the theory, is confirmed according to figure 20.

The bright-rolled somewhat tarnished anticorodal sheet is almost a specular reflector; the diffusely reflected part amounts to about 2.5 percent of the incident energy stream while, depending on the emission temperature, 80 to 90 percent undergoes specular reflection. The observation with the naked eye shows a sharply defined mirror image of the radiation source on the test plate upon which reddish haze is superposed. The difference $1 - \rho_{\nu_{spec.}}$ is to be reduced further by 0.025 (diffuse part) in order to obtain the total absorption coefficient $(1 - \rho_\nu)$, but gives qualitatively good information. In figure 21 the quotient $(1 - \rho_{\nu_{sp}})/(1 - \rho_{n_{sp}})$ is plotted in the polar diagram against the angle ν to

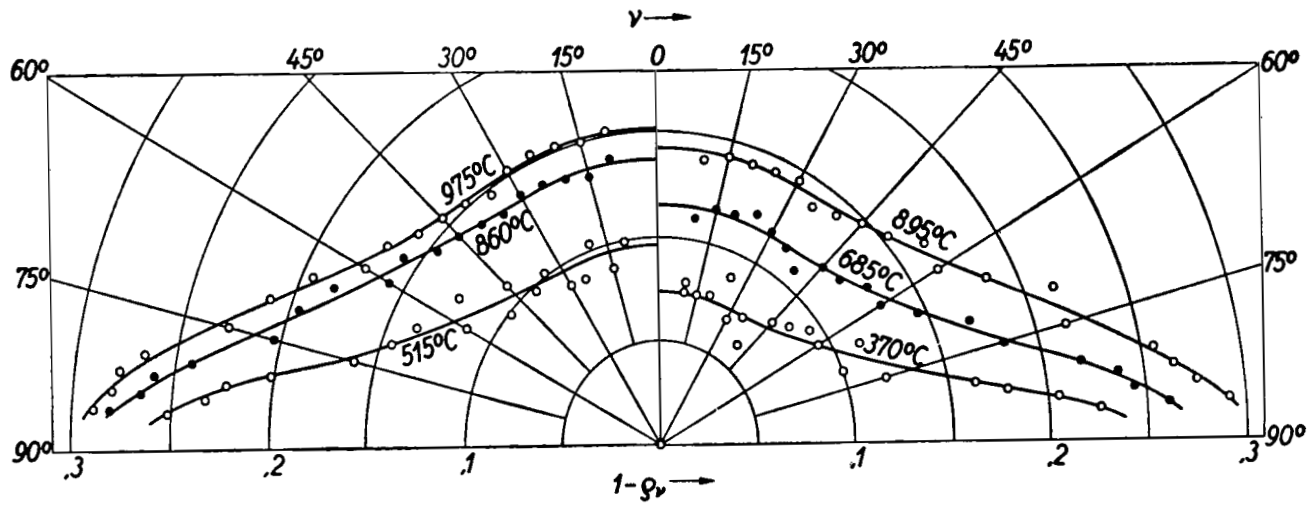

Figure 19. - Directional distribution of absorption coefficient ($1 - \rho_\nu$) for polished iron sheet at various emission temperatures. Test plate at room temperature.

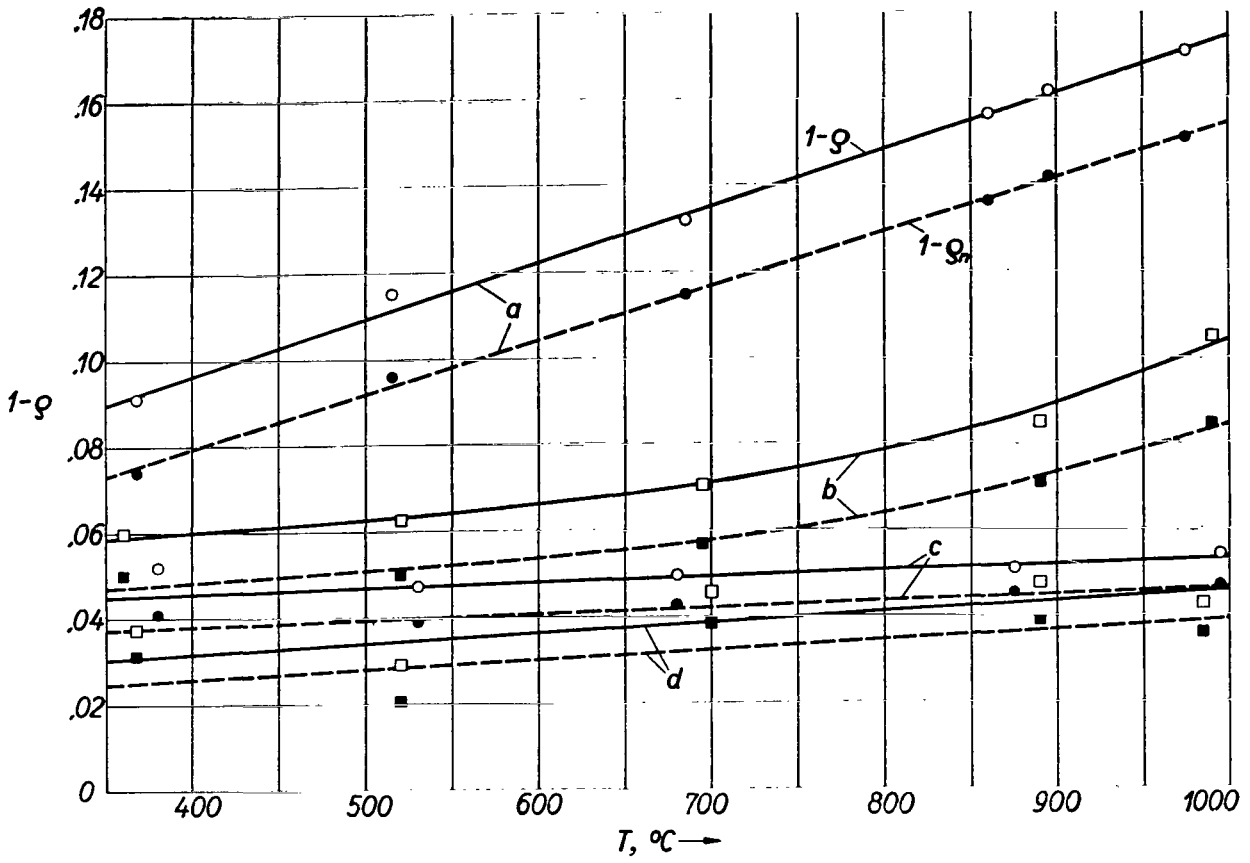

(a) Iron.
(b) Anticorodal (aluminum alloy).
(c) Brass.
(d) Copper.

Figure 20. - Absorption ratio of total incident reflection (1 - ρ) and of radiation in direction of surface normal (1 - ρ_n) as a function of emission temperature for polished metal surfaces. Test plate at room temperature.

the surface normal. This figure gives information on the directional distribution of the absorption coefficient at various emission temperatures. The tarnished anticorodal sheet absorbs the radiation of low emission temperature like the bright metal, while with increasing emission temperature the directional distribution, according to figure 21, increasingly approaches the directional distribution for nonmetals. The thin oxide skin on the surface is evidently barely "noticed" by the longer waves of the radiation of lower emission temperature, while radiation of higher emission temperature is the determining factor for the reflection behavior for the short-wave. Figure 22 finally gives the variation of (1 - ρ_{nsp}) referring to the plate normal, and of (1 - ρ_{sp}) referring to all directions of the half-space, as a function of the temperature T, compared with

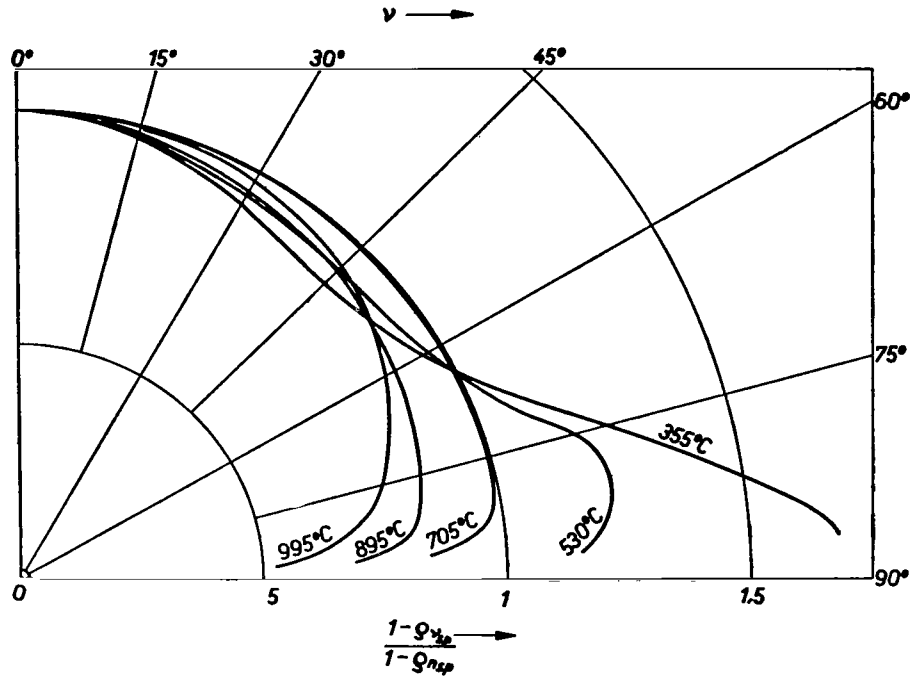

Figure 21. - Comparison of reflecting behavior of rolled-bright, slightly tarnished anticorodal sheet at angle γ to surface normal to that in direction of surface normal. Test plate at room temperature.

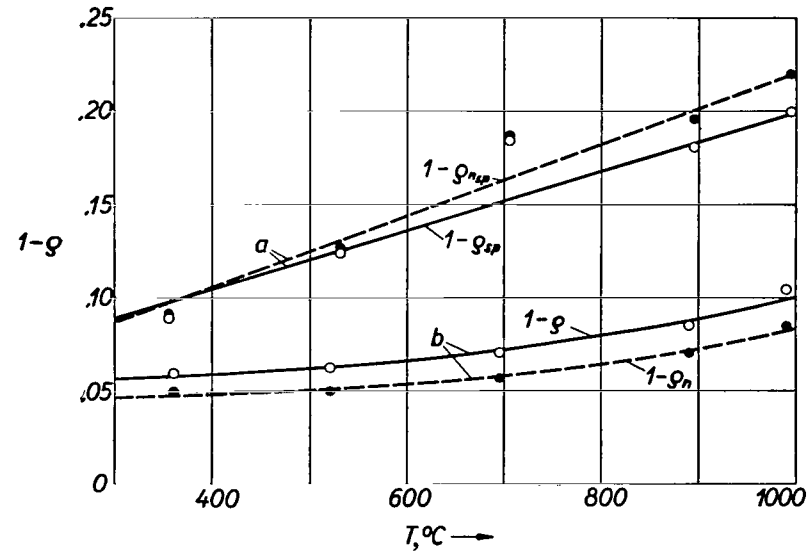

(a) Rolled-bright, slightly tarnished, anticorodal sheet.
(b) Polished anticorodal sheet. Test plates at room temperature.

Figure 22. - Dependence of radiation properties on emission temperature.

the absorption coefficients $(1 - \rho_n)$ and $(1 - \rho)$ of the polished anticorodal sheet.

All measured absorption coefficients refer to a test plate temperature of 10° to 20° C and to the given emission temperatures. According to the Kirchhoff law these absorption coefficients agree with the emission coefficients if we have the case of gray radiators. The investigated technical surfaces are, however, only approximately gray radiators.

For smooth surfaces, according to the electromagnetic theory of light, the absorption coefficients for the total radiation depend on the emission temperature (for monochromatic radiation, on the wavelength) and on the physical properties of the material, namely on the index of refraction for electrical nonconductors and on the specific electrical resistance for metals (see refs. 1 to 3). Since the material properties may also be temperature-dependent, the temperature of the test plate enters as parameter. Although the polished metal surfaces appear to approximate very closely the idealized assumptions of the electromagnetic theory of light, the measured absorption coefficients here generally lie higher and the experimental ratios $(1 - \rho)/(1 - \rho_n)$ lie lower than those demanded by the theory. Evidently, the invisible oxide and water films, which always exist at room temperature, become appreciable here.

The directional distributions of the emission and absorption coefficients, like their absolute amounts, are also dependent on the emission and plate temperature (refs. 2 and 3).

For the directional distributions of the reflection coefficient ρ' it may, on the contrary, be assumed that these are affected only by the emission temperature of the incident radiation but not by the plate temperature, since the structure of the surface, which is independent of the temperature, occurs here as "material property."

As is customary in technical radiation exchange computations, we shall in the following paragraphs always assume gray radiators, for which the Kirchhoff law holds without restriction. Accordingly, no distinction is to be made between emission coefficient and absorption coefficient and in the problems of heat transfer we shall only speak of the "emission coefficient" $\epsilon = (1 - \rho)$. If the temperatures of the radiating surfaces differ considerably and their radiation properties are dependent on the temperature the choice of the values to be substituted for ρ and ϵ must be decided for each case. For one of the measured surfaces, for example, its found absorption coefficient is to be substituted as ϵ if at low body temperature (room temperature) it undergoes radiation exchange with a surface which has one of the emission temperatures that are employed.

16. Surface Element Model

The directional distributions of the reflections found were all determined in a purely empirical way. We now ask whether the results can also be explained by computation. Is there an elementary law for the reflection mechanism that leads to the obtained results?

The mathematical model described herein (the "surface element model") gives, with good approximation, the reflection behavior for surfaces that approximate the specular reflector and for directions of reflection that lie near the direction of the specular reflection. It is based on the laws of radiation optics and neglects the wave character of the heat radiation. We imagine the surface to be composed of small surface elements equal to irregularly arranged mirrors. A single one of these surface elements dF_α is, according to figure 23, assumed to have the surface normal n that makes an angle α with the surface normal of the reflector. The ray e arriving with incidence angle ν is specularly reflected by dF_α with reflection angles μ and ψ in the direction r; e and r make the angle β with the normal n; the reflection coefficient for the specular reflection that takes place is denoted by ρ_β, which may depend on β. The surface is assumed isotropic, that is, the distribution of the surface element does not depend on the angle γ; all angles γ are equally possible. With regard to their angle of inclination, the dF_α are distributed according to a distribution function $\Phi(\alpha)$ characteristic for the reflector under consideration. Let the part $dF(\alpha)$ of the surface F of the test plate considered have an angle of inclination that lies in the interval $\alpha \ldots \alpha + d\alpha$.

$$\Phi(\alpha) = \frac{dF(\alpha)}{F\, d\alpha} \tag{20}$$

Integration over all angles of inclination gives

$$\int_0^{\pi/2} \Phi \, d\alpha = 1$$

Of the incident energy stream per unit area E_ν, the amount reflected by the surface element with the normal direction α, γ in the interval $(d\alpha, d\gamma)$ is

$$dR = E_\nu \rho_\beta \underbrace{\Phi(\alpha) d\alpha}_{\substack{\text{Part of } dF_\alpha \\ \text{in integral } d\alpha}} \underbrace{\frac{d\gamma}{2\pi}}_{\substack{\text{Part of } dF_\alpha \\ \text{in integral } d\gamma}}$$

With the solid angle element

$$d\Omega = \sin \mu \, d\mu \, d\psi$$

the reflected energy stream per unit area and unit solid angle is

$$R_{\nu\mu\psi} = \frac{dR}{d\Omega}$$

and according to definition (5) in section 11 the reflection coefficient is

$$\rho' = \frac{2\pi}{E_\nu} \frac{dR}{\sin \mu \, d\mu \, d\psi}$$

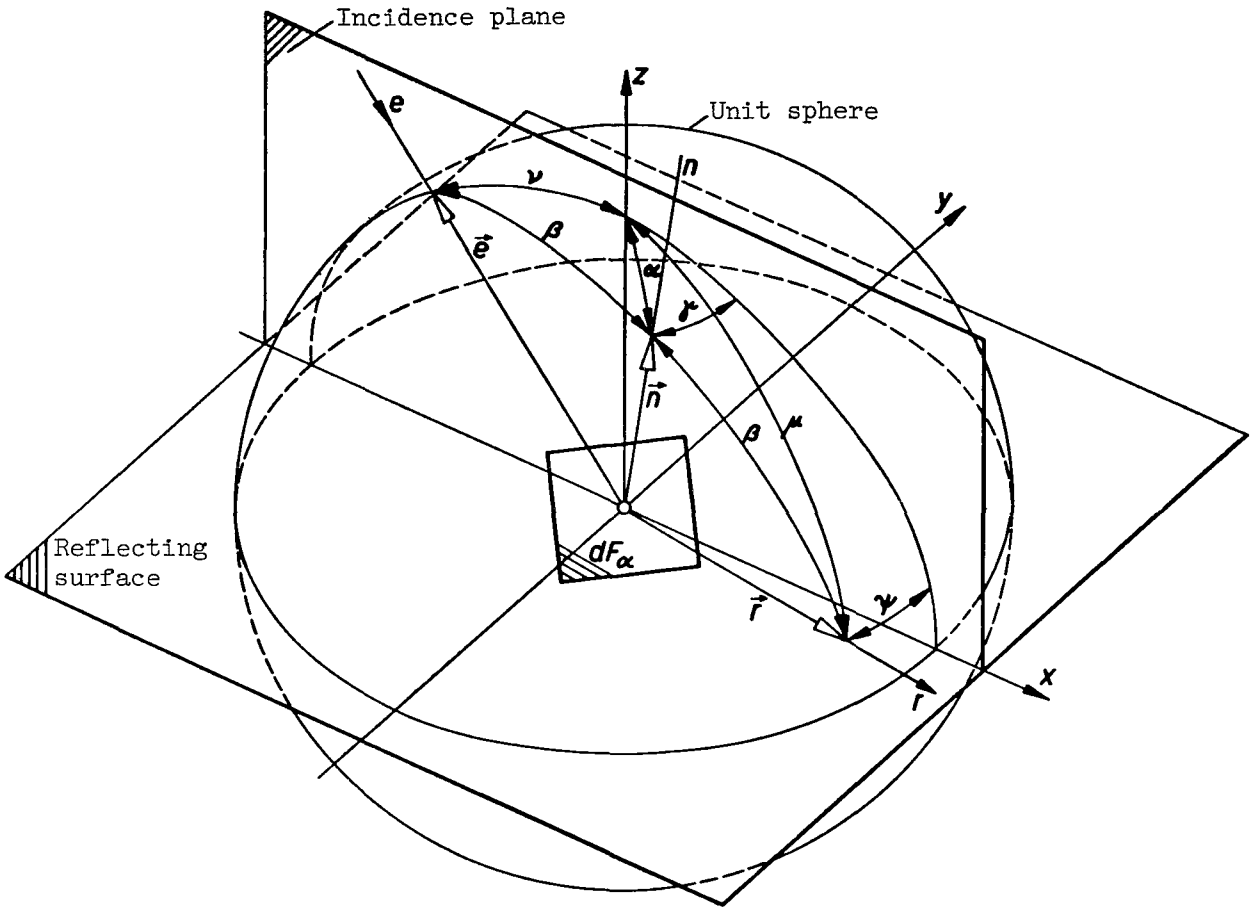

Figure 23. - Angle notations for surface element model.

With account taken of the expression for dR set up previously there is obtained for ρ':

$$\rho' = \frac{\Phi(\alpha)\rho_\beta}{\sin \mu} \frac{d\alpha \, d\gamma}{d\mu \, d\psi} \tag{21}$$

The functional determinant (Jacobian) Δ of the mapping of one coordinate system (μ, ψ) into the other system (α, γ) describes the relation between the two surface elements $d\mu \, d\psi$ and $d\alpha \, d\gamma$ as

$$\Delta = \begin{vmatrix} \frac{\partial \mu}{\partial \alpha} & \frac{\partial \mu}{\partial \gamma} \\ \frac{\partial \psi}{\partial \alpha} & \frac{\partial \psi}{\partial \gamma} \end{vmatrix} = \frac{d\mu \, d\psi}{d\alpha \, d\gamma} \tag{22}$$

In terms of equation (22) the expression for the reflection coefficient reads

$$\rho' = \frac{\Phi(\alpha)\rho_\beta}{\Delta \sin \mu} \tag{23}$$

To derive the relations between the introduced angles we substitute the three unit vectors $\vec{e}$, $\vec{r}$, and $\vec{n}$ in the directions e, r, and n, whose components in the (x,y,z) coordinate system are as follows:

Vector	x-Component	y-Component	z-Component
$\vec{e}$	$-\sin \nu$	0	$\cos \nu$
$\vec{r}$	$\sin \mu \cos \psi$	$\sin \mu \sin \psi$	$\cos \mu$
$\vec{n}$	$\sin \alpha \cos \gamma$	$\sin \alpha \sin \gamma$	$\cos \alpha$

From the condition of specular reflection the three vectors must lie in a plane. The vector $\vec{n}$ can therefore be presented as a linear combination of the other two. From figure 24 the relation can be read as:

$$\vec{e} + \vec{r} = 2 \cos \beta \vec{n} \tag{24}$$

taking account of the fact that $\vec{n}$ must be a unit vector. Equation (24), written in component form, gives the following system of equations:

$$\begin{aligned} -\sin \nu + \sin \mu \cos \psi &= 2 \cos \beta \sin \alpha \cos \gamma \\ \sin \mu \sin \psi &= 2 \cos \beta \sin \alpha \sin \gamma \\ \cos \nu + \cos \mu &= 2 \cos \beta \cos \alpha \end{aligned} \tag{25}$$

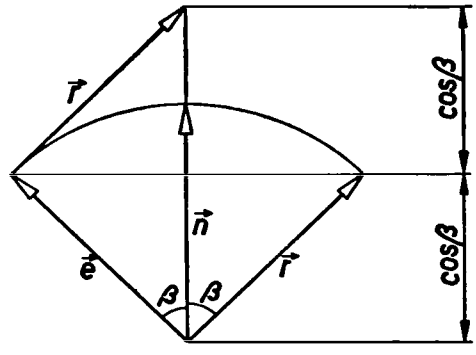

Figure 24. - Relations between three unit vectors.

From these three equations, β, μ, and ψ can be eliminated. The two terms $\sin \nu$ and $\cos \nu$ are first brought on the right side, the three relations are squared and added and there is obtained

$$\cos^2\beta - \cos \beta(\cos \alpha \cos \nu - \sin \alpha \sin \nu \cos \gamma) = 0$$

The case $\cos \beta = 0$ may be excluded since for $\beta = \pi/2$ the reflected ray must fall in the prolongation of the incident ray e and must go through the reflecting surface. The angle β is obtained as

$$\cos \beta = \cos \alpha \cos \nu - \sin \alpha \sin \nu \cos \gamma \tag{26}$$

From the third equation of equation (25) μ can now be computed as

$$\cos \mu = 2 \cos \alpha(\cos \alpha \cos \nu - \sin \alpha \sin \nu \cos \gamma) - \cos \nu \tag{27}$$

To eliminate ψ we bring the term $\sin \nu$ in the first equation of the system (25) on the right side, and then divide the second equation by the first equation so that,

$$\tan \psi = \frac{2 \sin \alpha \sin \gamma(\cos \alpha \cos \nu - \sin \alpha \sin \nu \cos \gamma)}{2 \sin \alpha \cos \gamma(\cos \alpha \cos \nu - \sin \alpha \sin \nu \cos \gamma) + \sin \nu} \tag{28}$$

The functional determinant Δ is to be determined according to equation (22) with the aid of transformation formulas (27) and (28). We consider first the special case of the incident radiation normal to the surface. The normal incidence is distinguished by $\nu = 0$, that is, $\cos \nu = 1$ and $\sin \nu = 0$. The relations (26) to (28) then simplify to:

$$\left.\begin{aligned} \cos \beta &= \cos \alpha; & \beta &= \alpha \\ \cos \mu &= 2 \cos^2\alpha - 1 = \cos 2\alpha; & \mu &= 2\alpha \\ \tan \psi &= \tan \gamma; & \psi &= \gamma \end{aligned}\right\} \tag{29}$$

The functional determinant Δ assumes the value

$$\Delta = \begin{vmatrix} 2 & 0 \\ 0 & 1 \end{vmatrix} = 2$$

If we restrict ourselves with the approximation

$$\sin \mu = \sin 2\alpha \approx 2\alpha$$

to small deflection angles α, that is, to directions that are not far removed from the direction of specular reflection, the reflection coefficient is obtained as

$$\rho' = \frac{\Phi(\alpha)\rho_\beta}{4\alpha} \tag{30}$$

In the general case of $\nu \neq 0$ we introduce further approximations to simplify the computation. Since the surface element model can be used only for directions in the neighborhood of the specular reflection, we again assume the angle α to be small:

$$\left.\begin{aligned} &\sin \alpha \approx \alpha \\ &\cos \alpha \approx 1 \\ \alpha^2 \ll 1 \qquad &\text{therefore} \qquad \alpha^2 \approx 0 \end{aligned}\right\} \tag{31}$$

Expressions (26) to (28) now become:

$$\left.\begin{aligned} \cos \beta &= \cos \nu - \alpha \sin \nu \cos \gamma \\ \cos \mu &= \cos \nu - 2\alpha \sin \nu \cos \gamma \end{aligned}\right\} \tag{32}$$

$$\tan \psi = \frac{2\alpha \sin \gamma (\cos \nu - \alpha \sin \nu \cos \gamma)}{2\alpha \cos \gamma \cos \nu + \sin \nu} \tag{33}$$

We assume further that we are situated neither in the neighborhood of glancing incidence (ν close to 90°) nor in the neighborhood of normal incidence (ν small), so that we may assume $\alpha \ll \sin \nu$ and $\alpha \ll \cos \nu$. For small deflection angles α and $\nu \neq 0$, ψ also becomes small so that the tangent may be replaced by the arc. Relation (33) then further simplifies to

$$\psi = 2\alpha \sin \gamma \cot \nu \tag{34}$$

With the transformation formulas (32) and (34) the partial derivatives of μ and ψ with respect to α and γ are obtained as

$$\frac{\partial \mu}{\partial \alpha} = \frac{2 \sin \nu \cos \gamma}{\sin \mu}$$

$$\frac{\partial \mu}{\partial \gamma} = -\frac{2\alpha \sin \nu \sin \gamma}{\sin \mu}$$

$$\frac{\partial \psi}{\partial \alpha} = 2 \sin \gamma \cot \nu$$

$$\frac{\partial \psi}{\partial \gamma} = 2\alpha \cos \gamma \cot \nu$$

and the functional determinant becomes

$$\Delta = \frac{4\alpha \cos \nu}{\sin \nu}$$

Substituted into equation (23), this gives the expression for the reflection coefficient as,

$$\rho' = \frac{\Phi(\alpha)\rho_\beta}{4\alpha \cos \nu} \tag{35}$$

which for $\nu = 0$, goes over into the formula (30) for normal incidence. Therefore, it is to be expected that the approximation formula (35) fails only in the neighborhood of glancing incidence.

The validity of the surface element model was tested on the two surfaces of the anodically oxidized and sand blasted anticorodal, that is, for two surfaces that closely approximate the specular reflector. If α is assumed to be small, β moves according to the first equation of equations (32) in narrow limits and the reflection coefficient ρ_β can be replaced by the constant value ρ_ν that depends only on the incidence angle. From the measurements the following expression is to be determined:

$$\Phi(\alpha)\rho_\nu = 4\alpha\rho' \cos \nu$$

and plotted for each incidence angle as a function of the angle of inclination α. The surface element model may be considered as valid if the various curves can be brought into coincidence through a normalization, by substituting, for example, the ratios ρ_ν/ρ_{45} of the reflection coefficients so that the curves of $\Phi(\alpha)\rho_{45}$ recomputed for all incidence angles coincide with the curve for $\nu = 45^\circ$. As can be seen from figures 25 and 26, this occurs for the two surfaces considered. The check is here restricted to angles of inclination α up to 12° at most, for which the introduced approximations of formulas (31) may still be substituted. The points for the incidence angle 60° scatter somewhat more strongly than the others because the simplifications assumed at the basis of the theory are no longer admissible in the neighborhood of glancing incidence. Each of the two surfaces has its own $\Phi(\alpha)$ distribution. The ratios ρ_ν/ρ_{45} of the reflection coefficients valid for the two test plates are as follows:

Anodically oxidized, anticorodal:

$\nu =$	30°	45°	60°
$\frac{\rho_\nu}{\rho_{45}} =$	1.294	1	0.825

Sandblasted, anticorodal:

$\nu =$	10°	30°	45°	60°
$\frac{\rho_\nu}{\rho_{45}} =$	1.258	1.091	1	0.916

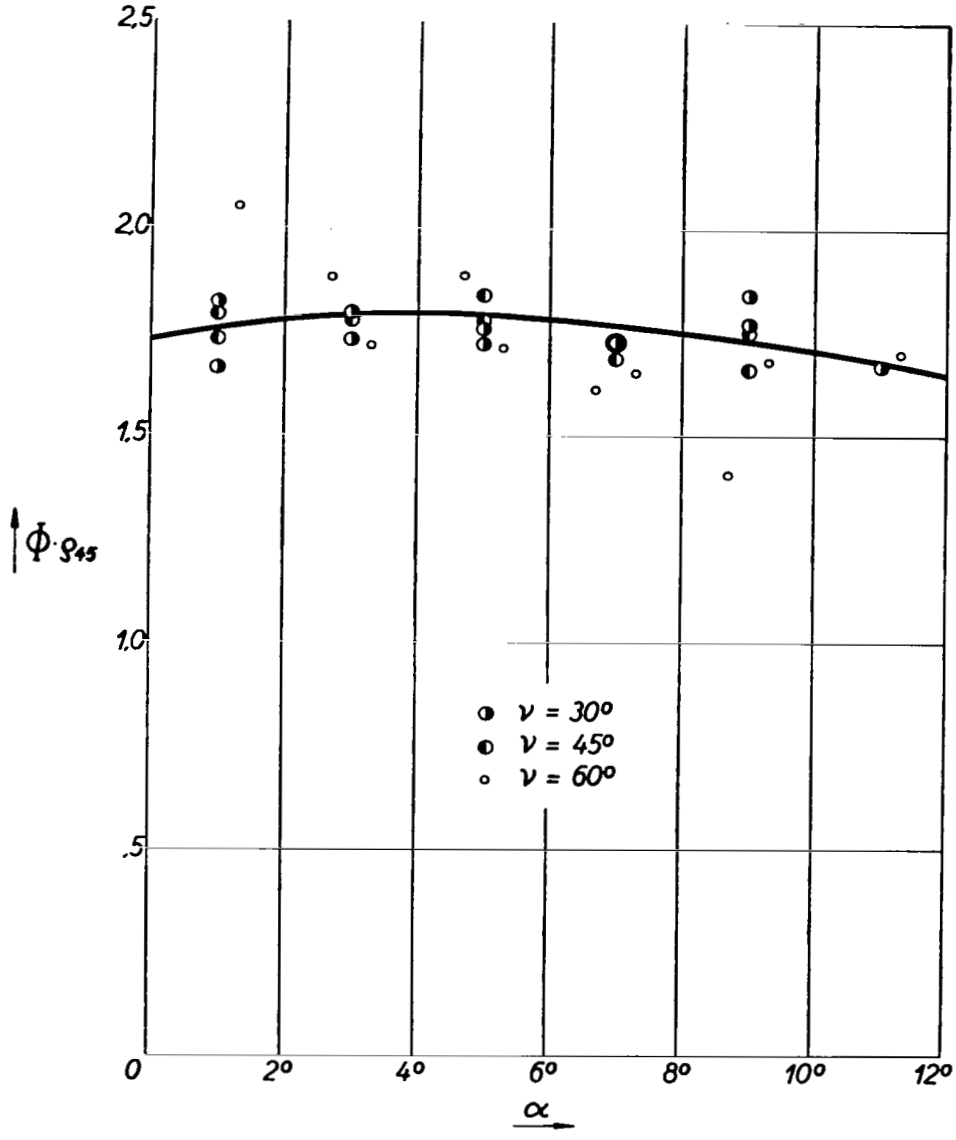

Figure 25. - Distribution of surface elements for anodically oxidized anticorodal.

The surface element model gives a good idea of the directional distribution of the reflection coefficients in the neighborhood of the direction of the specular reflection. According to formula (35) the distribution of ρ' is rotationally symmetrical with the direction of the specular reflection as axis of symmetry.

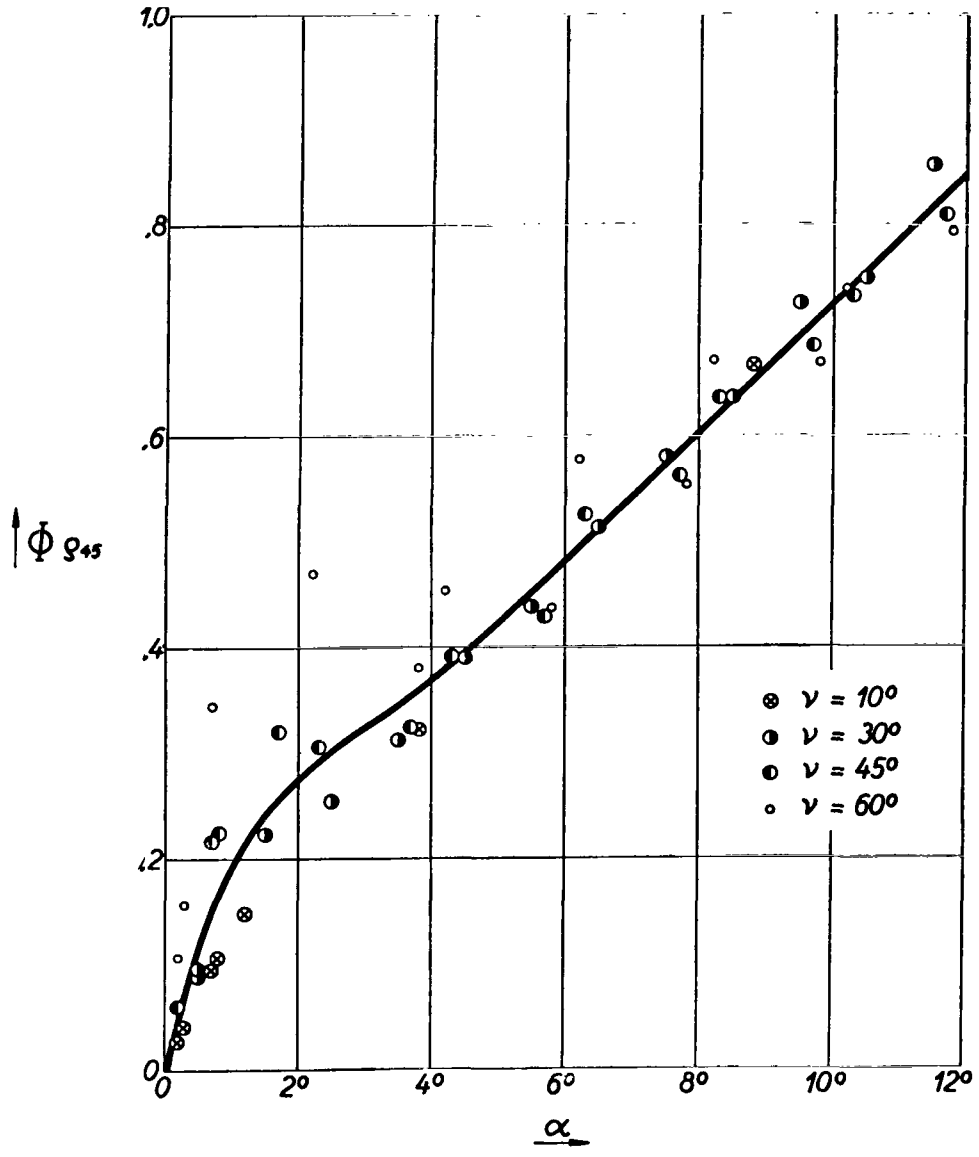

Figure 26. - Distribution of surface elements for sandblasted anticorodal.

2. HEAT TRANSFER FOR TWO-SURFACE SYSTEM

21. Definition of Two-Surface System, Assumptions for Computation

With the aid of the illustrative data gained on the directional distribution of the reflection coefficients we now turn to the computation of the heat transfer, taking account of the reflections. With the exception of a few considera-

tions in section 4, we shall restrict ourselves to the case of two surfaces that exchange radiation with each other. Each of these two surfaces is assumed to have the same temperature and the same radiation properties (emission and reflection coefficients) at each point. In regard to the geometrical arrangement of the surfaces, which in general are curved, we assume that from each element of the one surface only parts of the two surfaces F_1 and F_2 can be seen. Thus, F_1 and F_2 form a closed system with regard to the radiation exchange. We shall term a system with the properties just described as a two-surface system. The two surfaces may meet at a boundary line (fig. 27(a)) or be spatially separated from each other (fig. 27(b)).

The computation of the heat transfer in the case of the two-surface system cannot be accurately carried out except for a few geometrically simple cases. We are forced to make approximating assumptions.

Except for polished metals, almost all surfaces have a directional distribution of the emissions, which does not deviate strongly from the Lambert cosine law. We shall therefore always assume this law for the emission, but we shall take into account the directional distribution of the reflections. The following theory is also valid, however, without the assumption of the Lambert cosine law if in place of the solid angle ratio φ, there is substituted an incident radiation beam that is to be determined from the emission law and the geometrical arrangement.

Each emitted amount of energy is first reflected on one of the two surfaces of the two-surface system and then reflected, each time more weakly, a second time, a third time, and so forth. The first reflections contribute most of the energy. We shall make the assumption that the second, third, and further reflections are locally and directionally distributed in the same manner as the first.

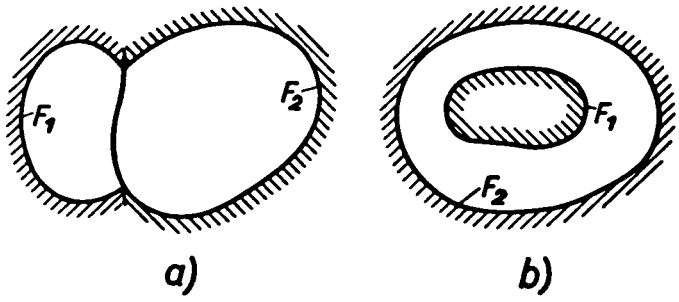

Figure 27. - Examples of two-surface systems.

22. Condition from Second Fundamental Law of Thermodynamics

Let the surface F_1 of a two-surface system have the temperature T_1. According to the Stefan-Boltzmann law the emitted radiation energy of the surface F_1 and all the resulting reflection energies are proportional to $(T_1/100)^4$. The same condition holds for the surface F_2. The exchanged heat quantity per unit time can first be expressed in the form

$$Q_{12} = k_1\left(\frac{T_1}{100}\right)^4 - k_2\left(\frac{T_2}{100}\right)^4$$

The second fundamental law of thermodynamics requires the vanishing of Q_{12} if the temperatures T_1 and T_2 are equal; therefore,

$$k_1 = k_2 = k$$

The radiation energy exchanged between the two surfaces of the two-surface system may therefore always be written in the form

$$Q_{12} = k\left[\left(\frac{T_1}{100}\right)^4 - \left(\frac{T_2}{100}\right)^4\right] \tag{36}$$

23. Beam Coefficient, Solid Angle Ratio and Reflection Factor

The surface F_1 of a two-surface system emits the radiation energy

$$q_1 = F_1 C_s \epsilon_1 \left(\frac{T_1}{100}\right)^4 \tag{37}$$

Of this amount the fraction $q_1\varphi_{12}$ strikes the surface F_2 while $q_1\varphi_{11}$ returns to the surface F_1. The two coefficients φ_{12} and φ_{11} are termed the beam coefficients of the surface F_1 with respect to F_2 and F_1, and depend both on the geometry of the two-surface system and on the directional distribution of the emissions of the first surface. Similarly the beam coefficients φ_{21} and φ_{22} are defined. The energy stream q_1, according to the definition of the two-surface system, is divided between the two surfaces F_1 and F_2. The beam coefficients φ_{11} and φ_{12} and similarly φ_{21} and φ_{22} satisfy the relations

$$\left.\begin{aligned} \varphi_{11} + \varphi_{12} &= 1 \\ \varphi_{21} + \varphi_{22} &= 1 \end{aligned}\right\} \tag{38}$$

According to our assumptions the two surfaces of the system emit according to the Lambert cosine law. The coefficients are therefore identical with the solid angle ratios that can be determined from the relation

$$\varphi_{12} = \frac{1}{F_1} \int_{F_1} \int_{F_2} \frac{\cos \nu_1 \cos \nu_2}{\pi r^2} \, dF_1 \, dF_2 \tag{39}$$

where F_1 and F_2 denote the surface areas of the two-surface system, r is the distance between the two surface elements dF_1 and dF_2 under consideration (fig. 28) and ν_1 and ν_2 are the angles between r and the surface normals n_1 and n_2.

On interchanging the indices in equation (39) the expression of the double integral remains unchanged. For the solid angle ratios φ_{12} and φ_{21}, the following relation therefore holds, so that

$$F_1 \varphi_{12} = F_2 \varphi_{21} \tag{40}$$

which is not true for generally defined beam coefficients. If φ denotes a general beam coefficient the theory of this section remains valid until equation (40) is introduced into the equation.

The surface F_2 absorbs the fraction $q_1 \varphi_{12} \epsilon_2$ from the energy stream $q_1 \varphi_{12}$ radiated by the surface F_1 while an amount $q_1 \varphi_{12} \rho_2$ is reflected. The part $q_1 \varphi_{12} \rho_2 f_{121}$ again reaches the surface F_1, and the part $q_1 \varphi_{12} \rho_2 f_{122}$ reaches the surface F_2. The reflection coefficient or reflection factor f_{121} gives that fraction of the energy stream reflected on the surface F_2 that is reflected back on the surface F_1 under the assumption that the reflection is produced by a beam from the surface F_1. It depends on the geometry of the two-surface system, on the directional distribution of the emissions of both surfaces and on the directional distribution of the reflections of the reflecting surface. The middle index j of the reflection factor f_{ijk} denotes the surface j (in the case of the two-surface system 1 or 2) whose reflections are being considered, the first index i gives information on the source of the incident energy stream that gave rise to these reflections, while the last index k gives the "address" to which the reflected part under consideration arrives. In the case of the two-surface system 8 such reflecting coefficients occur. Since the reflections of a surface can only be thrown back to the two surfaces F_1 and F_2 each two coefficients whose indices agree in the first two numbers add up to 1:

$$\left.\begin{aligned} f_{111} + f_{112} &= 1 \\ f_{121} + f_{122} &= 1 \\ f_{211} + f_{212} &= 1 \\ f_{221} + f_{222} &= 1 \end{aligned}\right\} \tag{41}$$

In general it is not immaterial whence the reflected radiation originates, that is

$$f_{121} \neq f_{221}, \qquad \text{and so forth}$$

In general, the reflection factors for the second, third, and further reflections do not agree with those that determine the distribution of the first reflections. In accordance with the approximation stated in section 21, in considering the second, third, and further reflections the same reflection coefficients are substituted that hold for the first reflection stages.

24. Heat Transfer for Two-Surface System

With the aid of the introduced notations the radiation exchange process may now be further investigated. Scheme I shows the splitting up of an energy q_1 emitted from a surface F_1 in the first and second reflection. Scheme II would have to be supplemented by adding a second scheme at the same stage with interchanged indices and serves for investigating an (i+1)th reflection starting out from the surface F_1 to the (i+2)th. As an end result we are interested in the heat quantity per unit time, which on the basis of the emission q_1 of the surface F_1, is transferred to the surface F_2. This quantity is obtained by summing all energy streams that are absorbed on the surface F_2. As shown by the two schemes, this sum is made up of the amount $q_1\varphi_{12}\epsilon_2$ absorbed after the emission and of the summation of amounts $p_{12}^{(i)}$ and $p_{22}^{(i)}$ reflected by F_2, multiplied by the factor ϵ_2/ρ_2, so that

$$Q_1 = q_1\varphi_{12}\epsilon_2 + \frac{\epsilon_2}{\rho_2}\left[\sum_{i=1}^{\infty} p_{12}^{(i)} + \sum_{i=1}^{\infty} p_{22}^{(i)}\right]$$

With the definition

$$\left.\begin{aligned} S_{11} &= \sum_{i=1}^{\infty} p_{11}^{(i)} \\ S_{12} &= \sum_{i=1}^{\infty} p_{12}^{(i)} \\ S_{21} &= \sum_{i=1}^{\infty} p_{21}^{(i)} \\ S_{22} &= \sum_{i=1}^{\infty} p_{22}^{(i)} \end{aligned}\right\} \qquad (42)$$

Q_1 may be written in the form

$$Q_1 = q_1\varphi_{12}\epsilon_2 + \frac{\epsilon_2}{\rho_2}(S_{12} + S_{22}) \tag{43}$$

The sums S_{12} and S_{22} must be computed first. The recursion formulas for the amounts p_{ik} are shown on scheme II.

$$\left.\begin{aligned} p_{11}^{(i+1)} &= p_{11}^{(i)} f_{111}\rho_1 + p_{21}^{(i)} f_{211}\rho_1 \\ p_{12}^{(i+1)} &= p_{11}^{(i)} f_{112}\rho_2 + p_{21}^{(i)} f_{212}\rho_2 \\ p_{21}^{(i+1)} &= p_{12}^{(i)} f_{121}\rho_1 + p_{22}^{(i)} f_{221}\rho_1 \\ p_{22}^{(i+1)} &= p_{12}^{(i)} f_{122}\rho_2 + p_{22}^{(i)} f_{222}\rho_2 \end{aligned}\right\} \tag{44}$$

We consider each of the relations (44) written with successive index i. Adding these formulas, there is obtained from each recursion formula one of the four following linear equations for determining the sums S_{jk}:

$$\left.\begin{aligned} S_{11} - p_{11}^{(1)} &= S_{11} f_{111}\rho_1 + S_{21} f_{211}\rho_1 \\ S_{12} - p_{12}^{(1)} &= S_{11} f_{112}\rho_2 + S_{21} f_{212}\rho_2 \\ S_{21} - p_{21}^{(1)} &= S_{12} f_{121}\rho_1 + S_{22} f_{221}\rho_1 \\ S_{22} - p_{22}^{(1)} &= S_{12} f_{122}\rho_2 + S_{22} f_{222}\rho_2 \end{aligned}\right\} \tag{45}$$

The first terms $p_{jk}^{(1)}$ of the sums S_{jk} are obtained from scheme I:

$$\left.\begin{aligned} p_{11}^{(1)} &= q_1\varphi_{11} f_{111}\rho_1^2 \\ p_{12}^{(1)} &= q_1\varphi_{11} f_{112}\rho_1\rho_2 \\ p_{21}^{(1)} &= q_1\varphi_{12} f_{121}\rho_1\rho_2 \\ p_{22}^{(1)} &= q_1\varphi_{12} f_{122}\rho_2^2 \end{aligned}\right\} \tag{46}$$

The solution of the system of linear equations (45) requires a tedious computation but otherwise offers no difficulties. Therefore, the results for the expression $S_{12} + S_{22}$ may be given immediately. With the abbreviated notation

$$N = (1 - f_{111}\rho_1)(1 - f_{222}\rho_2) - \rho_1\rho_2(f_{112}\rho_1 + f_{212} - f_{212}\rho_1)(f_{221}\rho_2 + f_{121} - f_{121}\rho_2) \tag{47}$$

this expression reads, with account taken of relations (41):

$$\frac{(S_{12} + S_{22})N}{\varphi_{12}\rho_2 q_1} = \rho_2 f_{122}(1 - f_{111}\rho_1) + (1 - f_{222}\rho_2 + f_{122}\rho_2)\frac{\varphi_{11}f_{112}}{\varphi_{12}}\rho_1$$

$$- \rho_1\rho_2(f_{112}\rho_1 + f_{212} - f_{212}\rho_1)(f_{221}\rho_2 + f_{121} - f_{121}\rho_2)$$

We write Q_1 in the form

$$Q_1 = q_1\varphi_{12}\epsilon_2 K_1 = F_1\varphi_{12}C_s\epsilon_1\epsilon_2\left(\frac{T_1}{100}\right)^4 K_1$$

where the correction factor K_1, according to equation (43), assumes the value

$$K_1 = 1 + \frac{S_{12} + S_{22}}{q_1\varphi_{12}\rho_2}$$

After a few further elementary transformations, taking account of equations (38), (41), and (47), there is obtained for K_1:

$$K_1 = \frac{1}{N}\left[1 + \rho_2(f_{122} - f_{222})\right]\left[1 + \rho_1\left(\frac{\varphi_{11}f_{112}}{\varphi_{12}} - f_{111}\right)\right] \tag{48}$$

and in analogous manner, if F_2 is assumed as the emitting surface, by interchanging the indices, the heat transfer

$$Q_2 = q_2\varphi_{21}\epsilon_1 K_2 = F_2\varphi_{21}C_s\epsilon_1\epsilon_2\left(\frac{T_2}{100}\right)^4 K_2$$

$$K_2 = \frac{1}{N}\left[1 + \rho_1(f_{211} - f_{111})\right]\left[1 + \rho_2\left(\frac{\varphi_{22}f_{221}}{\varphi_{21}} - f_{222}\right)\right] \tag{49}$$

If both surfaces of the system are emitting, the amount of heat transferred from F_1 to F_2 per unit time

$$Q_{12} = Q_1 - Q_2$$

must, according to the condition derived in section 22 from the second law of thermodynamics, be capable of being presented in the form of equation (36). Accordingly, the expressions for Q_1 and Q_2 must agree except for the factor $(T/100)^4$. At this point we shall introduce the assumption of the Lambert cosine law for the directional distribution of the emissions and, therefore, relation (40) in the computation. Except for the factor with the temperature T_1 or T_2, the agreement of the expressions for Q_1 and Q_2 exists if K_1 and K_2 coincide. This, as the comparison of equations (48) and (49) shows, is not in general the case because the approximating assumption according to which the second, third, and further reflections are distributed locally, and with respect to their directions in the same way as the first reflection, contradicts the second law of thermodynamics. The validity of the second law is theoretically an exact requirement. We postulate, therefore, the equality of K_1 and K_2 and through comparison of the formulas (48) and (49) we obtain the relations

$$\left.\begin{aligned} \varphi_{11} f_{112} &= \varphi_{12} f_{211} \\ \varphi_{22} f_{221} &= \varphi_{21} f_{122} \end{aligned}\right\} \tag{50}$$

which connect four of the eight reflection factors with the solid angle ratios. The reflection factors are, however, already determined by the assumed reflection laws and do not in general satisfy the conditions of equation (50). The failure to agree is connected with the error that is committed in the chosen approximation and vanishes if the second, third, and further reflections are actually distributed like the first. Of the eight reflection factors of the two-surface system, four can be eliminated with the aid of equations (41). We make the assumption that two of the remaining four unknowns, namely, f_{121} and f_{212}, are determined with the aid of the reflection law, while the last two are to be determined from equations (50). Their value does not agree with those that would be obtained according to the direct determination from the reflection law. The deviations correspond to the error of the approximation and make small corrections to the reflection factors necessary so that the approximating assumption made is compatible with the condition from the second law of thermodynamics. The radiant energy exchanged between the two surfaces of the system is finally obtained as

$$Q_{12} = F_1 \varphi_{12} C_s \epsilon_1 \epsilon_2 K \left[\left(\frac{T_1}{100} \right)^4 - \left(\frac{T_2}{100} \right)^4 \right] \tag{51}$$

with the factor K, taking account of equation (41):

$$K = \frac{\left[1 - \rho_1 (f_{212} - f_{112})\right]\left[1 - \rho_2 (f_{121} - f_{221})\right]}{(1 - f_{111}\rho_1)(1 - f_{222}\rho_2) - \rho_1 \rho_2 (f_{112}\rho_1 + f_{212} - f_{212}\rho_1)(f_{221}\rho_2 + f_{121} - f_{121}\rho_2)} \tag{52}$$

K has the significance of a correction factor to be applied to the Nusselt approximation. Its value represents the effect of the reflections on the heat exchange.

25. Two-Surface System with Convex Surface F_1

The computation of the heat exchange is considerably simplified if one of the two surfaces of the system, for example F_1, is convex. The emitted and reflected radiation from the convex surface F_1 excusively reach the surface F_2. Half of the solid angle ratios and reflection factors are therefore given without further computation:

$$\left.\begin{aligned} \varphi_{11} &= f_{111} = f_{211} = 0 \\ \varphi_{12} &= f_{112} = f_{212} = 1 \end{aligned}\right\} \tag{53}$$

The relation (40) between the solid angle ratios goes over into

$$\varphi_{21} = \frac{F_1}{F_2} \tag{54}$$

and, therefore, the computational determination of a solid angle ratio from the geometry of the two-surface system becomes superfluous. Of the conditions (50) the first condition becomes trivial. The radiation energy exchanged between the two surfaces is

$$Q_{12} = F_1 C_s \epsilon_1 \epsilon_2 K \left[\left(\frac{T_1}{100}\right)^4 - \left(\frac{T_2}{100}\right)^4\right] \tag{55}$$

with the correction factor as compared with the Nusselt approximation:

$$K = \frac{1 - \rho_2(f_{121} - f_{221})}{1 - f_{222}\rho_2 - \rho_1\rho_2(f_{221}\rho_2 + f_{121} - f_{121}\rho_2)} \tag{56}$$

26. Reflection Laws

The preceding computations do not contain assumptions in regard to the law of reflection that must be used to determine the reflection factors. The determination of the reflection factors on the basis of the empirically obtained reflection laws, that is, with the aid of the measured directional distributions of the reflection coefficient ρ', involves an almost insurmountable amount of computation which - except perhaps for several geometrically simple cases - makes this process appear unsuitable.

Another process leads more simply to the goal: We assume mathematically simple reflection laws as the basis of the computation of the reflection factors and, hence, of the radiation exchange. The obtained results, or rather the reflection factors arising from the reflection laws, can be superposed in order to attain as good an approximation as possible to the actual situation. In the two following sections (3 and 4), two reflection laws are more closely investigated.

The first law is the law of specular reflection; the corresponding surfaces are termed specular reflectors. The law states: If radiation energy falls on a specularly reflecting surface at the incidence angle ν, the nonabsorbed energy stream is reflected entirely in the incidence plane ($\psi = 0$), and with the angle of reflection $\mu = \nu$.

The counterpart of the specular reflection is a reflection law that prescribes a directional distribution for the reflection coefficients, that is independent of the direction of the incident ray, and therefore represents the most extreme case of a strongly scattering diffuse reflector. This is most simply realized mathematically through the law of Lambert reflection, which assumes the reflections to be distributed according to the Lambert cosine law. These reflections may now computationally be treated like emissions. A surface that reflects according to the Lambert cosine law is termed a Lambert reflector.

Specular reflectors occur in nature, for example, as polished metal surfaces. The Lambert reflector on the contrary is an ideal picture which, it is true, is very nearly approximated by the planed and polished white pine board, but which however (as is to be concluded from the measurements), is not quite actually realized. The two chosen reflection laws represent the extremes between which the measured directional distributions of the reflection factors can be ordered. From superposition of their reflection factors results may be expected, which with good approximation, give the heat exchange by radiation.

3. SPECULAR REFLECTION

The following computations of the reflection factors for both surfaces of the two-surface system are based on the law of specular reflection according to which, of the radiation energy E_ν incident at the angle ν, the nonabsorbed energy stream $E_\nu \rho_\nu$ is reflected with the angles of reflection $\mu = \nu$ and $\psi = 0$. In addition to the reflection law the assumed emission law, namely the Lambert cosine law, which is assumed valid for the two surfaces, enters in the reflection factors.

The surface F_1 of a two-surface system is assumed to send out rays in all directions, which may be combined in purely parallel beams. According to the Lambert cosine law of the emission all these beams have the same intensity over their cross section. In the visible region it would be observed that the surface F_1 radiates at each point and from all directions with equal brightness. We now consider specifically an emission direction R (fig. 29). The rays emitted from F_1 and specularly reflected on F_2 partly return to the surface F_1 and partly reach F_2. The proportion of all the rays of the beam that return to the surface F_1 is equal to the ratio of the cross section of the part of the beam reflected toward F_1 to that of the entire beam and is termed the direction-dependent reflection factor f'_{121}, which is coordinated with the direction R. The reflection factor f_{121} is obtained from it - as an averaged value - through integration over all directions of space, so that:

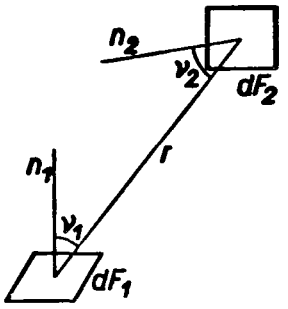

Figure 28.

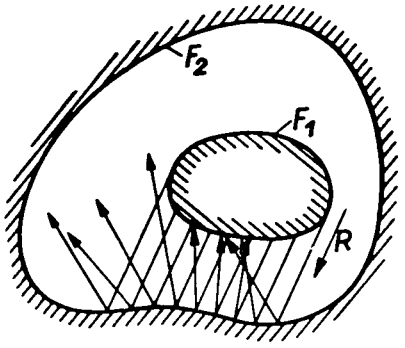

Figure 29.

$$f = \frac{1}{4\pi} \int f' \left(\frac{F_B}{F_m} \right) d\Omega \tag{57}$$

In equation (57) f' denotes a direction-dependent reflection factor and f its corresponding averaged reflection factor, F_B is the cross section of the bundle of rays in the direction R and F_m is the cross section of the bundle averaged over all directions of space according to:

$$F_m = \frac{1}{4\pi} \int F_B \, d\Omega \tag{58}$$

In the case of a configuration with rotational symmetry all planes through the axis of rotation are equivalent and the different directions of the space can

be characterized by a single direction angle, namely, the angle γ between the axis of symmetry and the direction R. The integral (57) simplifies to

$$f = \frac{1}{2}\int_0^{\pi} f'\left(\frac{F_B}{F_m}\right)\sin\gamma\, d\gamma \tag{59}$$

If a two-surface system consists of two general cylindrical or prism surfaces extending to infinity with parallel generatrices, all planes at right angles to the generatrices are equivalent, and we speak of a two-dimensional problem. The direction R can be fixed through an angle of rotation γ and the integral (57) goes over into the form

$$f = \frac{1}{2\pi}\int_0^{2\pi} f'\left(\frac{F_B}{F_m}\right)d\gamma \tag{60}$$

The reflections can be followed along in the projection of the system on a plane normal to the generatrices, since the law of specular reflection for rays that are oblique to the projection plane also holds for their projections.

In sections 31 to 34, four examples of two-surface systems are considered. Surface F_1 is a spherical or circular cylindrical surface, hence, convex, and therefore only one reflection factor (f_{121}) need be determined, on the basis of the reflection law. Further, the cross section of a parallel beam of rays issuing from F_1 is constant and therefore coincides with the averaged cross section F_m. The ratio F_B/F_m is equal to 1 for all directions of space. The computation of the direction-dependent reflection factors f'_{121} is conducted analytically in several cases, and in the other cases with the methods of projective geometry. The latter method, in the case of geometrically involved arrangements, is probably the only possible method.

31. Sphere and Plane Wall

A sphere, representing the surface F_1 of a two-surface system, exchanges radiation with a plane wall. The second surface F_2 encompasses both the wall and the infinite half-space above it. The center of the sphere is $d = \delta R$ distance from the wall (fig. 30).

We first compute the direction-dependent reflection factor f'_{121}. The problem is rotationally symmetrical, with the normal to the wall surface through the center of the sphere as axis of symmetry. A beam of rays starting out from the sphere with the direction angle γ (indicated in fig. 31 by the three rays s_1, s_2, and s_3) has a circular cross section and is thrown back by the wall as

a parallel beam with constant intensity and equal cross section (rays s_1', s_2', and s_3'). The sphere extends into the reflected beam by the amount a, which through elimination of the distances $\overline{CM}$ to $\overline{MA}$, is obtained from the following six equations:

$$a = R - \overline{CM} \qquad \overline{CM} = \overline{MB} \sin\gamma$$

$$\overline{MB} = R\delta - \overline{EB} \qquad \overline{EB} = \overline{EA}$$

$$\overline{EA} = \overline{MA} - R\delta \qquad R = \overline{MA} \sin\gamma$$

which can be easily read off from figure 31, so that

$$a = 2R(1 - \delta \sin\gamma) \tag{61}$$

The sphere intercepts the hatched part in figure 32 from the reflected beam, and the direction-dependent reflection factor $f'_{121}(\gamma)$ is equal to the ratio of the hatched area to the total area of the circle πR^2. Half the hatched area is the area of a circular segment with half the central angle ζ and is equal to

$$F_s = R^2(\zeta - \sin\zeta \cos\zeta)$$

from which the reflection factor is obtained as

$$f'_{121} = \frac{2F_s}{\pi R^2} = \frac{2}{\pi}(\zeta - \sin\zeta \cos\zeta)$$

In the preceding expression the angle ζ is to be replaced by γ. The relation

$$\cos\zeta = \delta \sin\gamma$$

is obtained by formulating $\cos\zeta$ and then eliminating a and R with the relation (61).

The reflection factor f_{121} averaged over all directions is found by evaluating the integral (59), which in our example assumes the form

$$f_{121} = \frac{1}{\pi}\int_0^{\gamma^*} \left[\arccos(\delta \sin\gamma) - \delta \sin\gamma\sqrt{1 - \delta^2 \sin^2\gamma}\right]\sin\gamma \, d\gamma \tag{62}$$

As upper integration limit there is to be put

$$\gamma^* = \arcsin\frac{1}{\delta}$$

and not π since for direction angles $\gamma > \gamma^*$, the reflected bundle of rays no longer strike the sphere and hence the direction-dependent reflection factor vanishes. The reflection factor f_{121} is a function of the nondimensional distance δ.

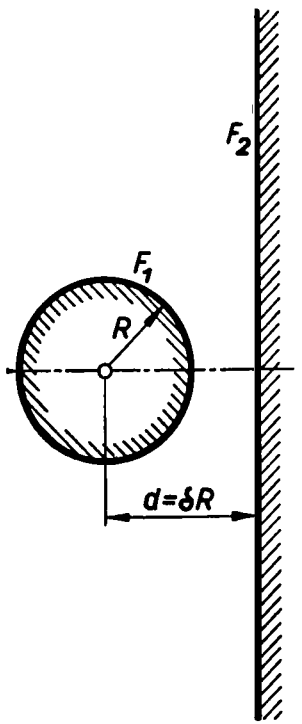

Figure 30.

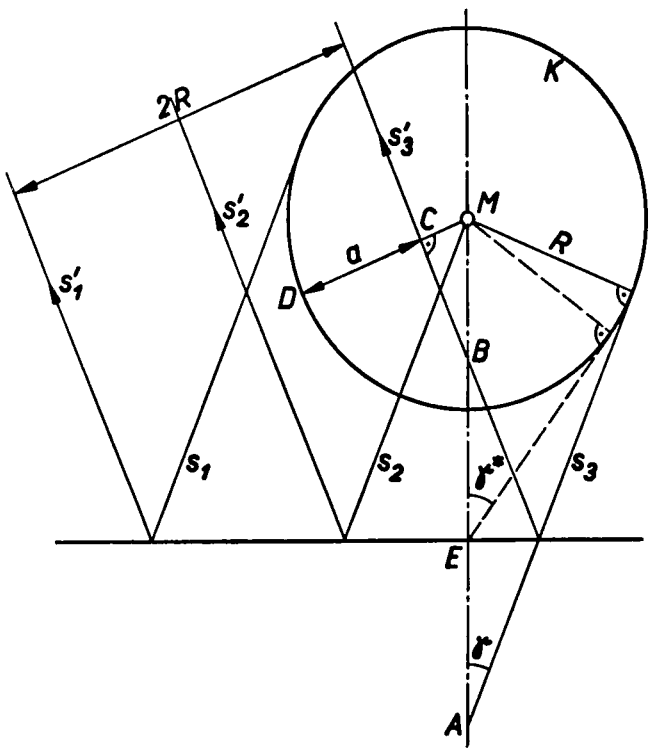

Figure 31.

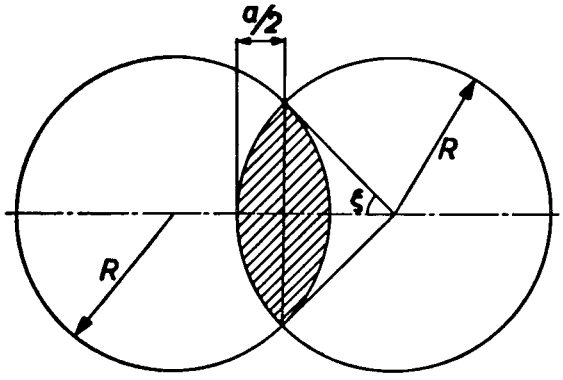

Figure 32.

We consider first the special case $\delta = 1$ for which the integral (62) is considerably simplified:

$$f_{121}(\delta = 1) = \frac{1}{\pi} \int_0^{\pi/2} \left(\frac{\pi}{2} - \gamma - \sin \gamma \cos \gamma \right) \sin \gamma \, d\gamma$$

The integration can be carried out in an elementary way and gives the result

$$f_{121}(\delta = 1) = \frac{1}{2} - \frac{4}{3\pi} \approx 0.0756$$

In the general case we remove the arc cos function in the first summand of the integrand by partial integration:

$$f_{121} = \frac{1}{\pi} \left[\frac{\pi}{2} - \delta \int_0^{\arcsin 1/\delta} \frac{\cos^2 \gamma}{\sqrt{1 - \delta^2 \sin^2 \gamma}} \, d\gamma \right.$$

$$\left. - \delta \int_0^{\arcsin 1/\delta} \sin^2 \gamma \sqrt{1 - \delta^2 \sin^2 \gamma} \, d\gamma \right]$$

We transform both partial integrals by the substitution

$$\sin \gamma = t$$

There is obtained

$$f_{121} = \frac{1}{\pi}\left[\frac{\pi}{2} - \delta\int_0^{1/\delta} \frac{\sqrt{1 - t^2}}{\sqrt{1 - \delta^2 t^2}}\,dt - \delta\int_0^{1/\delta} \frac{\sqrt{1 - \delta^2 t^2}}{\sqrt{1 - t^2}}\,t^2\,dt\right]$$

The two integrals are elliptic. We seek to obtain the solution in the form of a series expansion for the function $f_{121}(\delta)$ and for this purpose expand the factors $\sqrt{1 - t^2}$ and $1/\sqrt{1 - t^2}$ under the integral sign in a power series in t. Term by term integration leads to the very rapidly converging series

$$f_{121} = \frac{1}{16}\left(\frac{1}{\delta}\right)^2 + \frac{1}{128}\left(\frac{1}{\delta}\right)^4 + \ldots \qquad (63)$$

32. Circular Cylinder Parallel to Plane Wall

An infinitely long circular cylinder, representing surface F_1 of a two-surface system, interchanges radiation with a plane wall. The second surface encompasses both the wall and the infinite half-space lying above it. The axis of the cylinder is parallel to the wall and is $d = \delta R$ distance from it.

The notations are the same as for the case of the sphere and the plane wall. Figures 30 and 31 remain unchanged for the present two-dimensional problem and are now to be interpreted as sections normal to the cylinder axis. In the two-dimensional case the direction-dependent reflection coefficient f'_{121} is equal to the ratio of the distance a, by which the cylinder extends into the reflected band-shaped bundle of rays, to the width $2R$ of the reflected bundle:

$$f'_{121} = \frac{a}{2R} = 1 - \delta \sin\gamma$$

The reflection factor f_{121} averaged over all directions of space is, for the plane problem according to the integral (60), in our example found to be

$$f_{121} = \frac{1}{2\pi}\int_{-\gamma^*}^{\gamma^*} f'_{121}\,d\gamma = \frac{1}{\pi}\int_0^{\gamma^*} (1 - \delta \sin\gamma)\,d\gamma$$

The limit of integration γ^* - similarly to the case of the sphere and plane wall - is again

$$\gamma^* = \arcsin\frac{1}{\delta}$$

The reflection factor f_{121} is a function of the nondimensional distance δ:

$$f_{121} = \frac{1}{\pi}\left[\arcsin\left(\frac{1}{\delta}\right) + \sqrt{\delta^2 - 1} - \delta\right] \tag{64}$$

with the series expansion

$$f_{121} = \frac{1}{\pi}\left[\frac{1}{2}\left(\frac{1}{\delta}\right) + \frac{1}{24}\left(\frac{1}{\delta}\right)^3 + \frac{1}{80}\left(\frac{1}{\delta}\right)^5 + \ldots\right] \tag{65}$$

For the special case $\delta = 1$ the cylinder is tangent to the wall and there is obtained

$$f_{121}(\delta = 1) = \frac{1}{2} - \frac{1}{\pi} \approx 0.182$$

33. Eccentric Spherical Surfaces

A sphere, as surface F_1 of a two-surface system, is eccentrically situated in a hollow sphere (surface F_2) with which it exchanges radiation. In accordance with figure 33 we chose the ratio of the radii κ of the spherical surfaces and the nondimensional eccentricity δ as parameters of the problem.

The direction-dependent reflection factor f'_{121} is determined by the methods of projective geometry. The problem is one of rotational symmetry; hence a single angle suffices for characterizing the direction of the bundle of rays considered, namely the angle γ between the connecting line of the two sphere centers and the ray direction of the beam. For the graphical presentation it is most convenient to take this direction perpendicularly downward while the line connecting the sphere centers is oblique.

We consider first the relations in a meridional section (fig. 34) through the two sphere centers M_1 and M_2. Of all rays striking the spherical surface K_2 vertically downwards in the meridional section, the two "limiting rays" s_1 and s_2 are drawn and the reflected rays s'_1 and s'_2 just graze the sphere K_1. The reflections of all rays of the meridional section to the left of s_1 pass on the right of the sphere K_1, those to the right of s_2 pass on the left. Only the rays between s_1 and s_2 are thrown back on the sphere K_1 after reflection on K_2.

Figure 35 shows the projective geometrical construction in plan form (index ') and elevation (index ") for the rays outside the meridional section plane. We now consider all rays that are the generatices of a circular cylinder with the axis SM_2 and with the circle k_1 (in the elevation projected as a line) as the generating curve. Their reflections form a circular cone with the vertex S, the axis SM_2 and the base circle k_1 whose contour lines s_1 and s_2 are drawn in the elevation. Of the rays of the cylinder surface we shall

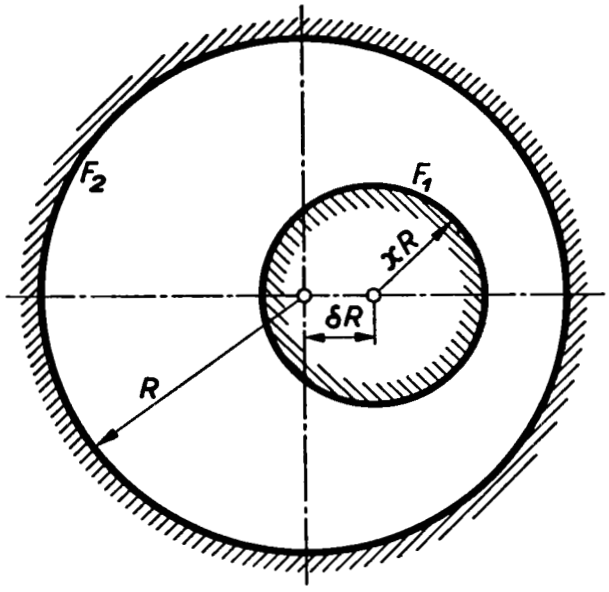

Figure 33. - Eccentric spherical surfaces.

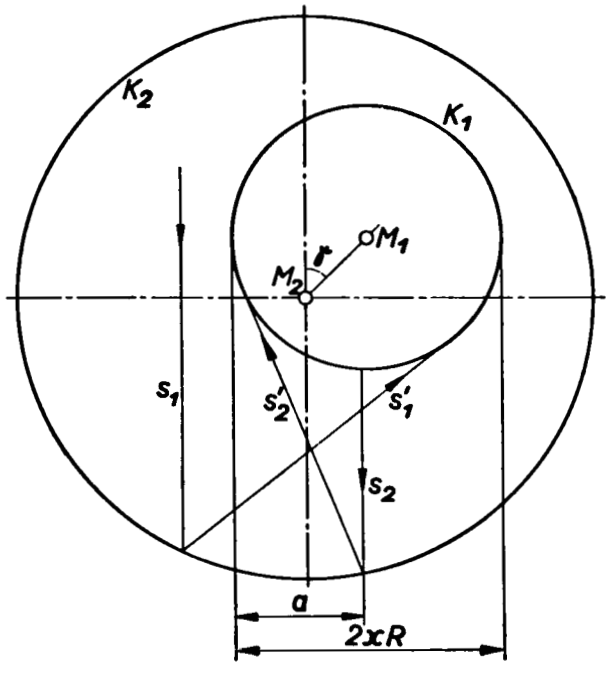

Figure 34.

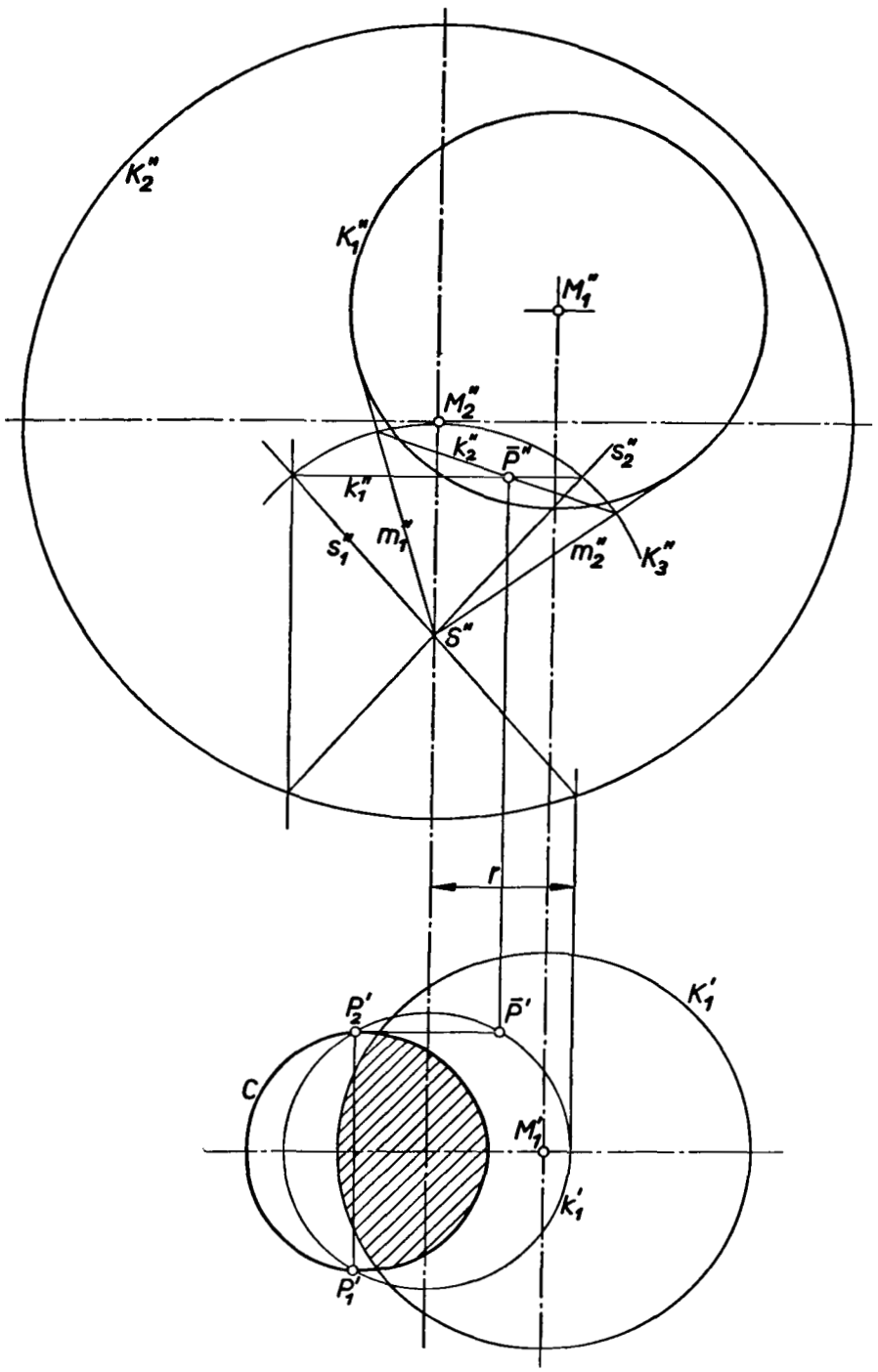

Figure 35. - Construction of f'_{121} in two-surface system for $\kappa = 0.5$, $\sigma = 0.4$, and $\gamma = 45^{\circ}$.

separate the rays whose reflections strike the sphere K_1 from the rays whose reflections pass by K_1. We seek the limiting rays whose reflections just touch K_1. These rays we obtain by the construction of the tangent generatrices of the cone to the sphere K_1 for which a geometric locus is the second circular cone formed on the tangents to K_1 from S. The contour lines m_1 and m_2 of the second cone (also with vortex S) are drawn in the elevation. The required tangent lines are the common generatrix lines of the two circular cones. We choose an auxiliary sphere K_3, with the center S, that cuts out the circles k_1 and k_2 from the two cones. The points of intersection of the two circles are points of the required tangent surface lines. Their elevations coincide at the point $\overline{P}''$, the point of intersection of the lines k_1'' and k_2'', and whose horizontal projections $\overline{P}'$ is drawn. The horizontal projections $\overline{P}_1'$ and $\overline{P}_2'$, of the penetration points of the two tangent surface lines with the sphere K_2, are obtained as points symmetrical to $\overline{P}'$ on the circle k_1'. They are the horizontal projections of the two limiting rays on the surface of the circular cylinder with the base circle k_1 whose reflected rays just touch the circle K_1. The perpendicular rays through the arc of the circle k_1 that lie on the left of P_1 and P_2 have reflected rays that strike the sphere K_1, those through the arc on the right have reflected rays that pass by K_1. By varying the radius of the circle k_1 there is finally obtained, point by point, a closed curve c, which encloses the bundle of all rays that strike the outer spherical shell vertically downward whose reflections fall on the inner sphere. The hatched part of this bundle originates from the sphere K_1 and the direction-dependent reflection factor f_{121}' is thus equal to the ratio of the hatched area to the area of the horizontal projection circle K_1' of the sphere K_1.

The construction of the direction-dependent reflection factor was now repeated for several angles γ (in steps of 45°) in order to obtain the reflection factor f_{121} averaged over all directions by evaluating the integral (59). This factor is a function of the ratio of the radii κ and of the dimensionless eccentricity δ and was determined as a function of κ in steps of 0.1 and as a function of δ in steps of 0.2 or, if required, of 0.1. Figure 36 gives the result. The dashed bounding curve corresponds to the case of the tangency of the two spherical surfaces and its point of intersection with the ordinate $\delta = 1$ to the case of a very small inner and a very large outer sphere (ratio of radii $\kappa = 0$), that touch each other. The reflection factor corresponding to this point originates from the computation of the example of sphere and plane wall at contact of the surfaces and amounts to 0.0756.

In the special case of concentric spherical surfaces, all the rays starting from the inner sphere after the specular reflection at the outer spherical surface again return to the inner sphere, and all of the rays starting from the outer sphere again return to the outer sphere after reflection at the outer sphere. The reflection factors are $f_{121} = 1$ and $f_{222} = 1$, not only for the first reflections but also for the second, third, and further reflections so that the basic approximation assumption of the second section is here exactly satisfied. Accordingly, the condition (36) from the second law of thermodynamics must

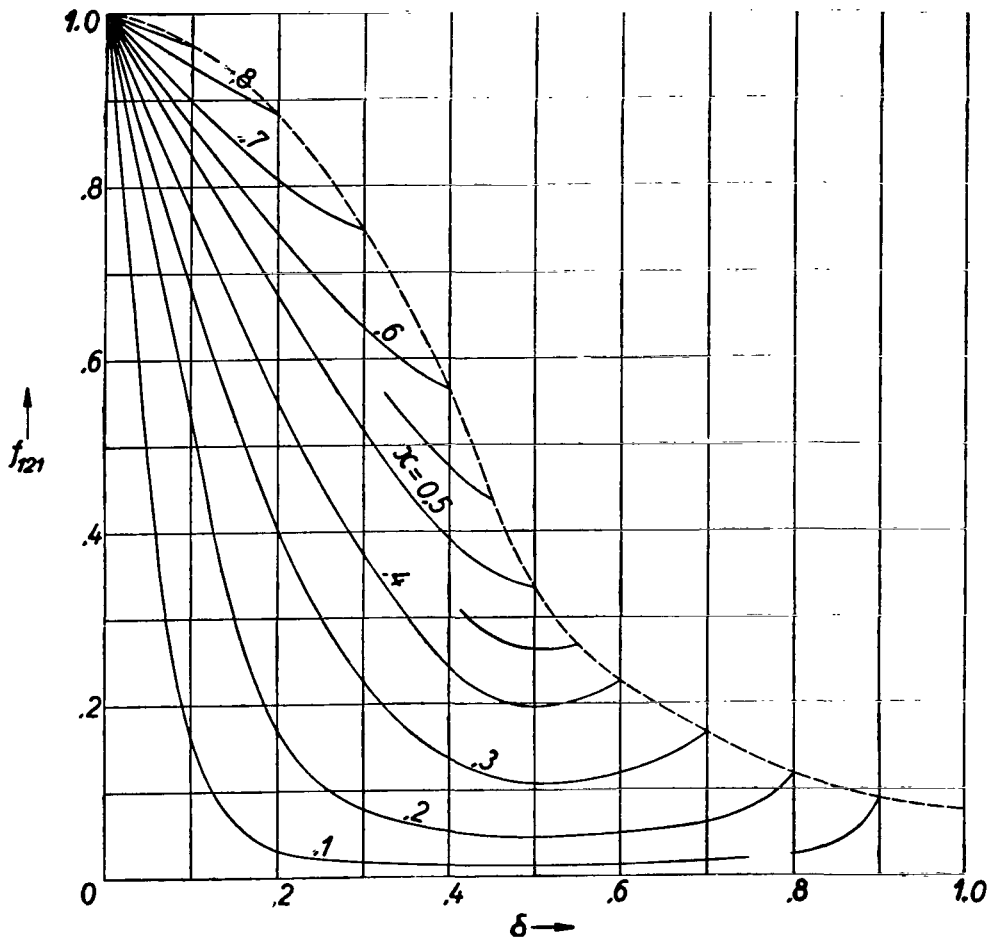

Figure 36. - Reflection factor f_{121} for eccentric spheres as function of ratio of radii κ and dimensionless eccentricity δ.

also be satisfied here. This is actually the case since for the convex surface F_1, the second equation of equations (50), which alone is essential, is satisfied with $f_{122} = 0$ and $f_{221} = 0$. For the correction factor to be applied to the Nusselt approximation there is thus obtained, in the case of concentric spherical surfaces, under the assumption of specular reflection at the outer surface, the exact solution

$$K = \frac{1}{\epsilon_1 + \epsilon_2 - \epsilon_1\epsilon_2} \tag{66}$$

which is also obtained in the case of parallel plates for any reflection laws.

34. Eccentric Circular Cylindrical Surfaces with Parallel Axis

A circular cylinder - as the surface F_1 of a two-surface system - is eccentrically situated in a hollow cylinder (surface F_2) with which it interchanges radiation. The two circular cylindrical surfaces have parallel axes and are infinitely long so that the case may be considered a two-dimensional problem. In accordance with figure 33 (which is now to be interpreted as the section normal to the cylinder axes), we choose the ratio of radii κ of the base circles of the cylinder and the dimensionless eccentricity δ as the parameters of the problem.

The direction-dependent reflection factor f'_{121} depends on a single rotation angle γ, and with the limiting rays introduced in figure 34 of the preceding example can be graphically determined:

$$f'_{121} = \frac{\alpha}{2\kappa R}$$

The graphical determination as a function of the angle γ was carried out in steps of 45°.

From the evaluation of the integral (60) there is obtained the reflection factor f_{121}, averaged over all directions, which was determined as a function of the ratio of the radii κ and of the dimensionless eccentricity δ in steps of 0.1 each. The result is shown in figure 37. The dashed limiting curve corresponds to the case of the contact of the two surfaces and its intersection with the ordinate $\delta = 1$, to the case of an inner cylinder with a small base circle radius and an outer cylinder with a very large base circle radius (ratio of radii $\kappa = 0$), that touch each other. The reflection factor corresponding to this point originates from the computation of the example of a circular cylinder parallel to a plane wall for contact of the two surfaces and amounts to 0.182.

For the special case of a concentric circular cylindrical surface with parallel axes, what has been said for the concentric spherical surfaces holds without change.

4. LAMBERT REFLECTION

The computations of this section are based on the law of Lambert reflection for both surfaces of the two-surface system: If heat radiation from any direction falls on a surface, the reflections are distributed according to the Lambert cosine law. The directional distribution of the reflection coefficient is accordingly independent of the direction of incidence. Since the Lambert cosine law was also assumed for the directional distribution of the emissions, we have in the case of the Lambert reflector, the important mathematical simplification that the emissions and reflections may formally be equally treated. The sum of all reflections can be combined with the emission into a new magnitude. In the visible wavelength region one would speak of the brightness of the surface at a definite point and this idea will also be carried over for the heat radiation.

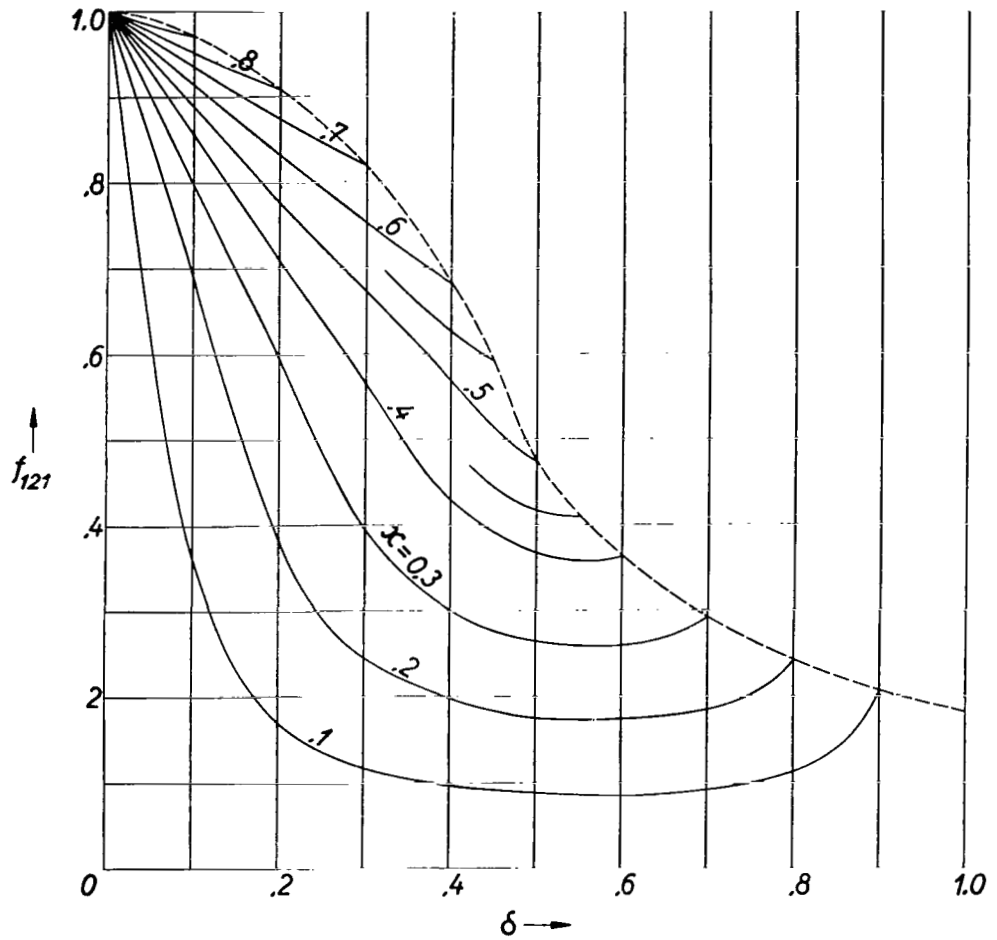

Figure 37. - Reflection factor f_{121} for eccentric circular cylinders with parallel axes as a function of ratio of radii $\varkappa$ and dimensionless eccentricity σ.

We first consider the computation of the reflection factors in the sense of the theory given in section 2. In the case of the Lambert reflection, the directional distribution of the reflected energies is independent of the origin of the beam. Hence, the reflection factors with different first and equal second and third index numbers coincide and the number of the reflection factors reduces to four, namely:

$$\left.\begin{aligned} f_{111} &= f_{211} \\ f_{112} &= f_{212} \\ f_{121} &= f_{221} \\ f_{122} &= f_{222} \end{aligned}\right\} \qquad (67)$$

The theory of the heat transfer for Lambert reflectors will then be generalized. We shall not only restrict ourselves to the treatment of the two-surface system, but also investigate more general arrangements of surfaces. We also drop the approximation assumption of the second section in accordance with which the second, third, and further reflections locally and directionally have the same distributions as the first. These discussions are given in sections 42 to 45.

Finally, the examples of the last sections will also be treated under the assumption of the law of Lambert reflection.

41. Computation of Reflection Factors

The surface F_1 of a two-surface system emits the radiation energy

$$q_1 = F_1 E_1 = F_1 C_s \epsilon_1 \left(\frac{T_1}{100}\right)^4$$

of which the fraction $F_1 E_1 \varphi_{12}$ falls on the surface F_2 that in turn again reflects the amount $F_1 E_1 \varphi_{12} \rho_2 f_{121}$ back to the surface F_1.

We fix a point on the surface F_1 by the coordinate x_1 and a point on the surface F_2 by the coordinate x_2. In general, x_1 and x_2 are each determined by two scalar magnitudes, the surface coordinates on the surfaces. Correspondingly, dx_1 and dx_2 are usually surface elements and the integrals over functions of x_1 or x_2 are double integrals.

Of the emission from the surface F_1, the radiation energy $F_1 E_1 \varphi_{1,x_2}$ falls on the surface element $dF(x_2)$ at the point x_2, which owing to the known relation

$$F_1 \varphi_{1,x_2} = dF(x_2) \varphi_{x_2,1}$$

between the solid angle ratios, is also equal to $E_1\, dF(x_2) \varphi_{x_2,1}$. Here φ_{1,x_2} denotes the solid angle ratio for the radiation exchange of the entire surface F_1 with the surface element $dF(x_2)$ and is, therefore, a differential. The solid angle ratio for the radiation exchange of the surface element $dF(x_2)$ with F_1 is denoted by $\varphi_{x_2,1}$. According to the Lambert reflection law the surface F_2 reflects back on F_1 the amount $\rho_2 \varphi_{x_2,1}$ times the incident radiation. Integrating over F_2, there is obtained the total radiant energy reflected by F_2 on the surface F_1:

$$E_1 \rho_2 \int_{F_2} \varphi_{x_2,1}^2\, dF(x_2)$$

Comparison with the expression formulated with the aid of the reflection factor leads to the relation

$$f_{121} = f_{221} = A_2 = \frac{\int_{F_s} \varphi^2_{x_2,1}\, dF(x_2)}{F_1 \varphi_{12}} \tag{68}$$

which by interchanging indices, goes over into an analogous expression for $f_{212} = f_{112} = A_1$.

The equations (50) stemming from the second law of thermodynamics go over for the Lambert reflection, taking account of equation (67), into the requirement $A_2 = \varphi_{21}$ and $A_1 = \varphi_{12}$, which is satisfied only if the solid angle ratio $\varphi_{x_2,1}$ and $\varphi_{x_1,2}$, depending on the point coordinates, are constant and therefore equal to φ_{21} and φ_{12}, respectively. The contradiction, as mentioned earlier in the report, is due to the approximating assumption according to which the second and further reflections are distributed in the same way as the first. We circumvent the difficulty by computing the reflection factors according to equation (68) and assume relations (51) and (52) as approximately valid, nevertheless.

42. Simplified Theory of Many-Surface System

We consider a system of n surfaces that exchange radiation with each other. Each surface is assumed to have the same temperature and the same radiation properties (emission and reflection coefficients) at each point and from each surface element of any surface, only parts of the surfaces of the system can be seen. We denote such a configuration, by analogy with the two-surface system, a multisurface, or more accurately, an n-surface system.

For the following computations we assume the Lambert cosine law for the directional distribution of the emissions and reflections and further make the approximating assumption that the reflections on each surface are locally uniformly distributed so that the brightness on each surface is a constant.

The k^{th} surface emits the radiation energy

$$F_k E_k = F_k C_s \epsilon_k \left(\frac{T_k}{100}\right)^4$$

and its brightness is made up of its emission per unit surface and the sum of all reflected radiations:

$$H_k = E_k + \sum R_k \tag{69}$$

The total surface radiation F_k, therefore, is $F_k H_k$. Of this total the part $F_k H_k \varphi_{ki}$ reaches the i^{th} surface, which again reflects the amount $F_k H_k \varphi_{ki} \rho_i$, and owing to the relation

$$F_k \varphi_{ki} = F_i \varphi_{ik}$$

between the solid angle ratios is also equal to $F_i H_k \varphi_{ik} \rho_i$. The sum of the reflections of the i^{th} surface is then obtained as

$$F_i \sum R_i = \rho_i F_i \sum_{k=1}^{n} \varphi_{ik} H_k$$

and, finally, from equation (69) the brightness H_i of the i^{th} surface

$$H_i = E_i + \rho_i \sum_{k=1}^{n} \varphi_{ik} H_k \tag{70}$$

The equation (70) can be written down for each index i, hence, n times altogether. This equation represents a system of n linear equations for the determination of the n unknown brightnesses of the n surfaces.

The concept of the heat transfer from one surface F_i to another surface F_k here becomes devoid of application in contrast to the computations where the reflections are neglected, for the heat exchange process is no longer a matter of two considered surfaces alone, but all other surfaces participate as reflectors. The heat exchange of group I of the first m surfaces F_i (index $i = 1 \ldots m$) with group II of the remaining $(n - m)$ surfaces F_k (index $k = m + 1 \ldots n$) is of interest. This heat exchange is expressed in the form of the double sum

$$Q_{I,II} = \sum_{i=1}^{m} \sum_{k=m+1}^{n} F_i \varphi_{ik} (H_i - H_k) \tag{71}$$

from an energy balance through comparison of all the radiations sent out from one group to the other. The sequence of the summations can be interchanged. The heat

$$Q_i = F_i \sum_{k=1}^{n} \varphi_{ik} (H_i - H_k) \tag{72}$$

given off by the i^{th} surface to all remaining surfaces follows as a special case ($m = 1$) from equation (71). The same result gives an energy balance for the surface F_i in which the sum of all absorbed amounts, namely $\epsilon_i F_i \sum_{k=1}^{n} \varphi_{ik} H_k$, is subtracted from the emission $F_i E_i$.

The solution of the system of equations (70) for a not too large number of surfaces n is best effected in closed form, for example, according to the Gauss algorithm. For large n the use of an iteration process is recommended. On the right side of the equations the emission energies E_i generally predominate so that the first approximation $H_i = E_i$ can be substituted on the right. The H_i obtained on the left side of the equation can again be substituted on the right side and the process can be repeated until the desired accuracy is attained.

The simplified theory of the multisurface system can be applied to the treatment of the two-surface system with account taken of the local distribution of the reflections by dividing the surfaces into partial surfaces. The accuracy can be raised by increasing the number of partial surfaces. The limiting case of infinitely many partial surfaces corresponds to the theory of the next section.

The system of equation (70) can formally be written as a vector equation if the n brightnesses H_i are taken as the components of a brightness vector H and the n emissions E_i are taken as the components of the emission vector. With the n-row and n-column coefficient matrix

$$M = \begin{pmatrix} \rho_1\varphi_{11} & \rho_1\varphi_{12} & \cdots & \rho_1\varphi_{1n} \\ \rho_2\varphi_{21} & \rho_2\varphi_{22} & \cdots & \rho_2\varphi_{2n} \\ \cdot & & & \cdot \\ \cdot & & & \cdot \\ \cdot & & & \cdot \\ \rho_n\varphi_{n1} & \rho_n\varphi_{n2} & \cdots & \rho_n\varphi_{nn} \end{pmatrix}$$

the system (70) assumes the form

$$H = E + MH \tag{73}$$

where the vector H occurs as column vector in the matrix product.

For the special case of the simplified theory of the two-surface system, the linear system of equation (70) becomes

$$H_1 = E_1 + \rho_1\varphi_{11}H_1 + \rho_1\varphi_{12}H_2$$

$$H_2 = E_2 + \rho_2\varphi_{21}H_1 + \rho_2\varphi_{22}H_2$$

The elimination of H_1 gives

$$H_1 = \frac{E_1(1 - \rho_2\varphi_{22}) + \rho_1\varphi_{12}E_2}{1 - \rho_1\varphi_{11} - \rho_2\varphi_{22} + \rho_1\rho_2(\varphi_{11}\varphi_{22} - \varphi_{12}\varphi_{21})}$$

The analogous relation for H_2 follows from the preceding relation by interchanging the indices. The expression for the heat transfer from the first to the second surface

$$Q_{12} = F_1\varphi_{12}(H_1 - H_2)$$

is obtained from equation (72), since in the case of the two-surface system, the heat given off by the first surface is equal to the heat Q_{12} transferred per unit time. We put it in the following form

$$Q_{12} = F_1\varphi_{12}C_s\epsilon_1\epsilon_2K\left[\left(\frac{T_1}{100}\right)^4 - \left(\frac{T_2}{100}\right)^4\right] \tag{51}$$

and by substituting the expressions for the brightnesses, obtain the correction factor

$$K = \frac{1}{1 - \rho_1\varphi_{11} - \rho_2\varphi_{22} + \rho_1\rho_2(\varphi_{11}\varphi_{22} - \varphi_{12}\varphi_{21})} \tag{74}$$

that is to be applied to the Nusselt approximation. Equation (74) also follows as a special case from equation (52) if the corresponding solid angle ratios are substituted in place of the reflection factors. If the first surface F_1 is convex, the correction factor K simplifies to the known relation

$$K = \frac{1}{\epsilon_2 + \varphi_{21}\epsilon_1 - \varphi_{21}\epsilon_1\epsilon_2} \tag{75}$$

For the single radiating surface (cavity of constant temperature) system (70) goes over into the single equation $H = E + \rho H$, from which it follows that the brightness of a cavity radiator is equal to that of the blackbody radiator (for equal temperature).

43. Integral Equation for Brightness Distribution

Starting from the notion of a many-surface system, we now make the limiting transition to infinitely many surfaces. We consider a system of surfaces whose temperature T and, therefore, the radiation emission E per unit surface, whose radiation properties (emission and reflection coefficients) and whose brightness H varies from point to point. As in section 41, we fix the position of a point by a point coordinate x, which in general, consists of two scalar magnitudes (surface coordinates).

For what follows we introduce a fixed point coordinate x and a current coordinate (integration variable) ξ. The solid angle ratio $\varphi_{x\xi}$ for the ra-

diation exchange of the surface element $dF(x)$ at the point x with that at the point ξ, $dF(\xi)$, is equal to

$$\varphi_{x\xi} = g(x,\xi)dF(\xi)$$

where g is the function

$$g(x,\xi) = g(\xi,x) = \frac{\cos \nu_1 \cos \nu_2}{\pi r^2} \tag{76}$$

of the two point coordinates, symmetrical in x and ξ; r is the distance between the two surface elements and ν_1 and ν_2 are the angles between the surface normals and connecting line of the elements (fig. 28).

From the surface element at the point ξ the radiation energy $dF(\xi)H(\xi)$ is emitted. Of this radiation, the part

$$\varphi_{\xi x}\, dF(\xi)H(\xi) = g(x,\xi)dF(x)dF(\xi)H(\xi)$$

strikes the surface element $dF(x)$, which again reflects the amount $\rho(x)g(x,\xi)dF(\xi)H(\xi)$. The total of all reflections sent out from the point x

$$\int_{\xi} \rho(x)g(x,\xi)H(\xi)dF(\xi)$$

is to be added to the emission per unit surface

$$E(x) = C_s\epsilon(x)\left[\frac{T(x)}{100}\right]^4$$

to obtain the brightness $H(x)$. The solution of the Fredholm integral equation for the brightness distribution is $H(x)$:

$$H(x) = E(x) + \rho(x) \int_{\xi} g(x,\xi)H(\xi)dF(\xi) \tag{77}$$

With reference to the theory of the multisurface system we divide the system of surfaces into two regions; namely, B_1 and B_2, and compare the radiations from one region to the other in an energy balance. Denoting the brightness and point coordinate on B_1 by H_1 and x_1, respectively, and the brightness and point coordinate on B_2 by H_2 and x_2, respectively, the radiation energy transferred from the first region to the second is

$$Q_{B_1B_2} = \int_{B_1}\int_{B_2} g(x_1,x_2)\left[H_1(x_1) - H_2(x_2)\right]dF(x_1)dF(x_2) \tag{78}$$

The heat given off per unit surface at the point x follows as a special case from the formula (78) if the region B_1 is assumed infinitely small; or through the subtraction of all absorbed amounts from the emission $E(x)$ per unit surface:

$$\frac{dQ}{dF}(x) = \int_{\xi} g(x,\xi)[H(x) - H(\xi)]dF(\xi) \tag{79}$$

The integral is to be taken over the entire system of surfaces.

The solving of integration equation (77) is best effected through iteration by substituting a first approximation function for the brightness distribution in the integral to obtain a second approximation from the equation. The iteration process is to be continued until the desired accuracy is attained. The process converges more rapidly the smaller the reflection coefficient $\rho(x)$, that is, the term $E(x)$ on the right side of the integral equation is more predominant.

The close connection of the results of this section with the simplified theory of the multisurface system is evidenced most clearly if the integral in equation (77) is formally expressed by an integral operator M, which carries over the brightness distribution into another point-dependent function; namely, in the result of the integration. The integral equation (77) then assumes the same form as the vectorially written system of equations (70), so that:

$$H = E + MH \tag{73}$$

The operation of the matrix multiplication, in the case of the multisurface system, corresponds to the integration; the emission and brightness vectors correspond to the point-dependent functions $E(x)$ and $H(x)$.

44. Two-Dimensional Problems

In the case of infinitely long cylindrical configurations the surface element $dF(x)$ can be taken as infinitely long narrow strips. The area of $dF(x)$ is equal to the product of the arc element ds in a section normal to the generatrices of the surfaces and a unit length, which is always eliminated from the computation by referring the emissions, brightnesses and heat transfers to unit length.

With the notation of figure 38 we compute the solid angle ratio of the radiation exchange of the surface element strip $dF(x)$ with $dF(\xi)$ through integration of the solid angle ratio for the radiation exchange between dF_1 and dF_2 over the length z:

$$\varphi_{x\xi} = \int_z \varphi_{dF_1, dF_2} = \int_{-\infty}^{\infty} g(x;\xi,z)ds(\xi)dz$$

The angles ν_1, α, and ν_1' are sides of a rectangular spherical triangle. The

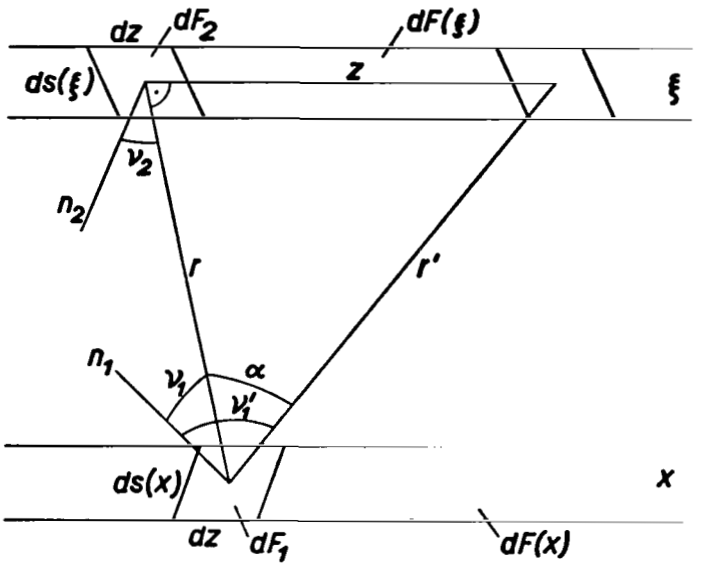

Figure 38.

spherical Pythagorean theorem leads to the relations

$$\cos \nu_1' = \cos \nu_1 \cos \alpha = \cos \nu_1 \frac{r}{r'} \qquad \text{and} \qquad \cos \nu_2' = \cos \nu_2 \frac{r}{r'}$$

By substituting in the expression for g

$$g = \frac{\cos \nu_1' \cos \nu_2'}{\pi r'^2} = \frac{\cos \nu_1 \cos \nu_2 \, r^2}{\pi r'^4}$$

there is obtained the solid angle ratio

$$\varphi_{x\xi} = \frac{\cos \nu_1 \cos \nu_2 r^2 \, ds(\xi)}{\pi} \int_{-\infty}^{\infty} \frac{dz}{(z^2 + r^2)^2}$$

or

$$\varphi_{x\xi} = \gamma(x, \xi) ds(\xi) \tag{80}$$

if the function is introduced then,

$$\gamma(x, \xi) = \gamma(\xi, x) = \frac{\cos \nu_1 \cos \nu_2}{2r} \tag{81}$$

symmetrical in x and ξ and dependent on the two point coordinates. For the remainder, the equations (77) to (79) also hold with the new surface elements except that in the formulas the function $g(x,\xi)$ is to be replaced by $\gamma(x,\xi)$ and the surface element dF by the arc element ds, whereby the emissions, brightnesses and heat transfers then refer to unit length.

45. Approximate Solution of Integral Equations for Two-Surface System

In the case of the two-surface system it is convenient to resolve the integral equation (77) into a system of two integral equations as follows:

$$\left.\begin{aligned} H_1(x_1) &= E_1 + \rho_1 \int_{F_1} g(x_1,\xi_1)H_1(\xi_1)dF(\xi_1) + \rho_1 \int_{F_2} g(x_1,\xi_2)H_2(\xi_2)dF(\xi_2) \\ H_2(x_2) &= E_2 + \rho_2 \int_{F_1} g(x_2,\xi_1)H_1(\xi_1)dF(\xi_1) + \rho_2 \int_{F_2} g(x_2,\xi_2)H_2(\xi_2)dF(\xi_2) \end{aligned}\right\} \quad (82)$$

where the index 1 refers to the point coordinate, brightness, emission coefficient and reflection coefficient on the first surface and the index 2 refers to the corresponding magnitudes on the second surface. The transferred radiation energy is obtained from equation (78) by making the regions B_1 and B_2 coincide with the surfaces F_1 and F_2.

To solve the integral equation system (82) we make use of the iteration method. On the right side, as first brightness distributions, we put the constant brightnesses $H_1^{(0)}$ and $H_2^{(0)}$ that are obtained from the simplified theory of the two-surface system (sec. 42) and, since these are already a fairly good approximation, we break off the computation after the first iteration step. On the left side of the system we then obtain the first brightness distributions $H_1^{(1)}(x_1)$ and $H_2^{(1)}(x_2)$, and this constitutes the only approximating assumption of the succeeding computations. On the right side of equation (82) we can now take the constants $H_1^{(0)}$ and $H_2^{(0)}$ outside the integral sign. The remaining integrals are solid angle ratios for the radiation exchange of a surface element with one of the two surfaces of the two-surface system, for example

$$\int_{F_2} g(x_1,\xi_2)dF(\xi_2) = \varphi_{x_1,2}$$

and the system (82) goes over into the form

$$\left.\begin{aligned} H_1^{(1)}(x_1) &= E_1 + \rho_1 H_1^{(0)}\varphi_{x_1,1} + \rho_1 H_2^{(0)}\varphi_{x_1,2} \\ H_2^{(1)}(x_2) &= E_2 + \rho_2 H_1^{(0)}\varphi_{x_2,1} + \rho_2 H_2^{(0)}\varphi_{x_2,2} \end{aligned}\right\}$$

or

$$\left.\begin{aligned} H_1^{(1)}(x_1) &= E_1 + \rho_1 H_1^{(0)} - \rho_1 \varphi_{x_1,2}\left[H_1^{(0)} - H_2^{(0)}\right] \\ H_2^{(1)}(x_2) &= E_2 + \rho_2 H_2^{(0)} - \rho_2 \varphi_{x_2,1}\left[H_1^{(0)} - H_2^{(0)}\right] \end{aligned}\right\}$$

To formulate the heat transfer from the first surface to the second we require the difference of the two brightness functions $H^{(1)}$. The brightnesses $H_1^{(0)}$ and $H_2^{(0)}$ are connected by the linear system of equations (70) written for the case $n = 2$. If the solid angle ratios φ_{11} and φ_{22} are replaced by $1 - \varphi_{12}$ and $1 - \varphi_{21}$ and the second equation is subtracted from the first there is obtained

$$E_1 - E_2 + \rho_1 H_1^{(0)} - \rho_2 H_2^{(0)} = \left[H_1^{(0)} - H_2^{(0)}\right]\left[1 + \rho_1 \varphi_{12} + \rho_2 \varphi_{21}\right]$$

whence there is finally obtained

$$H_1^{(1)}(x_1) - H_2^{(1)}(x_2) = \left[H_1^{(0)} - H_2^{(0)}\right]\left[1 + \rho_1 \varphi_{12} + \rho_2 \varphi_{21} - \rho_1 \varphi_{x_1,2} - \rho_2 \varphi_{x_2,1}\right]$$

We substitute in equation (78) and take the constants outside the integral sign. The remaining double integrals we express with the aid of the magnitudes A_1 and A_2, according to the definition of equation (68), so that

$$\int_{F_1}\int_{F_2} g(x_1, x_2)\, dF(x_1)\, dF(x_2) = F_1 \varphi_{12}$$

$$\int_{F_1}\int_{F_2} g(x_1, x_2)\, \varphi_{x_1,2}\, dF(x_1)\, dF(x_2) = \int_{F_1} \varphi_{x_1,2}^2\, dF(x_1) = F_1 \varphi_{12} A_1$$

$$\int_{F_1}\int_{F_2} g(x_1, x_2)\, \varphi_{x_2,1}\, dF(x_1)\, dF(x_2) = \int_{F_2} \varphi_{x_2,1}^2\, dF(x_2) = F_1 \varphi_{12} A_2$$

and obtain for the radiation energy transferred from F_1 to F_2:

$$Q_{12} = F_1 \varphi_{12}\left[H_1^{(0)} - H_2^{(0)}\right]\left[1 - \rho_1(A_1 - \varphi_{12}) - \rho_2(A_2 - \varphi_{21})\right] \qquad (83)$$

and for the correction factor to be applied to the Nusselt approximation according to equation (51):

$$K = \frac{1 - \rho_1(A_1 - \varphi_{12}) - \rho_2(A_2 - \varphi_{21})}{1 - \rho_1\varphi_{11} - \rho_2\varphi_{22} + \rho_1\rho_2(\varphi_{11}\varphi_{22} - \varphi_{12}\varphi_{21})} \tag{84}$$

If the surface F_1 is convex, we have $\varphi_{12} = 1$, $\varphi_{x_1,2} = 1$ and, therefore, $A_1 = 1$, which yields:

$$K = \frac{1 - \rho_2(A_2 - \varphi_{21})}{1 - \rho_2(1 - \varphi_{21}) - \rho_1\rho_2\varphi_{21}} \tag{85}$$

The expressions (52) - with the reflection factors for the Lambert reflection - and (84) are different approximations for the same correction factor K. Their comparison shows agreement except for terms in which at least two reflection coefficients occur as factors. Thus, in both approximations the first reflections are treated exactly; whereas, only the second and further reflections are approximate. Furthermore, a second iteration step can give only correction terms with two reflection coefficients as factors, and a third with only three reflection coefficients.

46. Sphere and Plane Wall

We investigate the radiation exchange of a sphere with a plane wall in the arrangement and with the notations of section 31. Since the surface F_1 is convex, we need to compute only the magnitude A_2. Further, the solid angle ratio $\varphi_{21} = 0$, because the surface F_2 is infinitely large.

The solid angle ratio $\varphi_{x_2,1}$ for the radiation exchange between a surface element on the wall (at A in fig. 39) and the sphere is to be determined first. We recall the graphical construction of the solid angle ratio in conformity with Nusselt (ref. 4), according to which the surface F_1 under consideration is to be projected a first time on the unit sphere about the point A as projection center, and the resulting image projected a second time on the tangential plane to the surface F_2 at A (in our case the wall itself). The required solid angle ratio is then equal to the ratio of the area of the image on the tangential plane to the area of the unit circle (π). In our case, the projection of the radiating sphere on the unit sphere is a small circle with the radius $\sin\omega$, and the projection on the wall is an ellipse with the semiaxes $\sin\omega$ and $\sin\omega\cos\alpha$. Thus, there is obtained

$$\varphi_{x_2,1} = \sin^2\omega\cos\alpha \tag{86}$$

As the surface element on the wall we choose a narrow circular ring surface with the normal projection E of the sphere center M on the wall as the center, the

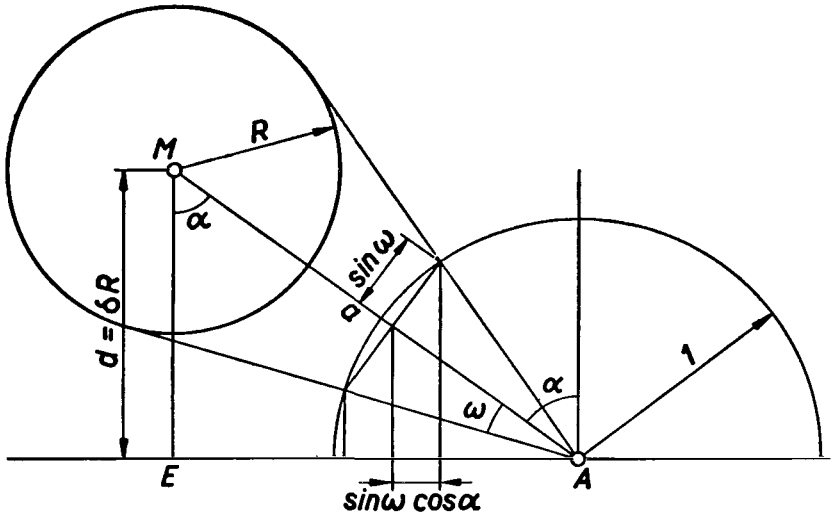

Figure 39. - Determination of solid angle ratio $\sigma_{x_2,1}$.

distance $\overline{EA} = Rx_2$ as the mean radius, $R\,dx_2$ as the width, and the surface area as

$$dF(x_2) = 2\pi R^2 x_2\,dx_2$$

From figure 39 the following relations are obtained:

$$\sin\omega = \frac{R}{a} \qquad \text{and} \qquad \cos\alpha = \frac{d}{a}$$

with

$$\overline{MA}^2 = a^2 = R^2\left(\delta^2 + x_2^2\right)$$

By substituting in equation (86) there is obtained

$$\varphi^2_{x_2,1} = \frac{\delta^2}{\left(\delta^2 + x_2^2\right)^3}$$

and, with $F_1 = 4\pi R^2$ as area of the radiating sphere, according to equation (68), the coefficient

$$A_2 = \frac{\delta^2}{2} \int_0^\infty \frac{x_2 \, dx_2}{(\delta^2 + x_2^2)^3}$$

and finally

$$A_2 = \frac{1}{8\delta^2} \tag{87}$$

47. Circular Cylinder Parallel to Plane Wall

An infinitely long circular cylinder exchanges radiation with a flat wall. The arrangement and notations are the same as in section 32. Again, as in the previous example, only the magnitude A_2 is to be computed and the solid angle ratio $\varphi_{21} = 0$.

For this two-dimensional problem we also make use of figure 39, which is now to be interpreted as a normal section to the axis of the circular cylinder, and permits us to derive the solid angle ratio $\varphi_{x_2,1}$ graphically. The central projection of the cylinder on the unit sphere about the point A is a spherical lune bounded by two great circle arcs; the normal projection of this surface on the wall is a lune bounded by two elliptical arcs. The required solid angle ratio is equal to the ratio of the area of the lune to the area of the unit sphere and this is equal to the ratio of the maximum width $2 \sin \omega \cos \alpha$ of the lune to the diameter 2 of the unit circle:

$$\varphi_{x_2,1} = \sin \omega \cos \alpha \tag{88}$$

As a surface element on the wall we choose an area (per unit length)

$$dF(x_2) = R \, dx_2$$

of a small strip parallel to the cylinder axis with the width $R \, dx_2$ at the distance $\overline{EA} = Rx_2$ from the normal projection of the cylinder on the wall. The angle functions $\sin \omega$ and $\cos \alpha$ are connected with the dimensions of the figure in the same way as in section 46. Substitution in equation (88) gives

$$\varphi_{x_2,1} = \frac{\delta}{\delta^2 + x_2^2}$$

and, with $F_1 = 2\pi R$ as area per unit length of the radiating cylinder,

$$A_2 = \frac{\delta^2}{2\pi} \int_{-\infty}^{\infty} \frac{dx_2}{\left(\delta^2 + x_2^2\right)^2}$$

and finally

$$A_2 = \frac{1}{4\delta} \tag{89}$$

48. Eccentric Spherical Surfaces

Two eccentrically situated spherical surfaces interchange radiation with each other. As in section 33, we choose the ratio of κ of the sphere radii and the dimensionless eccentricity δ as parameters of the problem. Again only A_2 is to be computed and the solid angle ratio for the radiation interchange between the outer and inner spherical surface amounts to $\varphi_{21} = \kappa^2$.

As the surface element of the external sphere we choose, according to figure 40, the surface area of a very low truncated cone and for determining the locus we choose the angle at the center ζ:

$$dF(x_2) = 2\pi R^2 \sin \zeta \, d\zeta$$

The visual rays from the point P to the contour of the inner sphere form a circular cone with the half aperture angle ω whose axis makes the angle α with the surface normal of the outer sphere. The solid angle ratio $\varphi_{x_2,1}$ is, in our example, again computed from the relation (86), with

$$\sin \omega = \frac{\kappa R}{\alpha}$$

$$\cos \alpha = \frac{R}{\alpha} (1 - \delta \cos \zeta)$$

and $a = \overline{M_1 P}$ according to the cosine law in the triangle $M_1 P M_2 \delta$

$$a^2 = R^2(1 + \delta^2 - 2\delta \cos \zeta)$$

and found to be

$$\varphi_{x_2,1} = \frac{R^3}{a^3} \kappa^2 (1 - \delta \cos \zeta)$$

With the area $F_1 = 4\pi R^2 \kappa^2$ of the inner sphere, after substitution in the expression (68), there is obtained

$$A_2 = \frac{\kappa^2}{2} \int_0^{\pi} \frac{(1 - \delta \cos \zeta)^2 \sin \zeta}{(1 + \delta^2 - 2\delta \cos \zeta)^3} \, d\zeta$$

In the special case of concentric spheres ($\delta = 0$) the integral is greatly simplified and there is obtained the well-known solution

$$f_{121} = A_2 = \kappa^2 = \varphi_{21} \tag{90}$$

In general, the magnitude A_2 is a function of both parameters κ and δ. We transform the integral through the substitution

$$\cos \zeta = t$$

into the form

$$A_2 = \frac{\kappa^2}{2} \int_{-1}^{1} \frac{(1 - \delta t)^2}{(1 + \delta^2 - 2\delta t)^3} \, dt$$

in which the integration can be carried out by means of decomposition into partial fractions:

$$A_2 = \frac{\kappa^2}{2} \left[\frac{1}{1 - \delta^2} + \frac{1 + \delta^2}{2(1 - \delta^2)^2} + \frac{1}{4\delta} \ln \left(\frac{1 + \delta}{1 - \delta} \right) \right] \tag{91}$$

For small eccentricity the series expansion

$$A_2 = \frac{\kappa^2}{4} \sum_{k=0}^{\infty} \left(2k + 3 + \frac{1}{2k + 1} \right) \delta^{2k} \tag{92}$$

is recommended. The function $A_2(k, \delta)$ increases monotonically with the eccentricity δ. Starting with horizontal tangent from the value κ^2, the rise becomes steeper with increasing eccentricity. The limiting case $\delta = 1$ and $\kappa = 0$ corresponds to a very small inner and very large outer sphere that touch each other. The corresponding coefficient A_2 can be taken from the computation of the example of a sphere and a plane wall in contact with each other and has the value

$$A_2(\kappa = 0; \ \delta = 1) = \frac{1}{8}$$

49. Eccentric Circular Cylindrical Surfaces with Parallel Axes

Two infinitely long circular cylinders with parallel axes eccentrically situated exchange heat through radiation. The arrangement and notations of the plane problem here considered correspond to the example of section 34. The solid angle ratio for radiation exchange from the outer to the inner cylindrical surface is $\varphi_{21} = K$ and again A_2 is to be computed as a function of the two parameters K and δ.

To determine the solid angle ratio $\varphi_{x_2,1}$ for the radiation exchange between a surface element on the outer cylindrical surface and the inner surface we again use figure 40, which is now to be interpreted as normal section to the axes of the circular cylinders. The visual rays from the point P to the contour of the inner cylinder form a wedge with the half aperture angle ω, whose plane of symmetry forms the angle α with the surface normal of the outer cylinder surface P. The required solid angle ratio is then found from formula (88) with account taken of the relation, already used in the last section, between the geometric magnitudes of the arrangement:

$$\varphi_{x_2,1} = \frac{R^2}{a^2} K(1 - \delta \cos \zeta)$$

As surface element on the outer cylinder we choose an infinitely long narrow strip in the direction of the generatrices of the width $R\, d\zeta$ with the area (per unit length)

$$dF(x_2) = R\, d\zeta$$

With the area $F_1 = 2\pi RK$ (referred to unit length) of the inner cylinder surface there is obtained, from equation (68)

$$A_2 = \frac{K}{2\pi} \int_{-\pi}^{\pi} \frac{(1 - \delta \cos \zeta)^2}{(1 + \delta^2 - 2\delta \cos \zeta)^2}\, d\zeta$$

The substitution

$$\tan \frac{\zeta}{2} = t$$

leads to the expressions

$$\cos \zeta = \frac{1 - t^2}{1 + t^2} \qquad \text{and} \qquad d\zeta = \frac{2\, dt}{1 + t^2}$$

and enables the elementary evaluation of the integral by means of resolution into partial fractions. The function

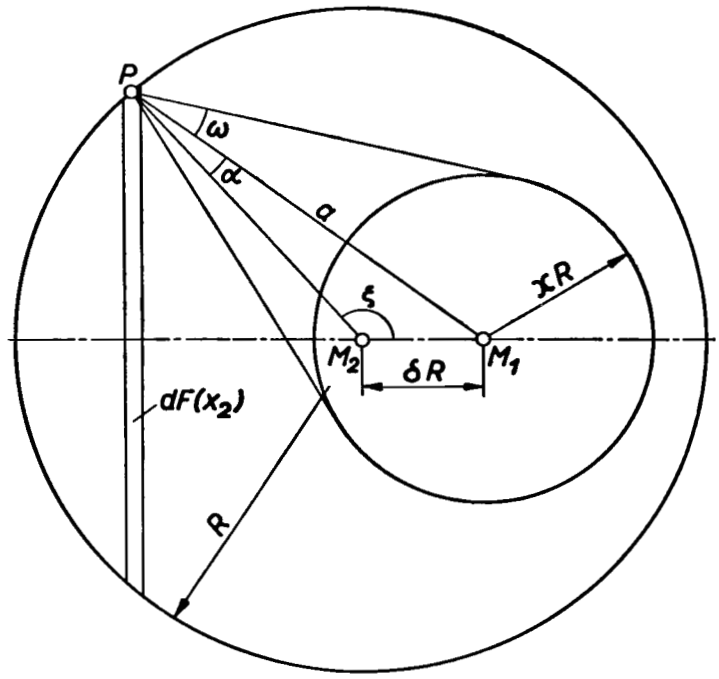

Figure 40. - Determination of solid angle ratio $\sigma_{x2,1}$.

$$A_2 = \frac{\kappa}{2}\left[\frac{2 - \delta^2}{1 - \delta^2}\right] \tag{93}$$

as in the preceding example, monotonically increases with the eccentricity δ. It starts with horizontal tangent with the value κ and rises with increasing eccentricity more and more steeply. The limiting case $\delta = 1$ and $\kappa = 0$ corresponds to an inner cylinder with a very small diameter and an outer cylinder with a very large diameter. The corresponding coefficient A_2 can be taken from the computation of the example of a circular cylinder parallel to a plane wall and has the value

$$A_2(\kappa = 0;\ \delta = 1) = \frac{1}{4}$$

5. SUPERPOSITION OF REFLECTION LAWS, RESULTS OF MEASUREMENTS FOR ECCENTRIC SPHERICAL SURFACES

51. Dispersion Coefficient

The specular and the Lambert reflector are mathematical models that enable a computation of the heat exchange through radiation with a tolerable amount of computation. As previously mentioned, the measured directional distributions of the reflections lie between the two extremes treated and, therefore, it appears to be a reasonable assumption that the true situation is best approximated by superposing the results of the two reflection laws.

We shall first apply this assumption to the differential reflection law, that is, to the incident angle-dependent directional distributions of the reflections. The approximation of the measured directional distributions of the reflection coefficient by a mixture of the laws of specular and Lambert reflection would then appear to be rather bold, since for a definite direction, considerable deviations may occur.

However, our assumption does not refer to the differential law but refers to the problem of the heat transfer. In each case, the exchanged radiation energy is obtained through repeated integration from the emission and reflection laws and, in accordance with the theory of the second section, is determined by the solid angle ratios and reflection factors of the problem under consideration. Let a certain reflection factor assume the value f_{sp} for the law of specular reflection and the value f_{Lam} for the Lambert reflection. For the resulting reflection factor to be substituted in computing the heat transfer we now assume the expression

$$f_{res} = (1 - \lambda)f_{sp} + \lambda f_{Lam} \tag{94}$$

that permits a best possible approximation to reality through a suitable choice of the coefficient λ in the interval between 0 and 1. We denote the coefficient λ as the dispersion coefficient or the degree of dispersion. The dispersion coefficient depends primarily on the reflection properties of the participating surfaces and secondly on their geometry. It is zero if there are only Lambert reflectors and thus gives a measure of the dispersion capacity of the reflecting surfaces. Because, however, surfaces with different reflection properties generally participate in the radiation exchange, λ is not a constant of the material but a characteristic magnitude of the particular problem under consideration.

In the case of the two-surface system we may ask which of the two surfaces has the greater effect on the determination of the dispersion coefficient. If one surface, for example F_1, is convex or nearly convex, formula (56) has shown that the second surface F_2 essentially determines the value of λ. In formula (56) only reflection factors that refer to a reflection at the surface F_2 appear; the other four reflection factors, according to formula (53) follow from

the convexity of the first surface. Accordingly, it is the more concave of the two surfaces (in the computed examples the enveloping cavity) on whose reflection properties the dispersion coefficient chiefly depends.

52. Results of Measurements for Eccentric Spherical Surfaces

Measurements of the heat transfer through radiation (e.g., eccentric spherical surfaces), were carried out by K. Elser (ref. 7) at the Institute for Thermodynamics and Combustion Engines of the Swiss Institute of Technology. In his test arrangement he used spherical surfaces with the ratio of radii $\kappa = 0.5$ and with various surfaces. He found that the heat transfer clearly increases with increasing eccentricity (not as much as with the computation with the law of specular reflection) and that for the variation with the eccentricity only the radiation properties of the outer spherical surface were of significance. These results agree with the prediction of the theory.

With a similarly constructed test arrangement tests were carried out by the present author using eccentric spherical surfaces with the ratio of radii $\kappa = 0.3$. An inner sphere of brass of 30 millimeters outer diameter exchanged radiation with a hollow copper sphere of 100 millimeters inner diameter. Both surfaces were black-oxidized; however, the oxide layers were less dense and black than those of the test plates of black-oxidized brass sheet mentioned in section 1.

The inner sphere had an interior cavity. This cavity contained a heating coil of canthal coils, which were loaded with about 40 watts during the test. The wall of the sphere was 4 millimeters thick and conducted the heat in tangential direction sufficiently to assure a uniform surface temperature. The temperature during the tests was about 490° to 500° C and could be determined with a copper-constantan thermocouple whose wires were mortised into two separated oppositely lying holes of 1 millimeter tangentially into the sphere wall. The thermo-electromotive force was measured without current by applying an equal and opposite compensation voltage. For heating the sphere a direct current source was used that was fed by a storage battery and had a very constant line voltage.

The inner sphere was suspended in the interior of the hollow sphere so as to swing on the heating wires. By inclining the outer sphere with the suspension the mutual position of the surfaces could be varied and adjusted to any desired eccentricity.

The outer hollow sphere was maintained at constant ambient temperature through a cooling jacket in which water circulated. The sphere was evacuated with the same high-vacuum apparatus, which was applied in the aparatus for the reflection measurements, and consisted of two hemispherical shells that were pressed together with a flange made airtight with vacuum grease. Its internal pressure was always maintained below 10^{-4} millimeters of mercury during the tests in order to suppress the heat conduction and convection of the intervening air layer.

The heat conducted away by the heating and thermocouple wires entered as a measuring error of the transferred radiation energy. This heat loss amounted to about 0.5 percent of the heating power and was taken into account. The heat conduction and convection in the air layer for the vacuum used was negligible. The electrical power was determined by measuring the current and voltage with precision instruments and the temperature of the inner sphere was determined within an accuracy of about 1° C so that the relative error of the measured heat transfer and of the other radiation magnitudes was less than 1 percent. The measurements were not, however, always reproducible because the radiating surface of the inner sphere slowly varied with time under the effect of the temperature.

From the measurements of the transferred radiation energy the factor $\epsilon_1\epsilon_2 K$ could, according to equation (55), be obtained as a function of the eccentricity. The result is given in the lower half of figure 41 (dashed curve and plotted measuring points). The emission coefficients ϵ_1 and ϵ_2 and the dispersion coefficient λ were at first still unknown. The theory was then applied for the determination of the measured results by making the computed curve, through a suitable choice of the emission ratios and the dispersion coefficient, coincide with the measured curve at two points (collocation points), namely at the point $\delta = 0$ (concentric position) and for $\delta = 0.437$, that is, at the point where the reflection factor f_{121} assumes the same value 0.121 for the laws of the specular and Lambert reflections; on the other hand care was taken to obtain as good as possible agreement of the computation with the results measured. There is to be substituted $\epsilon_1 = 0.76$ (for the inner sphere), $\epsilon_2 = 0.80$ (for the outer sphere), and $\lambda = 0.456$ in order to obtain the solid curve in the lower half of figure 41. In the example investigated an agreement of experiment with computation for the coefficient $\epsilon_1\epsilon_2 K$ can be attained within a relative deviation of 1 percent and the theoretically predicted variation of the heat transfer with the eccentricity is well satisfied. Smaller deviations can nautrally be ascribed to the simplified assumptions of the computation.

In the upper half of figure 41 the reflection factors f_{121} (plotted points) computed from the measurement results are compared with those obtained from the reflection laws and their superposition. The figure shows that the dispersion coefficient λ also depends on the eccentricity δ, that is on the geometry of the two-surface system.

As an example we shall compare various approximate solutions for the radiation exchange - as stages of an increasing approximation of the computation to the real situation. The computer, who knows nothing of the emission relations, will regard both surfaces as blackbodies and use the first rough approximation $\epsilon_1\epsilon_2 K = 1$. Considering the emission factors and neglecting the reflections leads to the Nusselt approximation with $\epsilon_1\epsilon_2 K = \epsilon_1\epsilon_2 = 0.608$. The reflections can be approximately taken into account by treating the configuration as concentric spherical surfaces with Lambert reflection according to equation (75) with $\epsilon_1\epsilon_2 K = 0.747$, or by computing with concentric spherical surfaces for specular

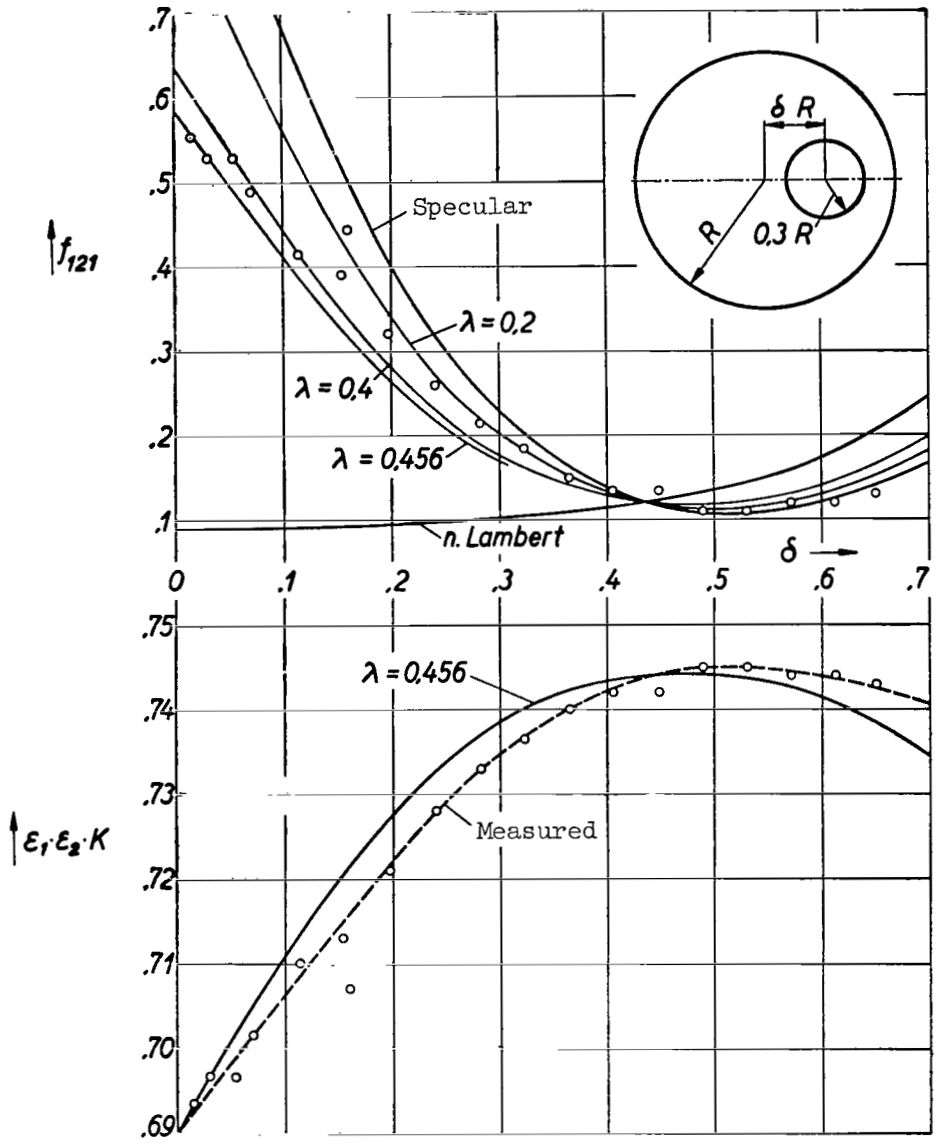

Figure 41. - Dependence of reflection factor f_{121} and of exchanged radiant energy on eccentricity δ for eccentric spherical surfaces (ratio of radii $\kappa = 0.3$).

reflection with the factor $\epsilon_1\epsilon_2 K = 0.638$, which gives the same emission relations as for parallel plates. In actuality $\epsilon_1\epsilon_2 K$ fluctuates, depending on the adjusted eccentricity, between 0.690 and 0.745 and the computation with more refined account of the reflections comes very close to the measured values.

53. Effect of Directional Distribution of Emission

Thus far we have taken into account only the directional distribution of the reflections. For the directional distribution of the emissions we assumed the Lambert cosine law. The computations, on this basis, correctly give the dependence of the heat transfer on the eccentricity for eccentric spherical surfaces. From this it can be concluded that the directional distribution of the reflection coefficients is the principal factor with respect to the dependence of the heat transfer on δ while the directional distribution of the emission coefficient only plays a subordinate part.

We shall see the effect of the directional distribution of the emission coefficient; for example, eccentric spherical surfaces with small ratio of the radii κ. In the concentric position the rays from the inner sphere fall almost perpendicularly on the surface of the outer spherical shell; correspondingly for the computation of the heat exchange the emission coefficient ϵ_n is to be substituted in the direction of the surface normals. If the spheres are situated in a very eccentric position almost all angles between 0° and 90° are represented in the incidence angles of the rays and an emission coefficient averaged over all directions (e.g., total radiation), is to be substituted.

Accordingly, an upper estimate of the effect of the directional distribution of the emissions is given by the ratio ϵ/ϵ_n of the emission coefficient ϵ of the total radiation to the coefficient ϵ_n of the normal radiation. According to the measurements of E. Schmidt (ref. 2) this ratio for bright metals is on the average about 1.2; for nonmetals (depending on the surface roughness) about 0.95 to 0.98.

In the experimentally investigated problem of section 52 the variability of $\epsilon_1\epsilon_2K$ (and, hence, the effect of the directional distributions of the reflections) constitutes about 8 percent of the value for concentric position. The effect of the directional distribution of the emissions should amount to a maximum of 2 percent since: (1) the extreme case described in our example (small ratio of radii κ with nearly perpendicular incidence of the rays on the outer spherical surface) does not apply and, (2) the occurring emission factors are rather high and therefore the directional distribution of the emissions must come close to the Lambert cosine law (as limiting case for the blackbody).

If the radiating surfaces are bright metals, the effect of the directional distributions of the emissions may amount up to about 20 percent. But then the emission factors are small and the reflections again play a much greater part.

Our example shows how to take an approximate account of the directional distribution of the ϵ_ν: Each individual case of the angles of incidence ν represented are to be investigated and the emission coefficients averaged over these angles are then to be substituted. A still more accurate computation requires the introduction of the ϵ_ν distribution in determining the reflection factors.

54. Approach and Focusing Effects

We wish to explain clearly how the reflection effect arises and for this purpose the example of eccentric spherical surface with small ratio of the radii K is again taken as a basis. We consider the inner sphere as primarily radiating.

We start with a medium eccentricity and bring the inner sphere closer to the nearest point of the outer sphere. The outer sphere then receives more radiation energy and, therefore, there is also an increase in the amounts reflected. The concentration of the reflections on the inner sphere at the closest position causes the inner sphere to receive more back reflections and the exchanged radiation energy to decrease. We shall denote this phenomenon, which occurs both for specular and Lambert reflection, the approach effect. The dependence of the heat exchange on the dimensionless distance δ for the examples of a sphere and a plane wall and for a circular cylinder parallel to a plane wall is controlled by the approach effect.

If we bring the inner sphere from a weakly eccentric position into the concentric position, the heat transfer is only slightly affected if the outer spherical surface is a Lambert reflector. However, if this surface is a specular reflector, the return reflections on the inner sphere greatly increase and the radiation energy correspondingly decreases. This phenomenon, which we shall call the focusing effect, takes place because the outer spherical surface (as a concave mirror) combines the reflections and concentrates them at its center. The focusing effect is a characteristic of the specular reflection and distinguishes the behavior of the latter from the Lambert reflection.

These two preceding notions enable a prediction of the effect of the reflections and make it possible to judge how the results deviate from each other, according to the laws of specular and Lambert reflection. Larger deviations are to be expected if the focusing effect plays the deciding part (e.g., in the case of the two-surface system, if one surface is uniformly and concavely curved), hence, specifically for concentric spherical and circular cylindrical surfaces. On the contrary, for irregularly curved surfaces no large deviations are to be expected and the computations may be conducted approximately with the more simple of the two reflection laws alone, that is with the Lambert law. For this reason the theory of the Lambert reflection was developed beyond the limits of the specular reflection.

SUMMARY

The thermal radiation properties of a technical surface can be characterized by its emission and reflection coefficients. An experimental apparatus is described for measuring the reflection coefficient as a function of the incident and reflection direction. A radiation source irradiates a surface, given in the form of a test plate, with definite intensity and in the given angle of incidence. A radiation measuring apparatus catches the reflections in a small solid angle region in the reflecting direction under consideration. The directional

distribution of the reflection coefficient clearly depends on the angle of incidence. All transitions are possible, from the purely specular to the strongly scattering reflector. The absorption coefficients can be obtained by integrating over all directions of the half-space.

A contribution is made to the theory of heat transfer by radiation: The computations are based both on the law of specular reflection, according to which a radiation energy with incidence angle ν is reflected with equal angle of reflection in the incidence plane, and on the Lambert law of reflection according to which the reflections are distributed in accordance with Lambert's cosine law. The superposition of the results gives the relations with good approximation as is shown by the tests for the example of the concentric spheres.

REFERENCES

1. Geiger, H., and Scheel, K.: Handbuch der Phys., Bds. 20-21, Springer (Berlin), 1928-1929.

2. Schmidt, E., und Eckert, E.: Über die Richtungsverteilung der Wärmestrahlung von Oberflächen. Forschung, bd. 6, 1935, p. 175.

3. Eckert, E.: Messung der Reflexion von Wärmestrahlen an technischen Oberflächen. Forschung, bd. 7, 1936, p. 265.

4. Nusselt, W.: Graphische Bestimmung des Winkelverhältnisses bei Wärmestrahlung. Z.V.D.I., bd. 72, 1928, p. 673.

5. Schack, A.: Der industrielle Wärmeubergang. Fourth ed., Stahleisen, Düsseldorf, 1953. (With Further References to the Literature.)

6. Kerkhof, F.: Vakuumthermoelemente für Strahlungsmessungen. Arch. tech. Messen, R. Oldenburg, München and Berlin, Oct. 1940. (With Further References to the Literature.)

Reports of the Institute for Thermodynamics and Combustion Engines of the Swiss Institute of Technology:

7. Elser, K.: Experimentelle Untersuchung des Strahlungsaustausches zwischen exzentrischen Kugelflächen. Rep. 205, 1949.

8. Ott, H. H.: Beitrag zur Theorie des Strahlungsaustausches zweier Flächen mit Anwendung auf den Fall exzentrischer Kugelflächen. Rep. 212, 1950.

Translated by S. Reiss
National Aeronautics and
Space Administration

SCHEME I

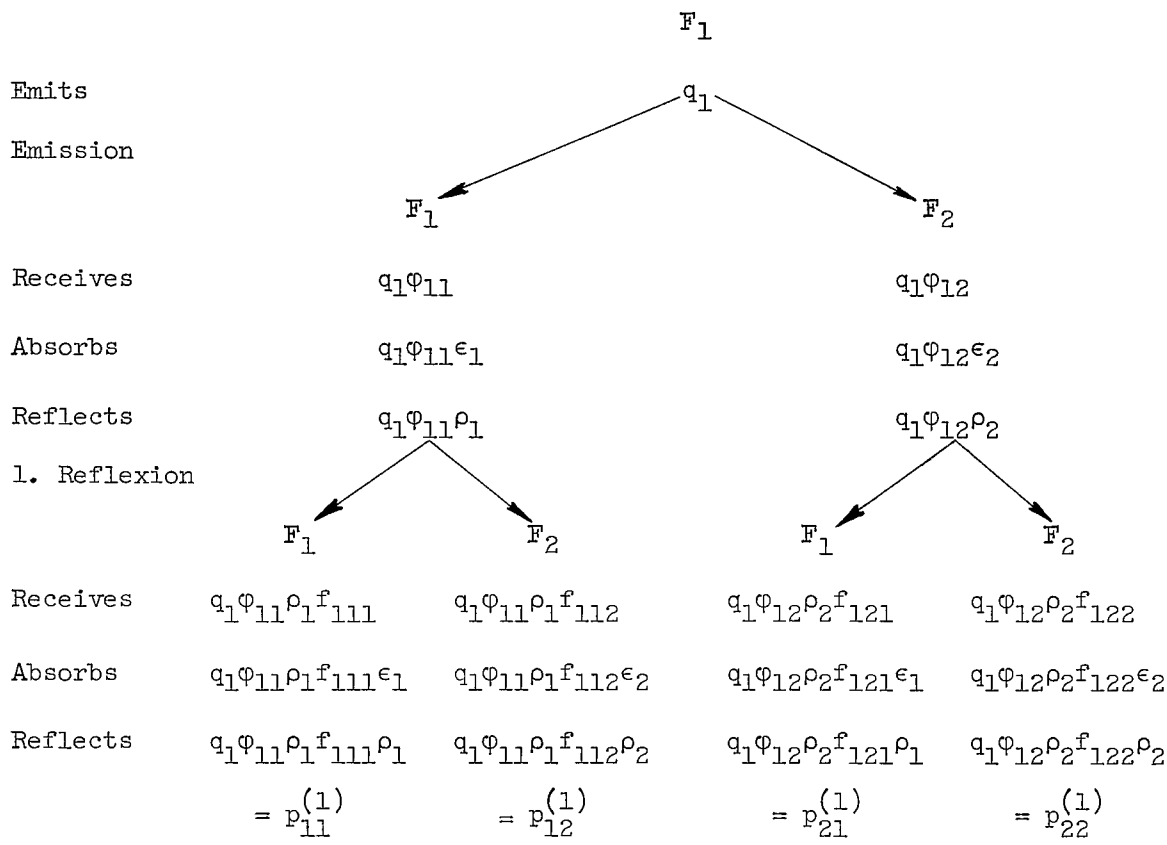

SCHEME II

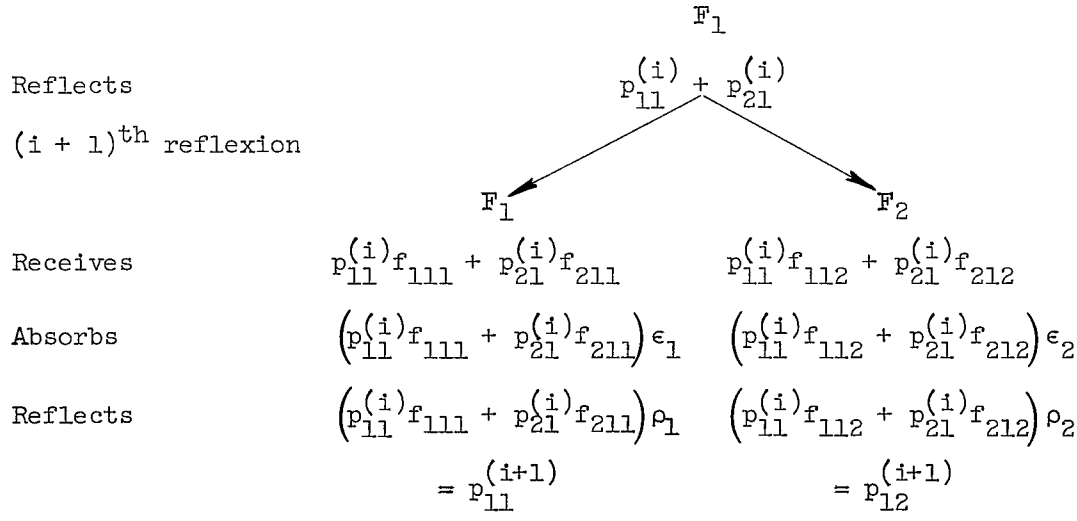

TABLE 1. - REFLECTION COEFFICIENT ρ' FOR

$\mu = \nu$ AND $\psi = 0$

Surface	$\nu = \mu = 30^\circ$	45°	60°	75°
Black-oxidized brass	0.506	0.710	2.27	17.4
White paper	.646	.798	1.50	10.2
Anodically oxidized anticorodal	77.2	89.5	184.4	770

TABLE 2. - AVERAGE REFLECTION COEFFICIENTS $\overline{\rho}$

FOR WHITE PAPER

[Emission temperature, $T_e = 905^\circ$ C.]

ν \ μ	0	15°	30°	45°	60°	75°
30°	0.485	0.464	0.396	0.322	0.221	0.106
60°	.390	.374	.344	.321	.284	.178

TABLE 3. - REFLECTION AND ABSORPTION COEFFICIENTS AS FUNCTION OF INCIDENT ANGLE FOR BLACK-OXIDIZED BRASS AND WHITE PAPER

Surface	ν	T_e, °C	ρ_ν	$1 - \rho_\nu$
Black-oxidized brass	0, 30°	910	0.086	0.914
	60°	910	.105	.895
White paper	0, 30°	905	.222	.778
	60°	905	.240	.760

TABLE 4. - ABSORPTION COEFFICIENTS DETERMINED FROM REFLECTION MEASUREMENTS

[T_e = emission temperature; surfaces are at room temperature.]

Surface	T_e in °C	$1 - \rho_n$	$1 - \rho$
Black-oxidized brass	520	0.889	0.870
	910	.914	.891
White paper	535	.848	
	905	.778	.753
White pine	910	.813	
Calorstea (steatite substance)	905	.567	
Anodically oxidized anticorodal	920	.636	
Sandblasted anticorodal	920	.510	

BIOGRAPHY

I was born on April 7, 1927 in Rorschach. I spent my early years at Horn (Thurgau), where I attended primary and secondary school from 1934 to 1942. In the spring of 1942 I entered St. Gallen, the higher modern school of the Canton school, and received the leaving certificate in September 1946. Since by inclination and aptitude I was drawn to the mathematical-scientific field, I began my course of study in the mechanical engineering division of the Swiss Technical College at Zurich in October 1946, which, with an interruption from 1950 to 1951 occasioned by military service and practical activity, I concluded at the end of 1951 with the receiving of the diploma. I was subsequently assistant to Prof. Dr. G. Eichelberg up to the end of November 1954. While there, I had the opportunity of undertaking the present work in March 1953.

NASA-Langley, 1968 —— 33 F-497

"The aeronautical and space activities of the United States shall be conducted so as to contribute . . . to the expansion of human knowledge of phenomena in the atmosphere and space. The Administration shall provide for the widest practicable and appropriate dissemination of information concerning its activities and the results thereof."

—NATIONAL AERONAUTICS AND SPACE ACT OF 1958

NASA SCIENTIFIC AND TECHNICAL PUBLICATIONS

TECHNICAL REPORTS: Scientific and technical information considered important, complete, and a lasting contribution to existing knowledge.

TECHNICAL NOTES: Information less broad in scope but nevertheless of importance as a contribution to existing knowledge.

TECHNICAL MEMORANDUMS: Information receiving limited distribution because of preliminary data, security classification, or other reasons.

CONTRACTOR REPORTS: Scientific and technical information generated under a NASA contract or grant and considered an important contribution to existing knowledge.

TECHNICAL TRANSLATIONS: Information published in a foreign language considered to merit NASA distribution in English.

SPECIAL PUBLICATIONS: Information derived from or of value to NASA activities. Publications include conference proceedings, monographs, data compilations, handbooks, sourcebooks, and special bibliographies.

TECHNOLOGY UTILIZATION PUBLICATIONS: Information on technology used by NASA that may be of particular interest in commercial and other non-aerospace applications. Publications include Tech Briefs, Technology Utilization Reports and Notes, and Technology Surveys.

Details on the availability of these publications may be obtained from:

SCIENTIFIC AND TECHNICAL INFORMATION DIVISION

NATIONAL AERONAUTICS AND SPACE ADMINISTRATION

Washington, D.C. 20546